Inorganic hole transport materials in perovskite solar cells arecatching up[*]

by

Sajid Sajid [a, b, c], Salem Alzahmi [a, b, **], Imen Ben Salem [c], Jongee Park [d], Ihab M. Obaidat [b, e, *]

Keywords: Inorganic HTM Optoelectronic feature Cost Performance Perovskite solar cell

Abstract

More research is required to further optimize device efficiency, stability, and reduce the materials cost as perovskite solar cells (PSCs) approach to industrialization. Modulating the optoelectronic features and chemical coupling of the hole transport materials (HTMs) remains a prominent field of study in PSCs due to the significant impact these materials have on the device performance and stability. In order to speed up the commercialization of these cells, it is also important to use cost-effective HTMs in PSCs. Inorganic- HTMs are superior to other types of HTMs in terms of their advantages in boosting device performance and producing PSCs at a reasonable cost, in addition to their superior charge transport capabilities, desired energy levels, and intrinsic thermal and chemical stability. A detailed overview of inorganic- HTMs, including metal oxides, cyanates, phthalocyanines, chalcogenides, nitrides, and carbides, is pre- sented in this review. After briefly discussing the primary physical and optoelectronic characteristics of inorganic-HTMs, the critical functions of the above-mentioned materials as HTMs in PSCs are addressed. This review concludes by offering suggestions for future research

[*] Published by Materials Today Energy, 10.1016/j.mtener.2023.101378. [a] Department of Chemical & Petroleum Engineering, United Arab Emirates University, Al Ain P.O. Box 15551, United Arab Emirates [b] National Water and Energy Center, United Arab Emirates University, Al Ain P.O. Box 15551, United Arab Emirates [c] College of Natural and Health Sciences, Zayed University, Abu Dhabi P.O. Box 144534, United Arab Emirates [d] Department of Metallurgical and Materials Engineering, Atilim University, Ankara, 06836, Turkey [e] Department of Physics, College of Sciences, University of Sharjah P.O. Box 27272, United Arab Emirates

that could considerably boost the performance of the PSCs with cost-effective inorganic-HTMs.

1. Introduction

The optoelectronic features of organic inorganic halide perovskites are appealing, including strong broadband absorption, high charge-carrier mobility, and long charge diffusion length [1]. Inexpensive perovskite and simple solution processing capabilities have accelerated the development of perovskite solar cells (PSCs). The PSCs can be made in two primary layouts: mesoporous architecture and planar architecture [2,3]. The device layout can further be divided into regular structure (n-i-p) and inverted structure (p-i-n) based on where the charge transport layers are located, as illustrated in Figs. 1a and b. The charge transport layers do make a substantial contribution, regardless of the PSC's architecture used [4]. When a perovskite layer is sandwiched between two elec- trodes, for instance, the direct contact of the perovskite with the electrodes will cause a high rate of charge-carrier recombination when electrons and holes are produced by incident light, which lowers the performance of the cell. Additionally, because perovskite is strongly affected by moisture, heat, and oxygen, the perovskite layer will break down very quickly. Therefore, choosing the right HTM will aid in preventing charge-carrier recombination and safeguard the perovskite layer from outside factors that may otherwise triggers degradation [5]. In addition to the high hole mobility, the energy levels of the HTM should be matched with corresponding contacts for efficient charge transport and collec- tion, as illustrated in Figs. 1 a and b. In the low-cost PSC fabrication, the cost of HTM should also be taken into account. Power conversion efficiencies (PCEs) of PSCs made with conventional organic-HTMs are typically around 26% [6]. For example, poly[bis(4-phenyl)(2,4,6-trimethylphenyl)amine (PTAA) is regar- ded as an outstanding HTM with a suitable energy level for both regular and inverted PSCs despite its high cost [7]. Another most

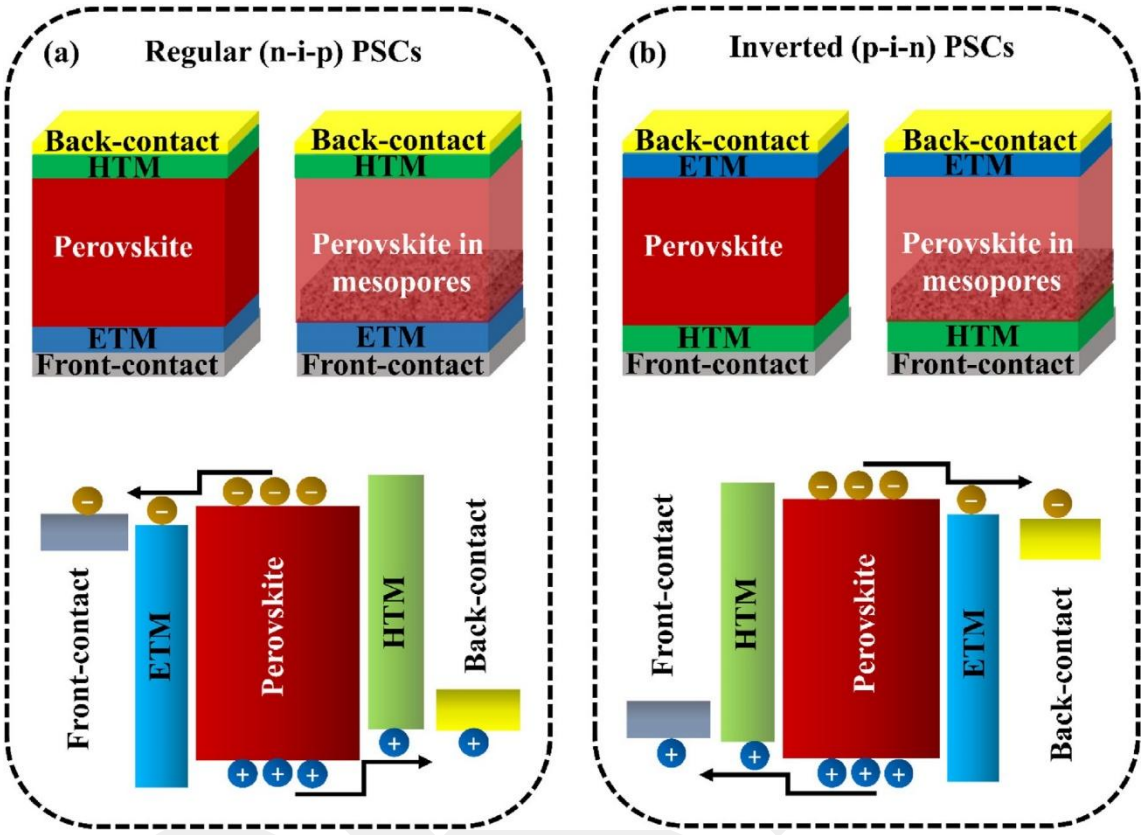

Fig. 1. Schematic illustrations of (a) Regular PSC configuration accompanied by charge-carriers generation and collection; (b) inverted PSC configuration accompanied by charge- carriers

generation and collection. PSC, perovskite solar cell.frequently used organic HTMs is 2,2′,7,7′-tetrakis[N,N-di(4- methoxyphenyl)amino]-9,9′-spirobifluorene (spiro-OMeTAD),

which possesses poor stability, low hole mobility, and high-cost. When spiro-OMeTAD is fabricated on top of the perovskite in the regular device structure, outstanding PCE can be achieved [6,8]. Unfortunately, the device's poor stability and high cost of the spiro- OMeTAD limit the commercialization of spiro-OMeTAD-based PSCs. For example, due to spiro-OMeTAD susceptibility to mois- ture [9], the regular PSCs can easily degrade. The irreversible interaction between migrated-iodine ions from the perovskite and components of the spiro-OMeTAD reduces the hole mobility and efficiency of the spiro-OMeTAD-based PSC [10]. Further investiga- tion showed that the performance of the spiro-OMeTAD-based PSCs

would be diminished by the diffusion of gold (Au) electrode through the HTMs, which react with the perovskite layer and trig its degradation [11]. The degradation at the interface between Au-
electrode and spiro-OMeTAD is regularly reported when PSCs were heated at 80 $^{\circ}C$ [12]. Despite the fact that additives
(LiTFSI tBP) and oxidants (FK209) are important dopants in PTAA or spiro-OMTAD, their hygroscopic and volatile nature causes se- vere morphological change, ion accumulation, and perovskite degradation, all of which seriously impair the performance and stability of the PSCs [13]. In the case of inverted PSCs, highly transparent HTMs are needed since the perovskite layer must receive the majority of the incident light in order to generate enough electrons and holes to achieve satisfactory performance. For instance, poly(3,4-ethylenedioxythiophene) polystyrene sulfo- nate (PEDOT:PSS) is one of the organic-HTMs that is often employed in inverted PSCs due to its suitable transparency,
acceptable conductivity, and appropriate workefunction [14,15]. Nevertheless, PEDOT:PSS triggers the decomposition of the PSCs because of its hygroscopic and acidic nature [16]. The conclusion drawn from the prior brief discussion is that, due to the afore- mentioned drawbacks, it is hard to preserve device stability and performance consistency based on the organic-HTMs. Thus, it is important to explore HTMs that operate with low-cost PSCs, have excellent stability, and have satisfactory efficiency.

Because of their exceptional optoelectronic features, low-cost, and excellent chemical and thermal robustness, inorganic-HTMs have recently emerged as the leaders among other HTMs. The primary contenders for emerging HTMs in PSCs are metal oxides and other inorganic semiconductors, including metal cyanates, phthalocyanines, chalcogenides, nitrides, and carbides. This review encompasses the newly emerging but continually growing field of alternative inorganic HTMs for PSCs, including metal cyanates, metal chalcogenides, nitrides, and carbides, despite the fact that numerous recent reviews [2,17e19] have widely discussed the integration of commonly used metal oxides as HTMs in PSCs. We, therefore, intend to present a comprehensive, updated, and critical assessment of various inorganic-HTMs in PSCs in this study. Following a discussion of the vital optoelectronic and physical features that inorganic-HTMs might have, we go into great details about the latest developments involving the integration of these HTMs in PSCs with a

focus on their various functionalities and their role in enhancing performance of the device. Finally, we give a forecast for further inorganic-HTMs development and utilization in PSCs, keeping in mind that the ground-breaking PSCs are anticipated to have a major influence on market applications very soon.

2. Demanding features of HTM

Regardless of the device configuration, integrating new HTMs has frequently been employed to obtain highly efficient and stable PSCs. After meeting at least a few of the following criteria, suitable HTMs can indeed be chosen: (i) desirable conductivity and hole-mobility to accelerate charge-carrier transport, (ii) high hydrophobicity and low surface energy to prevent water infiltration and the resulting moisture-induced deterioration, (iii) wide bandgap and high transparency in the visible wavelength spectrum to permit solar light to pass through, (iv) suppression of unwanted charge recombination at the corresponding interfaces, (v) inherent thermal, chemical, and photochemical stability to prevent PSC degradation during operation at high temperature and irradiation along with potential interactions with the perovskite layer, (vi) serving as a growth template to adjust the quality of the perovskite film, to boost its grain size and crystallinity, (vii) compact, pinhole-free layer formation with smooth surface enabling conformal coverage of the perovskite film to help stop shunting between the corresponding contacts, (viii) reducing device current-voltage (J-V) hysteresis and inhibiting perovskite ion diffusion in the forward and reverse scan conditions, and (ix) offering low-cost and facile fabrication processes.

Table 1 compares the costs and hole-mobility of the major HTMs used in PSCs. Fig. 2 shows the valence and conduction bands (CBs) of the inorganic-HTMs with those of typical perovskites. As can be seen, the majority of inorganic-HTMs have low-cost, sufficient hole-mobilities, and well-matched energy levels with the perovskites. This suggests that inorganic-HTMs are the best options for PSCs.

3. Transition metal oxides

3.1. *Nickel oxide*

A significant amount of effort was put into finding suitable HTMs as a result of the fast deterioration of the existing PSCs. Since it can be easily deposited using a variety of techniques, such as pulsed laser deposition (PLD), electro-deposition, spray pyrolysis, spin coating, sputtering, atomic layer deposition, and sol-gel, nickel oxide (NiO_x) is an appealing inorganic-HTM [2]. Additionally, it possesses a wide band gap, high transparency, excellent chemical stability, and convenient energy level alignment with perovskites. Together,

these characteristics support electron blocking and hole collecting. The often-found p-type conductivity in pristine NiO_x is typically attributed to the nickel vacancies, whereas stoichiometric NiO is insulating. However, due to the high ionization energy of Ni vacancies, the hole density in pure NiO_x is limited. External dopants with shallower acceptor levels can improve the hole density of NiO_x. The crucial functions of pristine and doped NiO_x in the development of highly efficient, stable, and affordable PSCs will be assessed in Sections 3.1.1 and 3.1.2.

3.1.1. *Pristine NiO_x*

In order to achieve optimal electrochemical coupling between perovskite and NiO_x, pristine NiO_x-based HTMs require surface modification, including ultraviolet (UV)-ozone and oxygen plasma [51], as depicted in Fig. 3. As an example, UV-ozone treatment can modulate energy levels of NiO_x and lessen open-circuit voltage (V_{oc}) loss in PSCs. Additionally, the surface wettability enhance- ment results in complete coverage of perovskite solution on the NiO_x-coated substrate. Oxygen plasma exhibits a comparable effect of enhancing the work function of NiO_x-HTM, which is desirable for high hole injection from perovskite layer to the HTM. Additionally, moderate plasma treatment may lead to a decrease in the $Ni^{2þ}$ and an increase in the $Ni^{3þ}/Ni^{2þ}$ proportion [52]. In non-stoichiometric NiO_x, $Ni^{3þ}$ can be found as NiOOH or Ni_2O_3. A higher $Ni^{3þ}$ concentration indicates the presence of more Ni vacancies, which leads to a higher hole conductivity.

Inverted planar PSCs were the first devices to employ NiO_x-based HTM in place of PEDOT:PSS [53]. The poor performance of NiO_x-based PSCs was due to insufficient perovskite coverage on the surface of the NiO_x, which caused charge transport layers to come into direct contact and resulted in a high rate of charge-carrier recombination. Wang et al. [54] used a mesoporous (mp) NiO_x to improve the perovskite's coverage. This approach demonstrated that adequate perovskite infiltration on mp-NiO_x enhanced light harvesting and reduced perovskite layer defect density, which led to the mp-PSC delivering a PCE of 9.51% as compared to the planar device's PCE of 7.40%. Additional research revealed that whether NiO_x-HTM is used to make planar or mp PSCs, the thickness of the layer is equally crucial to performance. Collectively, a thin layer of NiO_x could hardly cover the substrate completely, while a thicker layer would make it harder for the holes to move effectively and would prevent incident light from reaching the perovskite. For instance, spray pyrolysis was used by Chen et al. [55] to form a suitable NiO_x layer thickness in PSCs, which prevented the forma- tion of voids and reduced charge recombination. The PSC with NiO_x (10e20 nm) and mp-Al_2O_3 (90 nm) thus showed a PCE of 13.5%.

A low-temperature combustion process is also regarded as advantageous for forming NiO_x-HTMs with superior performance and better stability of the PSC. Due to the exothermic nature of the combustion process, NiO_x-HTM may be produced at low annealing temperatures (150e250 °*C*), which is suitable for flexible devices.

Additionally, compared to sol-gel-derived NiO_x, the combustion- based layer displayed more homogeneous surface covering [56]. It was found that high p-type doping density and enhanced con- ductivity can be easily obtained for NiO_x through combustion

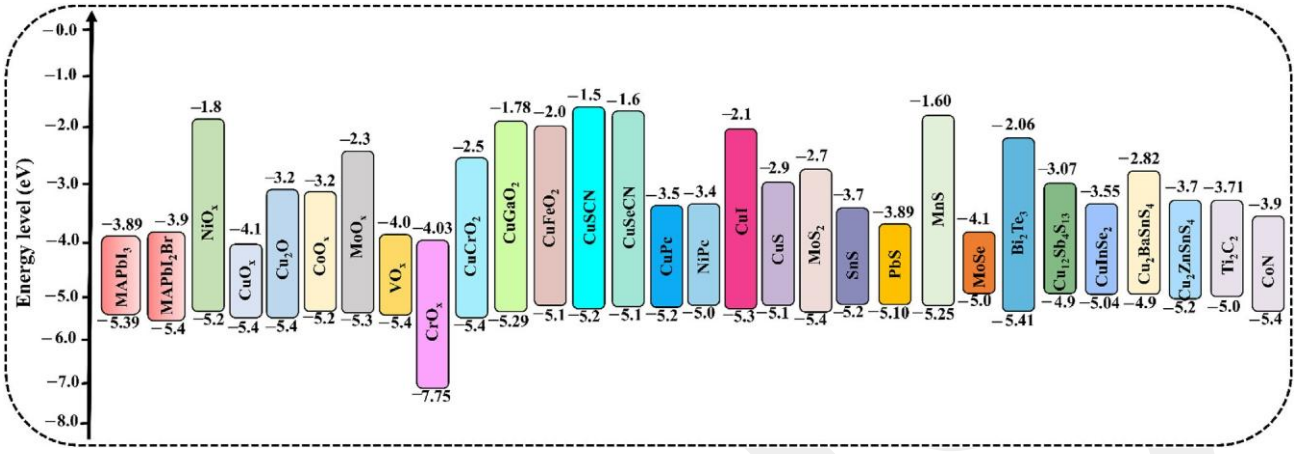

Fig. 2. Energy band diagram of the typical perovskites and inorganic-HTMs discussed in this review. HTM, hole transport material.

approach. Following optimization, combustion-based NiO_x layer (30 nm annealed at 250 ° *C*) displayed a PCE of 20.2% and high stability in inverted-planar PSC [56]. On an indium-doped tin oxide (ITO) substrate, Zhang et al. [56] spun-coated dispersion of NiO_x nanocrystals in deionized water and dried it at room temperature. Given that the concentration of NiO_x determines the film's thick- ness, a slightly greater concentration (2 wt%) of NiO_x displayed a high-quality film with appropriate thickness. For rigid and flexible inverted-planar PSCs, PCE of 17.60% and 14.53% were attained, respectively.

The performance of inverted planar PSCs based on NiO_x-HTMs can be improved by surface passivation as mentioned above. For instance, the efficiency of NiO_x-based inverted planar PSC has been improved to 22.18% with an excellent FF of 83.6% employing 2D/3D perovskite structure [57]. In another report, it was demonstrated that halide-substituted benzoic acid molecules coordinate through carboxyl and hydroxyl groups at the surface of NiO_x. On the opposite site of the molecules, strong halogen bonding can be formed by binding the undercoordinated iodine (I^-) at buried surface of the perovskite. This inhibited the generation of I_2 and thereby suppressed the formation of voids, led to a high PCE of 22.02% under continuous light soaking at 55 °*C* for 1000 h [57].

Recently, it was revealed that spinning a nickel nitrate solution at low temperatures might create homogeneous, ultra-thin nickel nitride (NiN) layer on the NiO_x surface. The Ni_xN-modified NiO_x- based inverted planar PSC had a PCE of 20.45% and long-term stability at nearly 82% of the initial efficiency after 1000 h [58].

Devices having charge transport layers made entirely of inor- ganic materials seem promising in the search for highly stable and relatively inexpensive PSCs. Low temperature processed inorganic transport materials,

in particular HTMs, that have satisfied thermal/ chemical compatibility with perovskites, have had a limited num- ber of successes. The NiO_x was used as HTM (prepared from nickel nitride) while ZnO was used as electron transport materials (ETM) in inverted PSCs by You et al. [59]. It was found that NiO_x-HTM can achieve appropriate coverage on the substrate and low series resistance by carefully regulating the layer thickness. This led to a PCE of 16.1% and a degradability of less than 10% after 1440 h of storage in ambient air at room temperature. Additionally, Liu et al.
[60] incorporated low-temperature NiO_x-HTMs into regular and inverted type PSCs (Fig. 4a). In addition to the increased work function of pristine NiO_x for the desirable energy level alignment with perovskite, the contact angle of NiO_x-dimethylformamide (DMF) precursor was lowered after 5 min of UV-ozone treatment. Final results showed that the inverted type of PSC had PCEs of 15.9%. The dispersion of pristine NiO_x-HTM in non-polar solvents for deposition onto the perovskite layer is challenging for the fabrication of regular PSCs. As a result, regular PSCs had clearly visible hysteresis behavior and had comparatively poor perfor- mance (9.11% PCE for reverse scan and 6.14% for forward scan) [60]. Other approaches, such as ligand exchange pathway, can be used to successfully use low-cost NiO_x-HTM in highly stable regular PSC by spin-coating. For instance, perovskite showed chemical compati- bility with NiO_x capped by oleylamine, which allowed NiO_x to be dispersed in non-polar solvent [61]. The PCE and stabilized power output of the PSC based on oleylamine-capped NiO_x were 12.71% and 10.99%, respectively. The NiO_x-based PSCs clearly displayed excellent durability compared to conventional spiro-OMeTAD, even if NiO_x as HTM in regular devices showed low PCEs, as shown in Fig. 4b. Li et al. constructed a bilayer of NiO_x/spiro-OMeTAD in regular PSC to increase PCE and stability, as shown in Fig. 4c [62]. The dispersion of NiO_x in chlorobenzene was obtained by adding
oleic acid. The spin-coated NiOx on perovskite layer was annealed
at 100 $^{\circ}C$, which is the desirable temperature that will not degrade the perovskite layer. In N_2 environment, the PSC based on NiO_x/ spiro-OMeTAD HTM demonstrated a PCE of 21.66% while main- taining 90% of original efficiency over 1200 h.

Vacuum-based deposition can also be used to fabricate high- quality NiO_x-HTMs as an alternative to the spin-coating tech- nique. For instance, Wang et al. used mp-NiO_x and low- temperature sputtered NiO_x compact layer, which performed bet- ter than solution processed NiO_x [63]. The optimum doping con-centration and desired thickness of the NiO_x were achieved by delicately adjusting the oxygen flow ratio and sputtering time, and the resulting mp-PSC displayed a PCE of 11.6% (Fig. 5a). Further- more, reactive magnetron sputtering delivered a homogenous and uniform morphology in comparison to spray pyrolysis-processed NiO_x, led to a 9.83% PCE in planar inverted PSC [64]. Low- temperature sputtered NiO_x film further enabled a 17.6% PCE in planar inverted PSC [65]. It was observed that annealing tempera- ture has almost no impact on the change of NiO_x grain sizes. Likewise, the as-sputtered NiO_x showed a minor increase in light absorption, permitting more incoming light in perovskite layer. Additionally, the conformance of sputtered NiO_x layer to silicon's pyramidal pattern makes low-temperature NiO_x highly suitable for use in tandem devices (Fig. 5b). The quality of pristine NiO_x-HTM was further improved by PLD. The PSC displayed

a PCE of 17.3% with an excellent fill factor (FF) of 81.3%, thanks to the effective electron blocking, strong hole extraction, and high transparency of PLD- based NiO_x [66]. Subsequently, Shalan et al. [67] improved the

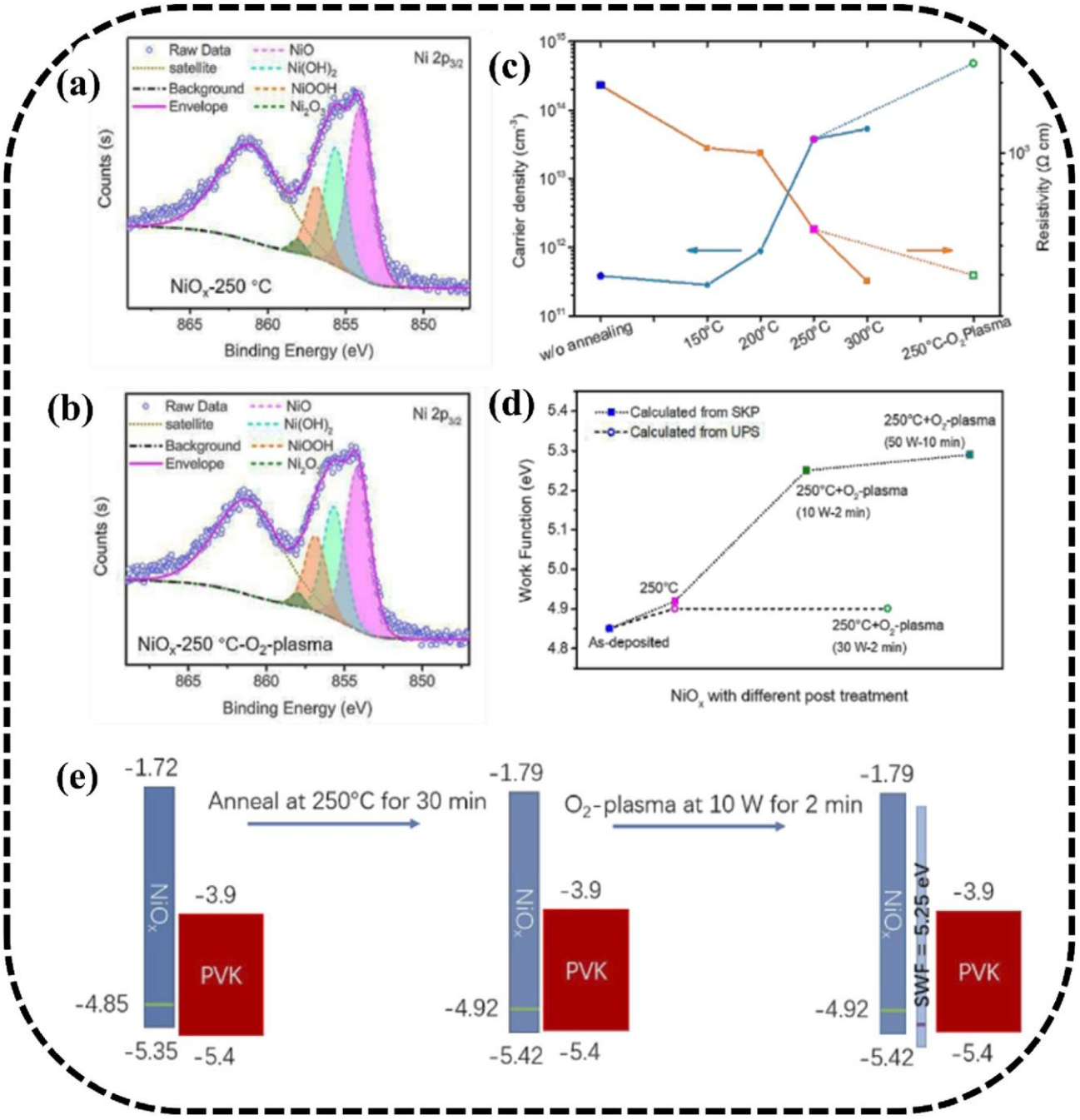

Fig. 3. X-ray photoelectron spectroscopy (XPS) spectra of (a) NiO_x annealed at 250 ° *C* for 30 min; (b) NiO_x annealed at 250 ° *C* followed by O_2-plasma for 2 min; (c) charge-carrier density and resistivity; (d) surface work function of NiO_x-film; (e) schematic of the energy levels alignment between NiO_x and perovskite. Reproduced with permission from the study by Zheng et al. [51]. Copyright 2012, Royal Society of Chemistry.

light harvesting and carrier extraction capabilities by sandwiching Au nano-islands between PLD-NiO_x and perovskite layer. The Au nano-island was shown to have contributed to the localization of long-wavelength light at the NiO_x/perovskite interface, which increased external quantum efficiency in the 500e800 nm range and produced high short-circuit current density (J_{sc}).

3.1.2. *Doped/modified NiO_x*

Since the stoichiometric NiO has inferior hole mobility, atten- tion should be paid to altering the electronic properties of NiO by adjusting the stoichiometric ratio or extrinsic dopants. In this sce- nario, p-type conductivity can indeed be generated through nickelvacancies. Low hole density produced by the high ionization energy associated with nickel vacancies, though. Non-stoichiometric NiO_x exhibits the self-doping phenomena generated by $Ni^{3þ}$ in the Ni vacancy. The $Ni^{3þ}$ acts as an electron acceptor, causing NiO to have p-type conductivity. There are several methods, including the annealing process, UV-ozone treatment, and elemental doping, to increase the amount of $Ni^{3þ}$ in NiO frameworks. Extrinsic dopants that have shallower acceptor levels are preferable in this aspect to boost the hole mobility. To improve charge-carrier mobility, extrinsic dopants such as Li, Cu, Mg, Cs, and Co, as well as co-dopants like Li:Cu and Mg:Li, have been added into NiO_x [2]. Since Cu doping causes acceptor energy levels to be closer to the valence band maximum than gap states of nickel vacancies in undoped NiO, Cu:NiO_x films are expected to have higher conduc- tivity than pristine NiO_x. The Cu can exist in the $Cu^{þ}$ and $Cu^{2þ}$ forms in Cu:NiO_x, and the replacement of $Ni^{2þ}$ with $Cu^{þ}$ results in an increase in carrier concentration and mobility. The Cu-doped NiO_x- HTM was initially used in inverted planar PSCs (with PCEs up to 15.4%) by Kim et al. [68], who utilized a simple solution-processed approach. The improved performance of the PSCs utilizing Cu- doped NiO_x was attributed to enhance conductivity and effective holes-collection at the corresponding interface. Using a combina- tion of cupric acetate monohydrate and nickel acetate tetrahydrate in anhydrous ethanol, Yue et al. reported varying amounts of cop- per doping [69]. The downward shift in Fermi level and valence band (VB) of Cu-doped NiO_x was beneficial for the collection of holes from perovskite. Particularly, the photogenerated holes were collected with minimal energy loss when there was a 5% Cu- doping. However, large Cu concentrations in NiO_x showed an up- ward shift in the VB position, which further raised the energy loss for interfacial hole transport. Through the solution combustion technique, a compact, smooth film with increased conductivity might be produced. For instance, Jung et al. [70] used a solution-

based combustion approach to deposit Cu-doped NiO_x layers at temperatures as low as 150 °*C*. To lower the reaction temperature, nickel nitrate hexahydrate and acetylacetone were used as oxidants and fuel. To improve conductivity, 5 mol% copper nitrate trihydrate was added to the combustion process. The good crystallinity, con- ductivity, and hole-extraction properties of Cu-doped NiO_x enabled the inverted planar PSC to have a high PCE of 17.74%. Additionally, Yao et al. [71] effectively implemented a bilayer of mp-Cu:NiO_x and compact layer of Cu:NiO_x in PSC, which resulted in a PCE of 19.6%. Moreover, He et al. [72] developed a large-area flexible PSC based on Cu-doped NiO_x nanoparticles, and their flexible device attained an average PCE of 15.1% on device with active area of 1.08 cm^2 (Fig. 6). One simple way for the controlled doping of Cu in NiO is the direct deposition of nanoparticle inks. For instance, the perfor- mance of PSCs has been significantly enhanced by room- temperature deposited Cu:NiO_x films made from nanoparticle inks (concentration of Cu with reference to Ni was 5.3 at%) [73]. This improvement can be attributed to the change in the work function of Cu:NiO_x and the significantly higher carrier concen- tration and mobility as compared to pristine NiO_x. For Cu:NiO_x and NiO_x, the best efficiencies on rigid substrates were 20.26 and

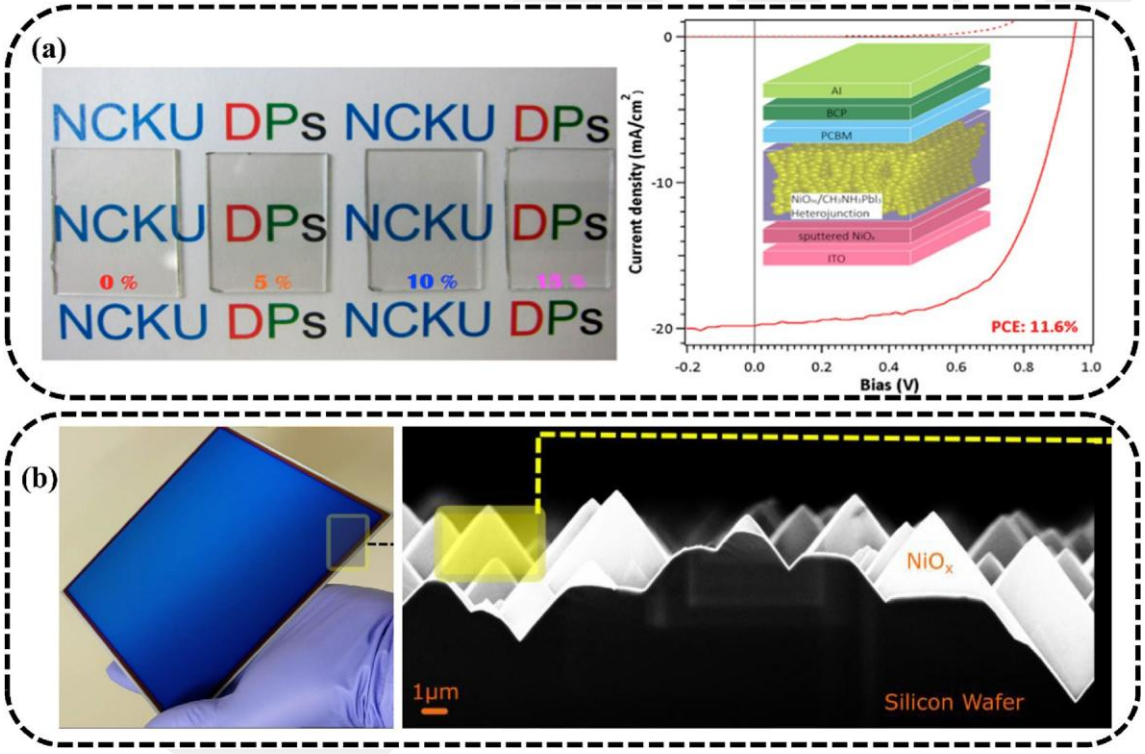

Fig. 5. (a) Sputtered NiO_x thin-films and J-V characteristic curve of as-prepared mesoporous inverted PSC (inset is the schematic of the device). Reproduced with permission from the study by Wang et al. [63]. Copyright 2014, American Chemical Society; (b) room temperature sputtered NiO_x thin-films on the device made of randomly textured silicon (blue colored layer) and pyramid conformal coating SEM cross-section images. Reproduced with permission from the study by Aydin et al. [65]. Copyright 2018, American Chemical Society. PSC, perovskite solar cell; SEM, scanning electron microscopy.

18.18%, respectively. The obtained PCE for Cu:NiO_x for larger 1.0 cm^2 device was 18.05%. The Cu:NiO_x ink was also used to manufacture the high-efficiency flexible PSCs, which had a PCE of 17.41%, which was much higher than that of undoped NiO_x (16.43%) (see Fig. 7).

It is obvious that a large concentration of dopants will increase the defect density and interfacial trap-states in NiO_x-HTMs, lowering the photovoltaic performance of the resulting devices. Additionally, Chen et al. showed that the cesium (Cs) dopant can produce higher $Ni^{þ3}$ acceptor ratio in the stoichiometry of NiO [74] because Cs has a larger atomic radius than Ni, the lattice distortion
in Cs:NiO_x produced more amorphous phase than NiO_x. The highest Cs:NiO_x performance was attributable to 1% Cs doping. The efficient hole extraction was further highlighted by a decreased work function. Potassium (K) doping in NiO_x can also be used to achieve more balanced charge-carrier transport. The K diffusing into perovskite would serve as a passivator at grain boundaries or in- terfaces in addition to improving mobility and conductivity. It should be noted that excessive K doping will cause the VB to move upward, substantially exacerbating the band mismatch with perovskite and degrading the V_{oc} of devices. Regarding this, K doping made sure that J_{sc} and FF have been increased, resulting in 18.05% PCE in inverted planar PSC with 5 vol% K-doped NiO_x-HTM [75]. Ge et al. [76] have examined the doping of a number of alkaline earth metals, including Mg, Ca, Sr, and Ba. It was discovered that this doping might significantly deepen the VB of NiO_x. In the meanwhile, carrier mobility and density can be increased. As a result, exceptional optoelectronic characteristics and desirable charge extraction capabilities were developed. It was found that the addition of dopant with low concentration up to 5% would not affect the intrinsic crystallization of the NiO_x. In addition, Sr was
found to effectively downshift the VB up to —5.34 eV, which is more
appropriate with $MAPbI_3$ (—5.4 eV) than pristine NiO_x (—5.04 eV) among the four alkaline earth metals (Fig. 6). Additionally, a high
V_{oc} of 1.14 V and PCE of 19.49% were obtained in the Sr-doped NiO_x- based PSCs. In addition to adding $Li^{þ}$ to NiO_x layer to improve conductivity, Chen et al. [77] also added $Mg^{2þ}$ to offset the upshift of the NiO_x VB caused by $Li^{þ}$ incorporation. In comparison to
PEDOT:PSS-based cells, PSC with NiMgLiO-HTM produced high FF of 82.7%, a V_{oc} of 1.083 V, and a PCE of 18.3%. Wang et al. reported on another co-doping strategy, such as Li and cobalt (Co) doping in NiO_x [22]. After adjusting the dopant concentration, it was discovered that 10 mol% Li and 5 mol% Co doped NiO_x achieved the greatest crystalline quality and increased conductivity. Addition- ally, the doped-NiO_x showed more advantageous band alignment. Inverted planar PSCs finally achieved a high PCE of 20.1%.

There have also been reports of some other alternate strategies, such as the use of boric acid (BA) as a dual-purpose additive to enhance the NiO_x film's quality while also modifying its electrical characteristics. It was revealed that by increasing the concentration and mobility of the holes inside, the boron (B) heteroatom in the NiO_x matrix can improve the energy band structure as well as the conductivity of the NiO_x film. The PSCs based on NiO_x-HTMs with BA aid showed a considerable rise in PCE from 18.71% to 21.40% with barely detectable hysteresis [78]. Additionally, the unsealed PSCs with BA-assisted-NiO_x were able to maintain 92.8% of their initial efficiency even after being exposed to ambient conditions for close to 1400 h.

Non-metal anions have hardly ever been used to dope NiO_x-HTM, although metal cations have been the majority of the known extrinsic dopants utilized in NiO_x so far. Due to the high nitrogen content of guanidine nitrate, Zhou et al. [79] employed it in this scenario to create N-doped NiO_x. The optimal guanidine nitrate doping was found to be 30 wt% when various guanidine

nitrate doping ratios were dissolved with NiO_x precursors, spin- coated onto cleaned substrates, and then annealed at 280 $^{\circ}C$ for

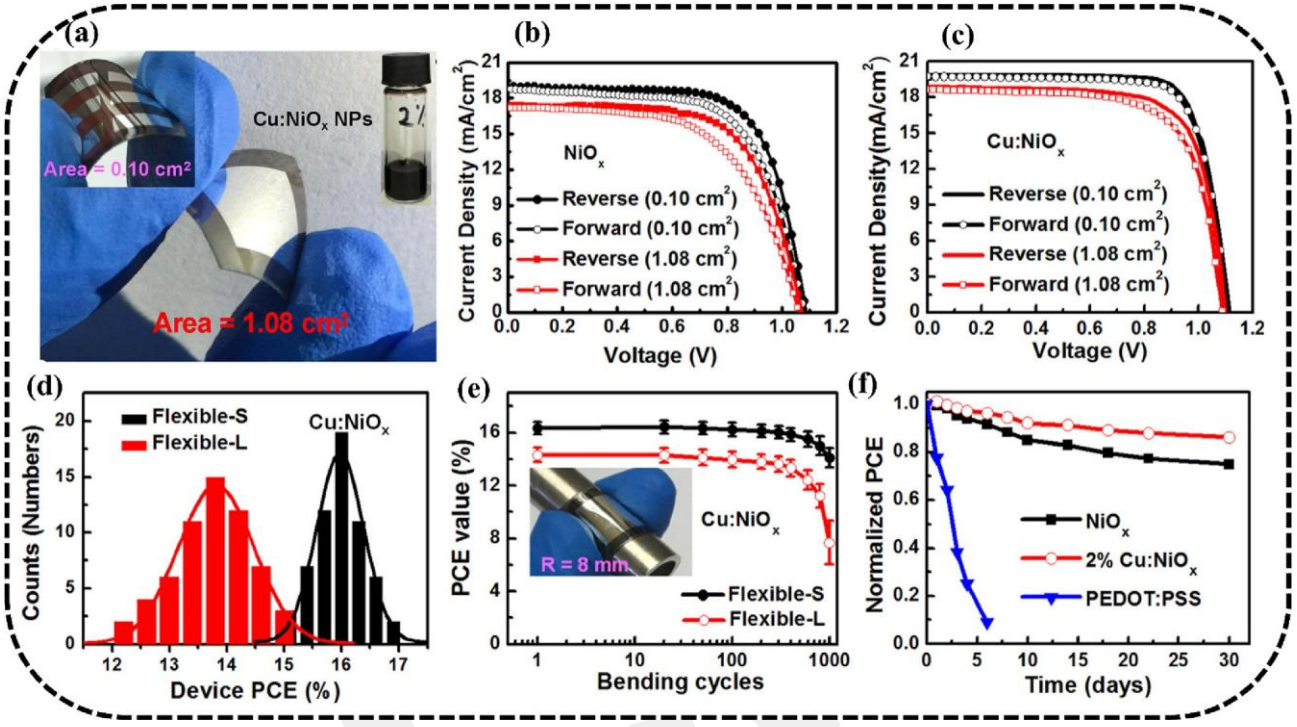

Fig. 6. (a) Photographs of fully assembled flexible Cu-doped-NiO_x-based PSC. Inset is the image of a small-area Cu-doped-NiO_x-based device; J-V curves in reverse and forward scans for the best-performing device; (b) NiO_x-based and (c) Cu-doped-NiO_x-based flexible cells with active areas of 0.10 and 1.08 cm^2; (d) histograms comparing the variation in the average PCEs calculated for 60 flexible PSCs; (e) PCE values as a function of bending cycles at a fixed bending radius of 8 mm for flexible PSCs with various active areas; (f) ambient air stability of the unencapsulated flexible devices using NiO_x, Cu-doped-NiO_x, and PEDOT:PSS as HTMs. Reproduced with permission from the study by He et al. [72]. Copyright 2017, American Chemical Society. HTM, hole transfer material; PCE, power conversion efficiency; PEDOT:PSS, poly(3,4-ethylenedioxythiophene) polystyrene sulfonate; PSC, perovskite solar cell.

60 min in air. When N-doped NiO_x was used, the PCE rose to 17.02% compared to the control device's PCE (15.28%). It should be mentioned that impurity ions, such as nitrate ions, have hindered the performance improvement of inverted planar PSCs using NiO_x as the HTM. In this context, Wang et al. [80] suggested a way to make high-quality NiO_x nanoparticles using an ionic liquid-assisted synthesis approach (IL:NiO_x). In order to produce IL:NiO_x HTM with high conductivity and robust hole-extraction capabilities, it was

found that the cation of the ionic liquid can hinder the adsorption of impurity ions on nickel hydroxide through a strong hydrogen bond and low adsorption energy. The redox reaction between the NiO_x and the perovskite layer was successfully suppressed by the elimination of impurity ions, which prevented the performance of the PSC from degrading. As a result, the improved inverted PSC showed an impressive PCE of more than 22.62%. Similarly, pyrolysis of urea lowered the high-valence state of nickel and replaced the adsorbed hydroxyl group with isocyanate, according to a reactive surface modification strategy based on the in-situ decomposition of urea on the NiO_x surface. With the perovskite, the modified NiO_x layer displayed low surface states and better transport energy level alignment. Modified-NiO_x-based PSC delivered a PCE of 23.61%

[81]. After 2000 h of thermal aging at 85 $^{\circ}C$, the device's PCE
maintained above 90%.

3.2. *Cupric/cuprous oxide*

Due to their advantages of low-cost, environmental friendliness, high hole-mobility, variety of preparation, and energy levels matching with perovskite, copper oxides, specifically cuprous oxide (Cu_2O) and cupric oxide (CuO), are typical p-type semiconductors that have been used as HTMs in PSCs. According to theoretical calculations, the photovoltaic performance of Cu_2O-based PSCswould produce a promising efficiency of above 25% [82]. Hossain et al. used simulation to model the regular planar PSCs with different HTMs made of NiO_x, CuI, CuSCN, spiro-OMeTAD, and Cu_2O [83]. The simulation of Cu_2O-based PSC showed the maximum ef- ficiency of 25.86%. Despite the fact that the modeling findings indicated significant PCEs in regular PSCs, direct deposition of inorganic-HTM can harm the perovskite layer beneath. So, it is crucial to consider the deposition techniques. For instance, in order to deposit a uniform, dense, and pinhole-free crystalline layer of Cu_2O on the perovskite surface, Nejand et al. [84] used a reactive magnetron sputtering approach with carefully controlled DC power and deposition duration. In order to prevent the bombardment damage on the perovskite layer, the sputtering procedure involved

tilting a perovskite-covered substrate at a 45° angle in front of a
metallic Cu target. To make hole collection from the perovskite layer faster, an excellent perovskite/Cu_2O interface was formed during the deposition procedure. At a PCE of 8.93%, a regular planar PSC was demonstrated. To increase the device efficiency above 9%, a Cu_2O film with high hole-mobility and low resistance was created after the Cu_2O layer's thickness was optimized to be 300 nm. The Cu_2O in PSC efficiently impeded the passage of oxygen and water, resulting in the high device's stability. By substituting organic/ inorganic hybrid HTM of FBT-Bh4/CuO_x for conventional HTM of spiro-OMeTAD, extremely efficient PSCs with long-term stability were demonstrated [85]. The FBT-Bh4 and CuO_x were sequentially coated on perovskite layer using solution process and vacuum thermal deposition, respectively. The FBT-Bh4/CuO_x in contact with perovskite showed a quicker extraction rate than the spiro- OMeTAD equivalent.

The FBT-Bh4/CuO_x-based device produced a PCE of 18.85% (Figs. 8aed). When the PSC was stored at 70e80% relative humidity without sealing, the device demonstrated sta- bility for 500 h.

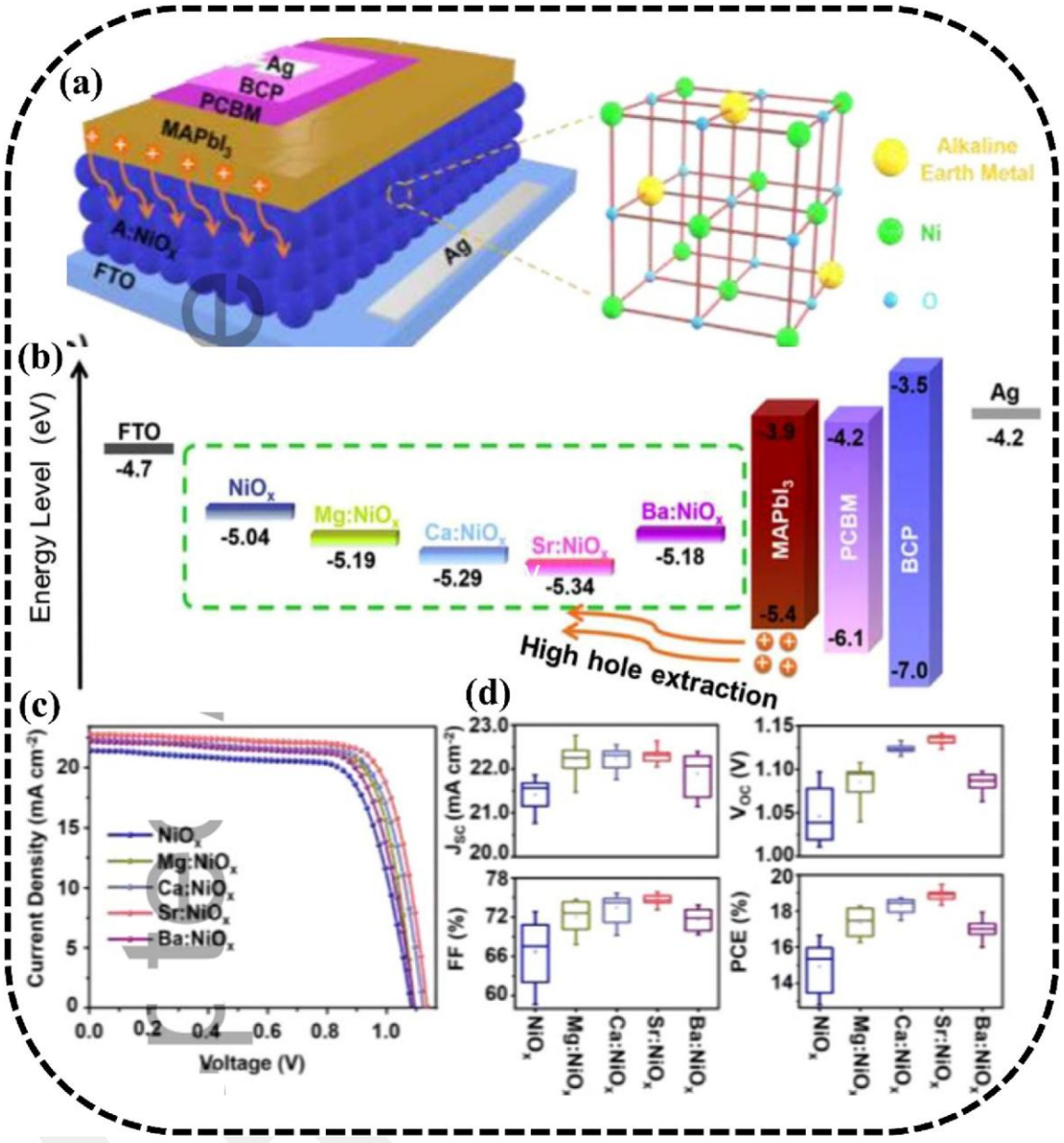

Fig. 7. (a) Inverted planar PSC layout and alkaline earth metal doped NiOx crystal structure (Mg, Ca, Sr, Ba are represented by yellow balls, respectively); (b) an energy level diagram showing how photoinduced holes are transferred between the different layers of the PSCs; (c) J-V characteristics of PSCs based on pure and alkaline earth metal doped NiOx-HTMs tested under AM 1.5G irradiation; and (d) statistics of the device performance with various NiOx-HTMs. Reproduced with permission from the study by Ge et al. [76]. Copyright 2019, WILEY-VCH Verlag GmbH & Co. KGaA, Weinheim. PSC, perovskite solar cell.

When compared to organic-HTM-based devices, inverted planar PSCs with Cu_2O or CuO as HTMs have also been found to be highly efficient and robust. For instance, compared to PSCs using PEDOT:PSS, PSCs

containing Cu_2O and CuO produced improve- ments in V_{oc} of 1.07 and 1.06 V and increased J_{sc} of 16.52 and

15.82 mA/cm^2. These improvements led to the PSCs superior PCEs of 13.35% and 12.16%, respectively. The enhanced V_{oc} is largely attributable to the aligning of energy levels of perovskite and Cu_2O/CuO. On top of Cu_2O and CuO, highly crystalline perovskite was also created to improve carrier transport, which advantages the device with a greater J_{sc} [86]. A PCE of 8.23% was reported in PSCs with solution processed and highly crystalline Cu_2O-HTM. Due to the high hole mobility of Cu_2O, low energy loss between Cu_2O and perovskite, negligible charge-carrier recombination, and good perovskite crystallinity on Cu_2O film, the Cu_2O-based device

outperformed PSCs including NiO_x or Cu:NiO_x [87]. Furthermore, Yu et al. [88] demonstrated the significance of managing the Cu_2O thickness by fabricating an ultrathin Cu_2O compact layer for the inverted PSCs using thermal oxidation of sputtered-Cu thin-film. The Cu_2O thickness was carefully regulated in order to maximize optical transmission and reduce series resistance. The best PCE of 11% was attained by a PSC using 5 nm layer of Cu_2O. Further reports showed that solution-processed CuO_x-HTM exhibits high trans- parency in the visible spectrum, efficient hole transport and decreased contact resistance at the perovskite/CuO_x interface [89]. In comparison to its PEDOT:PSS equivalent, the CuO_x-based device displayed a PCE of 17.1%, a high J_{sc} of 23.2 mA/cm^2, minimal hys- teresis, and superior air stability [89]. Yu et al. used the spin-coating process to create CuO_x as HTM and ZnO as ETM in order to produce efficient and stable PSCs [90]. The PCE for the inverted planar PSC

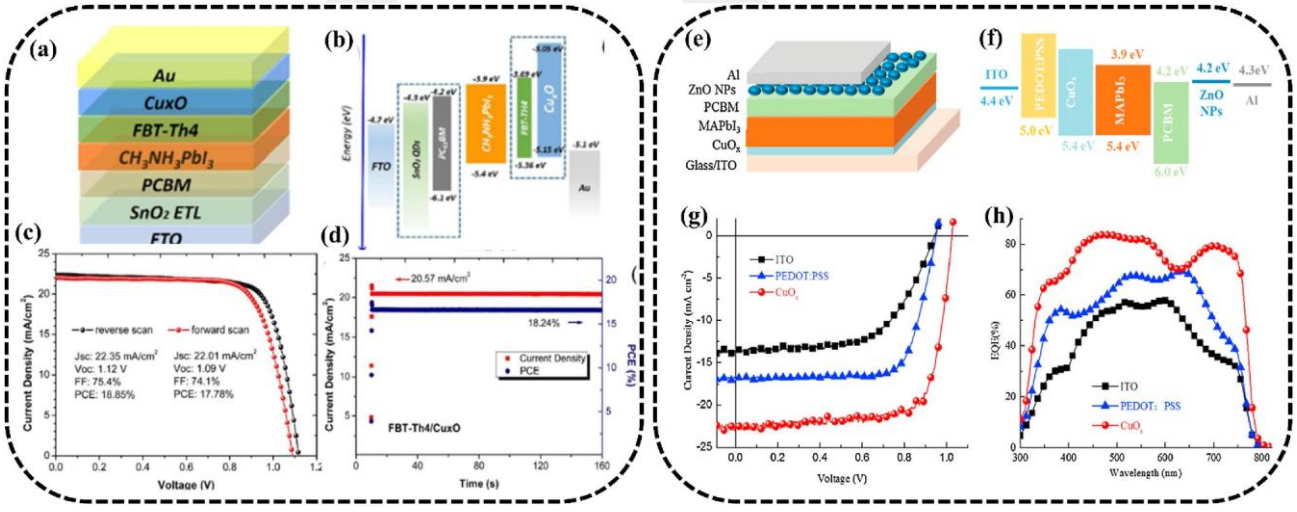

Fig. 8. (a), (b) Schematics of the corresponding device accompanied by energy levels diagram; (c) The J-V characteristics of the champion devices while using FBT-Th4/Cu_xO and spiro-OMeTAD; (d) stabilized PCEs for the top-performing FBT-Th4/Cu_xO-based PSC at a maximum power point. Reproduced with permission from the study by Guo et al. [85]. Copyright 2012, Royal Society of Chemistry; (e, f) schematics of the corresponding PSC using CuO_x-HTM accompanied by energy levels diagram; (g) J-V characteristic curves; (h) external quantum efficiencies of PSCs using CuO_x or PEDOT:PSS as HTMs. Reproduced with

permission from the study by Yu et al. [90]. Copyright 2017, Elsevier B.V. HTM, hole transport material; PCE, power conversion efficiency; PSC, perovskite solar cell; spiro-OMeTAD, 2,2′,7,7′-tetrakis[N,N-di(4-methoxyphenyl)amino]-9,9′-spirobifluorene.

with CuO_x-HTM was 17.43% (Figs. 8eeh), and kept 90% of its orig- inal efficiency, while the PEDOT:PSS-based device lost about 70% of it. The improved J_{sc} was attributed to the efficient hole transport/ extraction by CuO_x-HTM. Moreover, the CuO_x-HTM promoted the formation of large-grains perovskites, which led to decreased grain boundaries and suppression of recombination loss. The perfor- mance of the device can be correlated using impedance spectros- copy and capacitance-frequency measurement to examine the charge accumulation at perovskite/HTMs interfaces. In order to study the charge accumulation behaviors, Galatopoulos et al. [91] constructed the inverted planar PSCs using three representative HTMs, including PEDOT:PSS, Cu:NiO_x, and CuO. Due to the efficient hole extraction, it was demonstrated that reduced charge accu- mulation for Cu:NiO_x and CuO-based PSCs promoted the J_{sc}. Moreover, it should be highlighted that perovskite, which was coated on CuO-HTM has the highest grain size, measuring around 625 nm, and fewer grain boundaries. In terms of decreased inter- face capacitance and enhanced recombination resistance, the smaller grain boundaries resulted in less charge accumulation/ recombination [91]. Rao et al. optimized the quality of the perov- skite film [92] on ultrathin CuO_x film of 5 nm by solution method for the inverted planar PSC and obtained one of the highest PCEs of 19.0% among inorganic-HTM-based PSCs. The device's impressive V_{oc} of 1.11 V was mostly attributable to the improved perovskite morphology brought on by Cl-doping. In comparison to the $MAPbI_3$ perovskite, the $MAPbI_{3-x}Cl_x$ perovskite produced through rapid deposition crystallization exhibited larger grain size and fewer intrinsic defects. Impedance spectroscopy demonstrated that the $MAPbI_{3-x}Cl_x$-based device had stronger recombination resistance than its $MAPbI_3$-based equivalent, which improved V_{oc} and FF.

Given the low throughput and limited size of the spin-coating process, the commercialization of the solution-processed PSCs is hampered. As a result, Bu et al. [93] used electrospray deposition to create the perovskite layer and the CuO_x-HTM beneath it, which can aid in the production of PSCs on an industrial scale. Due to the optimized 48 nm thick CuO_x film and sufficient substrate coverage, the PSC showed a PCE of 5.83%. On the ITO substrate, the electrospray-deposited CuO_x film, though, found it challenging to create a compact layer, which led to substantial shunting loss and inferior FF. Liu et al. [94] also formed Cu_2O-HTM for the inverted planar PSC through electrodeposition. It was revealed that Cu_2O crystallization aided by the growth of Cu_2O particles on the ITO substrate. The Cu_2O-based PSC displayed an optimum PCE of 9.64% with the controlled particle size by the deposition time. However, the direct contact between perovskite and ITO considerably decreased the V_{oc}, FF, and the resulting device performance due to the randomly scattered Cu_2O particle rather than the compact layer. The low carrier extraction capability within the PSCs causes a se- vere loss in V_{oc} and FF, which is a bottleneck for the development of PSCs and integrated perovskite/organic bulk

heterojunction solar cells (IPSCs). Therefore, the incorporation of CuO_x and black phos- phorous quantum dots into IPSCs was used by Shi et al. [95], and successfully extended the single-component PSCs light response to 930 nm while also dramatically lowered the V_{oc} and FF loss of the devices. The electron/hole transport behaviors of perovskite and bulk heterojunction films were improved by black phosphorous quantum dots with bipolar charge transport and strong mobility properties. The introduction of CuO_x layer between bulk hetero- junction and spiro-OMeTAD produced a good driving force for the transportation of holes and had matching energy levels. The PCE for the best device was 23.52%. Moreover, the IPSCs exhibited excep- tional long-term stability.

3.3. *Cobalt oxide*

Cobalt oxide (CoO_x) is another potential HTM due to its favor- able energy levels alignment with perovskites and efficient hole extraction. Inverted planar PSC with CoO_x-HTM showed higher PCE of 14.5% than that of PSCs based on PEDOT:PSS (PCE ¼ 12.2%), NiO_x (PCE ¼ 10.2%), and CuO_x (PCE ¼ 9.4%) [96]. Here cobalt acetate tetrahydrate precursor was spin-coated on top of the ITO substrate to create an ultrathin CoO_x film, which displayed exceptional transparency for the visible spectrum. Furthermore, when the CoO_x layer displayed complete substrate coverage and the appropriate roughness, the formation of smooth and well-packed perovskite films as well as reduced charge-carrier recombination were made possible. However, the solution procedure for fabricating CoO_x is time-consuming and necessitates high temperature treatment. For instance, preparing the CoO_x precursor requires 3 days and fabri- cating the CoO_x thin film requires more than 3 h. Concerns about the energy usage arose from the high annealing temperature of more than 400 °*C*. To properly cover the substrate with a Cu-doped CoO_x film, Huang et al. [97] reported employing a quick and affordable method known as direct current magnetron sputtering in order to shorten processing time and temperature. The trans- parency of the as-prepared CoO_x film was high. It was found that the replacement of Co ion by copper improves the carrier mobility and adjusts the energy levels between CoO_x and the perovskite layer. Because of the diminished energy level misalignment and increased carrier mobility, both the loss during carrier transport in CoO_x and the loss from recombination at the CoO_x/perovskite interface were minimized. In comparison to PEDOT:PSS, the Cu- doped CoO_x-based PSC demonstrated a PCE up to 9.98% with bet- ter stability.

Other nanostructures such as Co_3O_4 have also been used in PSCs as alternative HTMs. The Co_3O_4 displayed a typical *Fd3m* space group spinel crystal structure, where the high-spin $Co^{2þ}$ ions and the low-spin $Co^{3þ}$ ions were found in the tetrahedral sites and octahedral sites, respectively. The Co_3O_4-based HTM fabricated by chemically precipitating approach showed reasonable performance improvement of PSCs. For instance, the well-aligned frontier energy levels and efficient hole extraction between Co_3O_4-HTM and perovskite layer

enabled PSC to deliver a higher PCE of 13.27% than that of control device (PCE ¼ 11.25%) [98]. Moreover, the unencapsulated Co_3O_4-based device demonstrated stable PCE for 100 days at 70% relative humidity and 25 °*C*. Lee et al. doped Co_2O_4 with nickel in order to improve the optoelectronic features of the corresponding HTM [99]. The high density of $Ni^{3þ}$ in thin-film (annealed at 340 °*C*) contributed to the increase in hole-mobility because $Ni^{3þ}$ state causes oxygen deficit in $NiCo_2O_4$. High optical transparency, well-matched energy bands, a smooth film morphology, and reasonable electrical conductivity were obtained for the $NiCo_2O_4$ layer produced by the sol-gel method. The solution-processed $NiCo_2O_4$ was capable of producing device efficiency up to 18.16% for the planar PSCs thanks to these excellent characteristics (Figs. 9a and b). Another nanostructure such as $LiCoO_2$ has also been employed in the PSC as HTM. The $LiCoO_2$ is a layered solid-state material comprised of sheets of CoO_6 octahedra that share their edges and layers of lithium. A high-temperature solid state reaction and a solution technique both are methods that can be used to transform lithium and cobalt salts into $LiCoO_2$ powder or crystals. The $LiCoO_2$ films may also be made from $LiCoO_2$ target material using magnetron sputtering to produce a thin film that is compact, highly pure, and has no restrictions on the target or substrate. With minimal current hysteresis, PSC with sputtered-$LiCoO_2$ HTM in this scenario produced a PCE of 19% (Figs. 9c and d) [25]. Without encapsulation, the device demonstrated great stability at 90 °*C* in an inert atmosphere, and the PCE only dropped by 2% even after the cell was heated to 100 ° *C* for 30 min. Nevertheless, under the same heating conditions, efficiency of the PSC based on PEDOT:PSS completely lost.

3.4. *Molybdenum oxide*

Given its ambient stability, affordability, and low toxicity, molybdenum oxide (MoO_x) is one of the potential HTMs in photovoltaics. Nevertheless, due to its misaligned energy level, particularly at the $MAPbI_3/MoO_x$ interface, barely a few reports about the MoO_x-HTMs in PSCs are published. More often, the MoO_x is used as a dopant in PEDOT:PSS to improve perovskite layer formation with more uniform coverage or as an interfacial layer between ITO and PEDOT:PSS to improve hole-mobility. In order to fabricate PSCs with MoO_x/N,N-di(1-naphthyl)-N,N-diphenyl-(1,1-biphenyl)-4,4-diamine (NPB) as a hybrid HTM, Kim et al. employed the vacuum deposition process [100]. The PSC with MoO_x/NPB showed remarkable reproducibility, a PCE of 13.7%, and a V_{oc} of 1.12 V. The advantageous band alignment between perovskite and MoO_x/NPB-HTM was credited for the increased V_{oc}. The MoO_x-doped-PEDOT:PSS showed crystal nucleation sites for MoO_x nano-spots that aided in the crystallization of perovskite [101]. The PEDOT:PSS-MoO_x-based PSCs displayed better PCE than that of the PEDOT:PSS-based devices because of superior hole transportation and perovskite crystallinity.

Modifying the charge collection and recombination pathway is also made possible by interface engineering on the corresponding electrodes. For instance, solution-processed MoO_x and titanium (IV) oxide bis(2,4-pentanedionate) as interfacial modifiers decreased the charge transfer resistance (Fig. 10), resulted in an improved PCE from 11.2% to 16.04% in inverted PSCs [102]. In order to replace noble metals like Ag and Au in regular planar PSCs, Zhao et al. employed MoO_x/Al as a hole extraction layer coated on spiro-OMeTAD [103]. The performance of the best device with an Al electrode attained a PCE of 11.4% with an optimal thickness of MoO_x (10 nm), only under that of the control device (Ag electrode), which had a PCE of 12.36%. Further research revealed that the holes extraction and J_{sc} of the device can be improved by MoO_3 nano- particles spread between the perovskite layer and HTM. For example, PCE of 18.27% and J_{sc} of 23.67 mA/cm^2 were obtained with optimum content (0.5 mg/ml) of the MoO_3 compared to 16.97% with a J_{sc} of 21.84 mA/cm^2 for the controlled device [104]. These findings suggest the potential ways to boost the performance of MoO_x-based PSCs even more.

3.5. *Vanadium oxide*

Due to its desirable energy levels, high hole-mobility, simple solution-processing, wide bandgap, and high transmittance, vana- dium oxide (VO_x) is another promising HTM. In the inverted planar PSC with a structure of ITO/VO_x/perovskite/PCBM/Al, Sun et al. documented the very first application of VO_x as HTM [105]. The author achieved a homogeneous, pinhole-free surface by depos- iting VO_x on an ITO substrate using a low-temperature solution process approach. Given the outstanding transmittance and quenching capabilities of VO_x, PSC with VO_x-HTM displayed a PCE of 14.23% with minimal hysteresis [105]. The solution-processed VO_x on ITO substrate with the deposition of aminopropanol acid as interfacial modifier resulted in low charge-carrier recombination [106], as displayed by transient photovoltage measurements. As a result, the PCE of 19.57% was obtained in the VO_x-based inverted planar PSC. The photovoltage and PCE of printable PSCs were enhanced by Li et al. [107] using a simple post-treatment method for the deposition of VO_x at the carbon/perovskite interface (Fig. 11a). Due to advantageous energy level alignment, VO_x can facilitate the charge transfer from perovskite to carbon because it has a high work function of 5.39 eV. The V_{oc} increased from 0.892 to 0.922 V as a result and produced a champion PCE of 15.77% with barely detectable hysteresis.

In order to alter the PEDOT:PSS, Peng et al. [108] used V_2O_x as an interface modifier in inverted planar PSCs. The device with hybrid V_2O_x/PEDOT:PSS layer showed improved PCE from 14.8% to 17.5%. With negligible change in TRPL compared to the PEDOT:PSS equivalent, it was noticed that such improvement might not credit to the charge quenching ability of the V_2O_x/PEDOT:PSS, but rather come from less charge-carrier recombination at the inter- face of V_2O_x/perovskite. As a hybrid HTM for regular mp-PSCs, Cheng et al. used solution-processed nickel phthalocyanine (NiPc) and V_2O_5 to substitute spiro-OMeTAD [27]. The spin-coated V_2O_5 film and afterward annealed at 120 $^\circ C$ for 10 min resulted in

full coverage on perovskite layer. In comparison to the controlled PSC, the deposition of V_2O_5 on NiPc improved the ability for

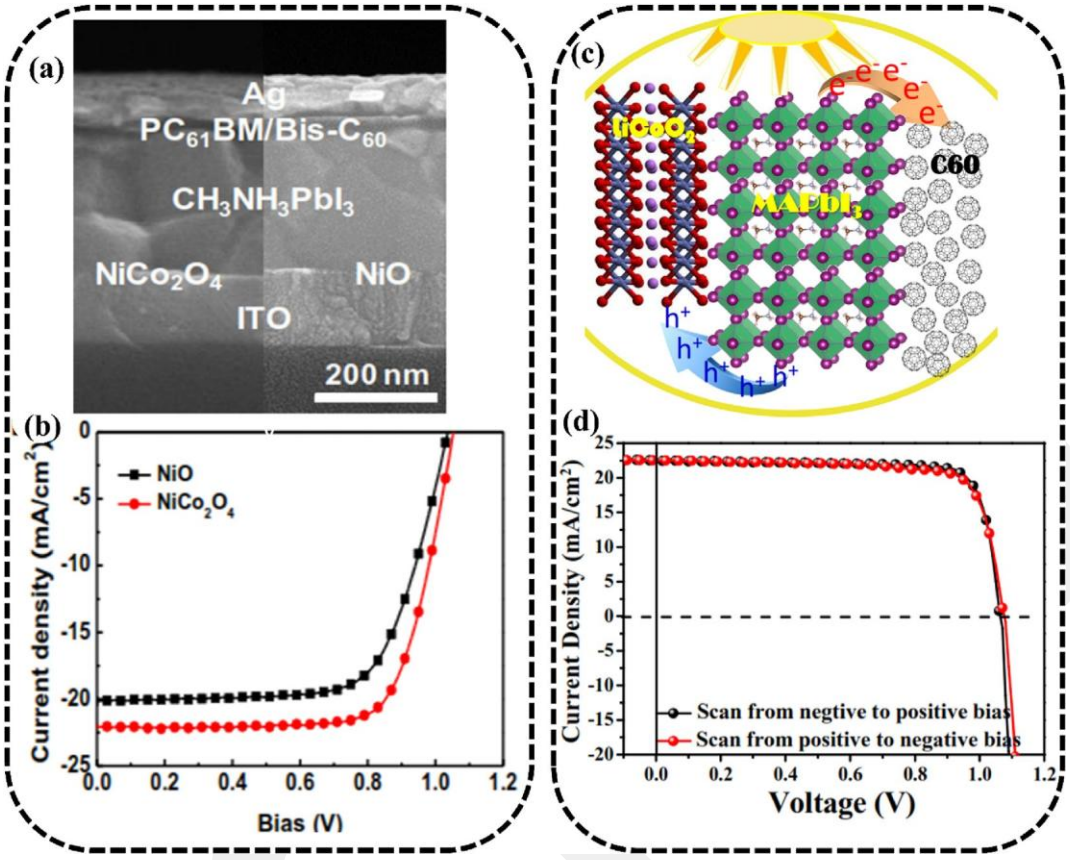

Fig. 9. (a, b) Cross-sectional SEM image and J-V characteristic curves of inverted planar PSCs using $NiCo_2O_4$ and NiO_x as HTMs. Reproduced with permission from the study by Lee et al. [99]. Copyright 2019, Royal Society of Chemistry. (c) Schematic of the charge-carrier extraction within the $LiCoO_2$-based PSC; (d) the resulted J-V characteristic curves of the $LiCoO_2$-based PSCs. Reproduced with permission [25]. Copyright 2018, Royal Society of Chemistry. HTM, hole transport material; PSC, perovskite solar cell; SEM, scanning electron microscopy.

charge extraction, increasing the PCE from 10.6% to 18.3%. The use of a MoO_x interlayer, which was initially added to boost opera- tional stability, was implicated in interfacial degradation mecha- nism, according to Schloemer et al. [109]. The HTM/MoO_x interface, as stated by the author, buckles under illumination at 70 $^{\circ}C$, which causes delamination and quick J_{sc} losses, with an average t80 of 55 h. By carefully comparing different HTM, in- terlayers, and contacts, the finding revealed that, regardless of the other parts of the device, simply switching out the MoO_x inter- layer for a VO_x interlayer significantly improved PSC operational stability by resolving the buckling problem. Under continual illumination and bias, unencapsulated VO_x-based devices aged in an ambient environment retain, on average, 71% of their initial PCEs (Fig. 11b).

3.6. *Chromium oxide*

The hole collection within PSC can be improved by chromium oxide (CrO_x) as HTM. By producing flexible PSCs using a configu- ration of PET/PEDOT:PSS/$MAPbI_{3-x}Cl_x$/PTCDI or PCBM/Cr_2O_3/Cr, Au, Cu, or Al, Kaltenbrunner et al. investigated these metal protective layers [110]. The author added a Cr_2O_3/Cr interlayer that successfully shields the metal top contacts from interactions with the perovskite to enable air-stable operation. Under AM1.5 irradiation, flexible PSC using an ultrathin Cr_2O_3/Cr layer produced stabilized PCE of 12% and a power-per-weight of 23 W/g, which at the time set a record for photovoltaics. It is widely speculated that since the energy level of pristine CrO_x does not match that of perovskite, it is still an undesirable option for HTM. The CB and VB of CrO_x are at 4.03 eV and 7.78 eV, respectively, which contrasts with the energy levels of perovskite, whose CB and VB are at 3.9 eV and 5.4 eV. Extrinsic doping can be used to solve the energy level issue. For instance, Cu-doping was developed by Qin et al., and the energy level of CrO_x was tuned [111]. The CrO_x and Cu:CrO_{x-1} films displayed the bandgap of 3.72 and 3.70 eV, respectively. The pris- tine CrOx film had a VB of —7.78 eV and a CB of —4.03 eV, while Cu:CrO_{x-1} showed a CB of —5.08 eV, which is closer to that of perovskite. In contrast to CrO_x-based PSC (9.27%), a Cu:CrO_{x-1}- based device displayed a higher PCE of 10.99%. Moreover, the Cu:CrO_{x-1}-based device demonstrated a 60% increase in stability over a control device after a 150 h storage period in air with 25% humidity. The suppressed $Cr^{6þ}$ oxidation state, which causes a redox reaction with the perovskite product, was believed to have been accountable for the stability.

Similarly, $NiCrO_3$ films have been employed by Zheng et al. [112] as HTMs in PSCs. The homogeneous and pinhole-free $NiCrO_3$-HTMs exhibited greater electrical conductivity and a deeper VB than the most common NiO_x-HTMs, ensuring optimum hole transport and energy level alignment. A better PCE of 19.93% was obtained by the PSC with $NiCrO_3$-HTM than by NiO_x-based device (18.35%) as a result of these advantages. Salehi-Abar et al. [113] added Cr_2O_3 to MWCNT, and the results showed superior morphological properties and better energy level alignment, which made it easier to collect holes. Moreover, the PCE was increased from 12.22% (bare Cr_2O_3) to 16.29% (MWCNT/Cr_2O_3 nanocomposite) and the hysteresis and interfacial recombination of charges were decreased. These studies

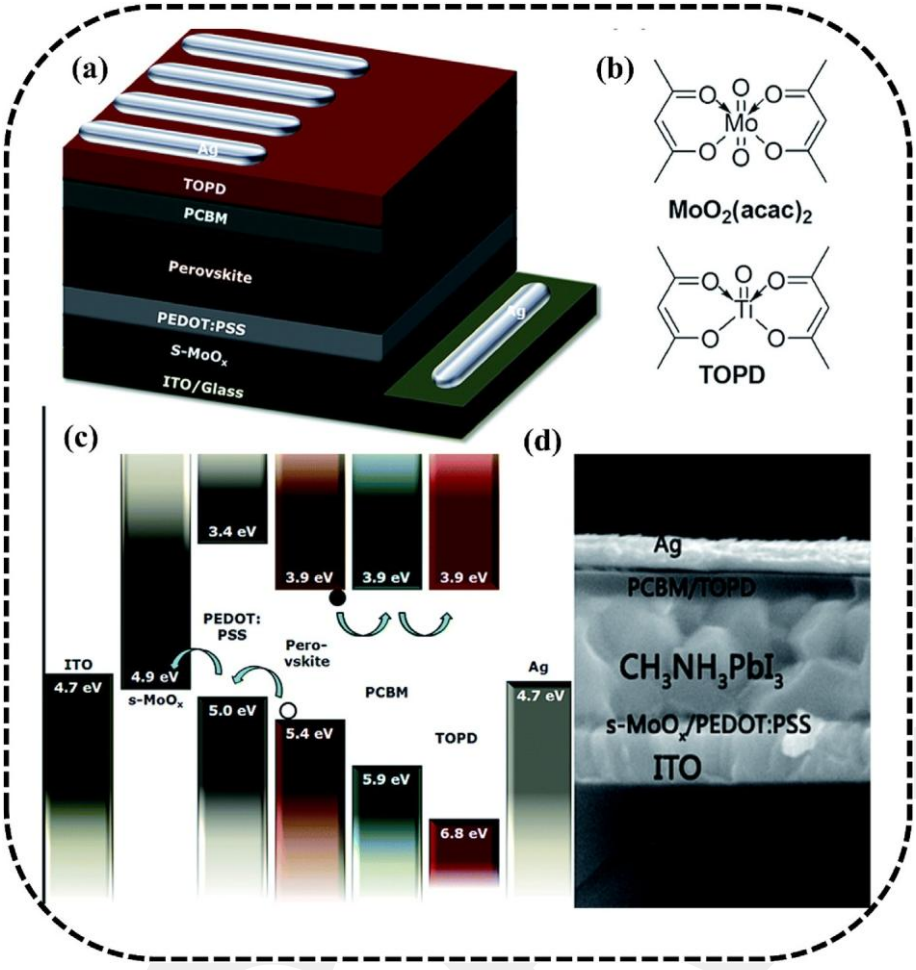

Fig. 10. (a) Device's schematic layout; (b) $MoO_2(acac)_2$ and titanium(IV) oxide bis(2,4-pentanedionate) (TOPD) molecular structures; (c) schematics energy band diagram of the corresponding materials; (d) Cross-sectional SEM of the device. Reproduced with permission from the study by Zhang et al. [102]. Copyright 2017, Royal Society of Chemistry. SEM, scanning electron microscopy.

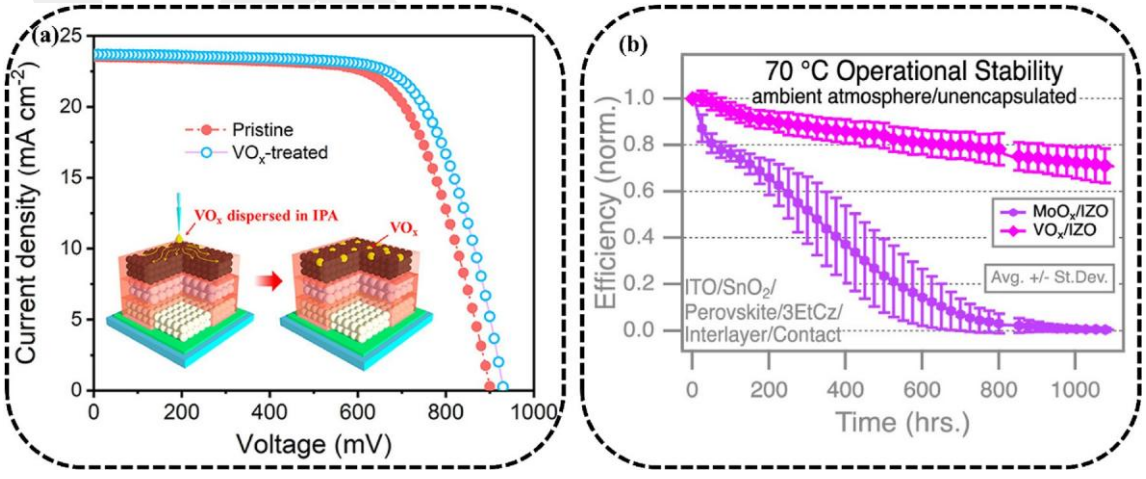

Fig. 11. (a) J-V characteristic curves of control and VO_x-treated PSCs (inset is the schematic of VO_x-based device design). Reproduce with permission from the study by Li et al. [107]. Copyright 2019, American

Chemical Society; (b) PCEs for unsealed PSCs tested at 70 ° *C* with constant load, continuous illumination, and exposure to ambient air. Reproduced with permission from the study by Schloemer et al. [109]. Copyright 2020, American Chemical Society. PCE, power conversion efficiency; PSC, perovskite solar cell.

emphasize that CrO_x improves hole transport and prevents hole accumulation in PSCs. However, more study is required to promote the methods of fabricating extremely efficient and robust PSCs in order to fully realize the capabilities of CrO_x-HTMs.

3.7. Other metal oxides

Due to their decent hole-mobility and desirable energy levels, $CuAlO_2$, $CuCrO_2$, and CuGaO metal oxides have also been used in PSCs as HTMs. According to reports [114], p-type $CuAlO_2$ has good optical transparency, excellent thermal, chemical, and environ- mental stability, and it comprises non-toxic, affordable, and abun- dant components. The $CuAlO_2$ was used by Igbari et al. [115] as the hole-selective buffer layer between the ITO electrode and PEDOT:PSS in inverted planar PSCs. Using the direct current magnetron sputtering method, thin films of $CuAlO_2$ were produced from a pre-fabricated polycrystalline $CuAlO_2$ ceramic target. The optimized device produced a J_{sc} of 21.98 mA/cm^2, a V_{oc} of 0.88 V, a FF of 75%, and a PCE of 14.52%. The $CuCrO_2$ is a good choice for enhancing the performance of PSCs due to its wide bandgap (2.9e3.1 eV), acceptable VB (5.3 eV), excellent carrier mobility (0.1e1 cm^2/V/s), and UV-light stability [29]. For example, $CuCrO_2$ spin-coated atop of the perovskite layer in a regular PSC, yielded in a PCE of 16.7%, and maintained roughly 88% of its initial PCE after 500 h under continuous illumination in a N_2 environment at ambient temperature [116]. Furthermore, inverted planar PSC with $CuCrO_2$-HTM produced a PCE of 19% [117], demonstrated UV light blocking and effective hole transport, and kept roughly 95% of its initial efficiency after 1000 h of constant 1-sun illumination in argon environment (Figs. 12aed). Similarly, Qin et al. developed PSC using $CuCrO_2$-based HTM, demonstrated 17.19% efficiency on rigid substrate and 15.53% efficiency on flexible substrate [118]. By promoting the crystallinity, grain size, and surface morphology of the absorber layer, the inserted $CuCrO_2$, served an important role in improving the performance of the cells. Further reports showed that $CuCrO_2$ nanoparticles can be used in PSCs, but difficult con- version from nanoparticles to uniform thin-films and their lengthy reaction times (50e60 h) at high temperatures during hydrother- mal synthesis need to be addressed. Wang et al. [119] reported a straightforward, inexpensive, and highly reproducible technique for the spray pyrolysis deposition of Cu-deficient $CuCrO_2$ films. In comparison to the extensively investigated NiO_x, the resultant $CuCrO_2$ films showed advantages in terms of transparency, rough- ness, and electrical characteristics. In comparison to NiO_x-based PSCs, the optimized $CuCrO_2$-based device delivered a high PCE of 18.86%.

The $CuGaO_2$, which has an appropriate bandgap of 3.6 eV, a VB of 5.3 eV, and hole-mobility of 10^{-2}-10^{-1} cm^2/V/s, is another promising candidate within the metal oxide group. In addition, compared to spiro-OMeTAD, $CuGaO_2$ exhibits adequate thermal

and environmental stability. Compared to the spiro-OMeTAD- based PSCs, $CuGaO_2$ spin-coated on top of the perovskite layer in a regular planar; PSC produced a PCE of 18.5% and preserved over 90% of its initial PCE following storage in ambient atmosphere at 25 $^{\circ}C$ and 30e55% relative humidity for 30 days without sealing [30].

The PCE of a mesoporous $CuGaO_2$ coated on top of NiO_x was 20%, which was higher than that of a planar device (16.7%) [120], and it retained more than 80% of its initial PCE after 1000 h in a N_2 atmosphere at 85 $^{\circ}C$ for unencapsulated devices. Another relatively affordable, thermally stable, and photostable metal oxide is $CuFeO_2$. Compared to PSCs based on spiro-OMeTAD, devices with $CuFeO_2$ exhibit adequate thermal, moisture, and photostability [31]. As demonstrated in Figs. 12eeg, unencapsulated PSCs with $CuFeO_2$ maintained roughly 85% of their initial PCE for over 1000 h, but spiro-OMeTAD devices decreased to 10%. According to thermal and humidity stability testing, $CuFeO_2$-based devices maintained over 90% of their initial PCE after 300 h of exposure to 85% relative humidity and 70 $^{\circ}C$, respectively. These primarily results demonstrate that highly efficient, photostable, moisture tolerant, and

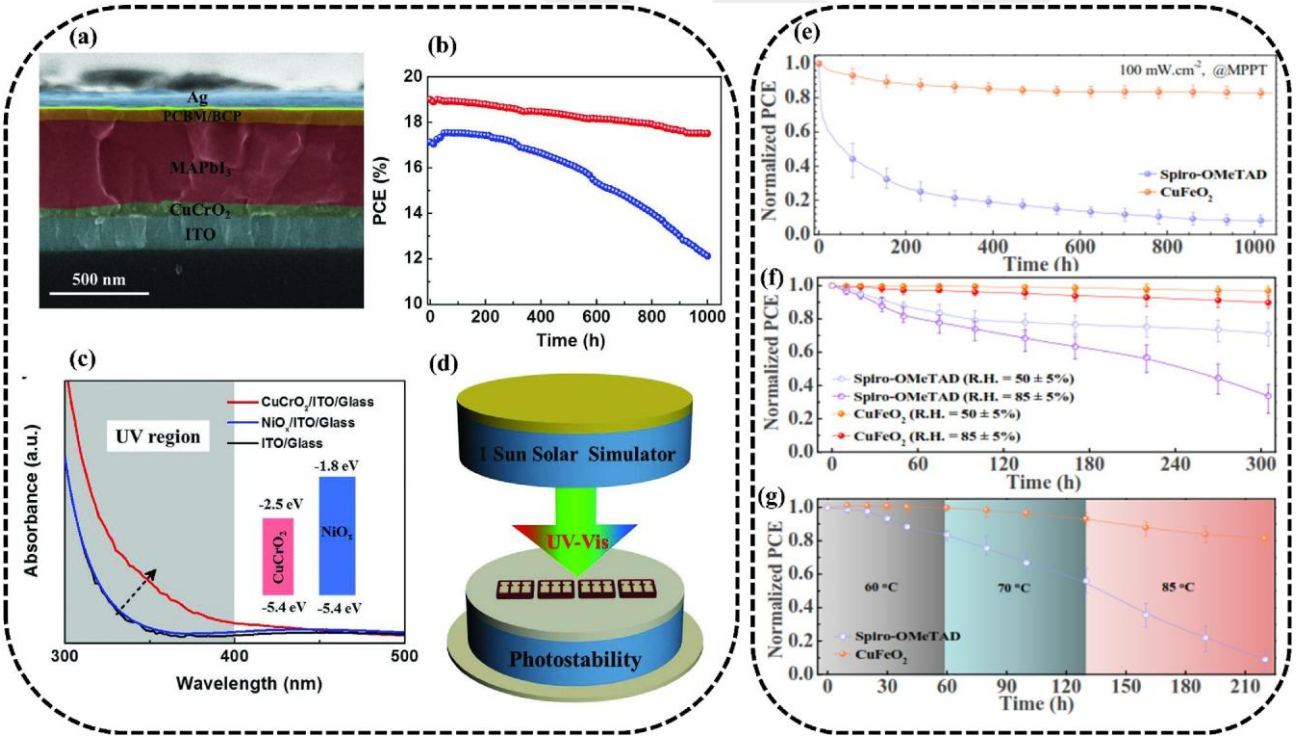

Fig. 12. (a) Cross-sectional SEM of the $CuCrO_2$-based PSC; (b) stability analysis of the PSCs with $CuCrO_2$ or NiO_x as HTMs; (c) $CuCrO_2$ and NiO_x layer UVevis spectra, inset is the energy level of each layer corresponding optical bandgap; (d) the photostability investigation set up with both of the unsealed devices exposed to UV light from a xenon lamp under 1-sun illumination. Reproduced with permission from the

study by Zhang et al. [117]. Copyright 2018, WILEY-VCH Verlag GmbH & Co. KGaA, Weinheim. Stability analyses of the PSCs with $CuFeO_2$ or spiro-OMeTAD as HTMs; (e) PCEs at maximum power point tracking; (f) PCEs under different relative humidity conditions; (g) PCEs under different temperature conditions. Reproduced with permission from the study by Akin et al. [31]. Copyright 2019, American Chemical Society. HTM, hole transport material; PCE, power conversion efficiency; PSC, perovskite solar cell; SEM, scanning electron microscopy; spiro-OMeTAD, 2,2′,7,7′-tetrakis[N,N-di(4-methoxyphenyl)amino]-9,9′-spirobifluorene; UV, ultraviolet.

thermally stable PSCs can be further developed with metal oxides HTMs. A summary of the available data on the performance of PSCs based on metal oxide HTMs is shown in Table 2.

By using metal oxides-based inorganic HTMs, which improved the photovoltaic performances of inverted and regular PSCs, it has been demonstrated that the improvements in built-in voltage, hole collection ability, and minimized charge recombination are further possible. Instead of the traditional organic HTMs, many efficient, inexpensive, and simple to process inorganic HTMs such as NiO_x, Cu_2O, CuO_x, MoO_x, VO_x, CrO_x, $CuCrO_2$, $CuGaO_2$, and $CuFeO_2$ were employed. These materials have some beneficial qualities as well as some disadvantages. Due to its desirable bandgap, effective hole collection, low electrode polarization, high photo- and thermal stability, and significant potential for low-temperature with large- scale production, for instance, the most favorable inorganic HTM is NiO_x. Nevertheless, the photovoltaic performances were

$(I_{0.85}Br_{0.15})_3$	n-i-p (planar)	1.01	23.6	65.0	15.6

[31hampered by the poor intrinsic conductivity and mismatched Fermi level of NiO_x in comparison to the perovskite layer. A number of methods, including oxygen plasma treatment, extrinsic doping, and modifying the surface, were developed to address the aforementioned problems. Among these, the PSCs for the surface- modified NiO_x with urea revealed PCEs greater than 23% whereas the PSCs for the Cu-doped NiO_x HTMs gave PCEs up to 20.5%.

4. Metal cyanates, phthalocyanines, and halide

4.1. *Metal thiocyanate*

A molecular copper single-ion pseudohalide is known as copper thiocyanate (CuSCN). The CuSCN has been extensively used in PSCs since it has shown the most positive outcomes as an inorganic HTM. The suitable work function and the high hole-mobility (10^{-2} to 10^{-1} $cm^2/V/s$) of the CuSCN facilitate the charge-carriers transport and ensure effective carrier transfer [124]. The CuSCN was used as HTM for the first time by ITO et al. in 2014 via integrating it into regular mesoscopic PSCs by the doctor-blading method [125]. As anticipated, the high hole-mobility and desirable energy levels enhanced the transportation and separation of charge-

carriers in comparison to CuSCN-free PSCs. The PSC using CuSCN yielded a PCE of 4.8%, with the sequential coating method further optimizing the perovskite layer [126]. Regular planar PSCs with CuSCN-HTMs were first fabricated by Chavhan et al. [127]. The CuSCN-based planar PSCs delivered J_{sc} of 14.4 mA/cm^2, V_{oc} of 0.72 V, FF of 62%, and PCE of 6.4%. The poor performance of the CuSCN-based device was attributed to the inadequate covering of perovskite layer on top of the substrate. Furthermore, the smooth surface formed by the deposition of a perovskite layer and subsequent dripping of MAI solution on it allowed the CuSCN-based planar PSC to deliver a PCE of 7.19% [124]. The approach, however, only partially resolved the

CuSCN film penetration issue. Similar to this, Sepalage et al. re- ported a strategy using a protective solvent to lessen CuSCN penetration [128]. Between the perovskite and doctor-bladed CuSCN layers, a few drops of chlorobenzene were used to create a protective solvent layer. The as-prepared CuSCN-HTM enabled PSC with a PCE of 9.6%.

Since the uniform perovskite surface effectively decreased direct contacts between the charge transport materials, which may have limited short-circuiting contact, slowing down the rapid crystalli- zation of perovskites and enlarging its grains through two-step sequential method typically results in a uniform film with grain size of 1 m m. Regarding this, Qin et al. reported that, mp-PSC with CuSCN as HTM exhibited a J_{sc} of 19.7 mA/cm^2, a V_{oc} of 1.01 V, an FF of 62%, and a PCE of 12.4% [129]. Similar to the modification of the perovskite layer, the CuSCN homogeneity with a suitable thickness is crucial. Snaith et al. used the spray-coated method to fabricate CuSCN with a controllable and uniform thickness, delivered a PCE of 13.3% in regular mp-PSCs [130]. After 1000 h of thermal stressing

at 85 $^{\circ}C$ in an ambient atmosphere, the PCE of CuSCN-based PSC

with encapsulation maintained 77% of its initial value. In order to make thermally stable PSCs, Jung et al. developed a CuSCN-based PSC with a mixed-cation/anion perovskite (Figs. 13aec) and ob- tained a PCE of 18% [131]. Arora et al. used the drop-casting tech- nique to produce very compact and highly conformal CuSCN layer on top of perovskite layer [132]. The authors also added a layer of reduced graphene oxide as a separator between the CuSCN and Au electrode in order to prevent an electrical potential-induced interaction between the gold and the thiocyanate anions that would have resulted in the formation of an undesirable barrier. With a J_{sc} of 23.2 mA/cm^2, a V_{oc} of 1.11 V, a FF of 78%, and a PCE of 20.4%, the PSCs displayed remarkable performance. Often, the diethyl sulfide (DES)-dissolved CuSCN is spin-coated onto the perovskite layer followed by post-annealing to obtain dense and

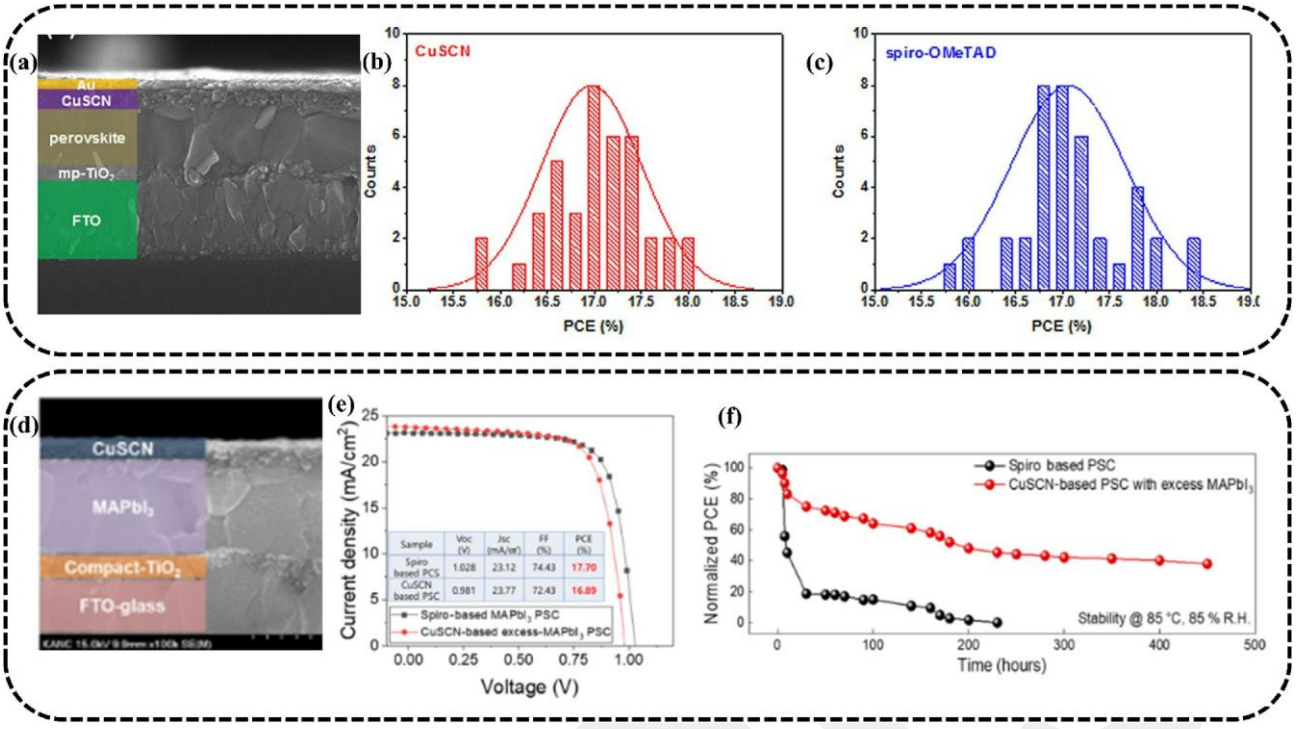

Fig. 13. (a) SEM image and (b, c) statistical data of the regular mesoporous PSCs with CuSCN or spiro-OMeTAD as HTMs. Reproduced with permission from the study by Jung et al. [131]. Copyright 2016, WILEY-VCH Verlag GmbH & Co. KGaA, Weinheim. (d) SEM image, (e) J-V characteristic curves, and (f) long-term stability of the regular planar PSCs with CuSCN or spiro-OMeTAD as HTMs. Reproduced with permission from the study by Kim et al. [133]. Copyright 2022, American Chemical Society. HTM, hole transport layer; SEM, scanning electron microscopy; spiro-OMeTAD, 2,2′,7,7′-tetrakis[N,N-di(4-methoxyphenyl)amino]-9,9′-spirobifluorene.

high-quality CuSCN layers. However, prolonged post-annealing at high temperatures has been linked to the unintended dissociation of perovskites. Moreover, the polar solvent DES, which is used as a CuSCN solvent, degrades the surface of perovskites and impairs the interfacial features between the perovskite layer and HTM. In order to overcome this problem, Kim et al. [133] looked into the impact of the molar ratio of methylammonium iodide (MAI) and PbI_2 in the $MAPbI_3$ precursor solution. By employing DES polar solvent for the CuSCN solution, the increased MAI molar ratio in the $MAPbI_3$ pre- cursor solution decreased $MAPbI_3$ surface damage. Moreover, after an appropriate post-annealing step, dissociation of $MAPbI_3$ to PbI_2 was effectively reduced. The MA loss might be made up for by the excess MAI molar ratio in the $MAPbI_3$ precursor, which would also successfully prevent the phase separation of $MAPbI_3$ into MAI and PbI_2 during post-annealing. In CuSCN-based regular planar PSC, the PCE of 17% was attained. The CuSCN-based device likewise demonstrated superior stability over the traditional spiro-OMeTAD

at 85 $^{\circ}C$ and 85% relative humidity (Figs. 13def). Similar to this,

Nideesh et al. used an antisolvent treatment to remove DES residue from CuSCN [134]. With the use of diethyl ether, the antisolvent treatment produced a dense and excellent CuSCN film with enhanced surface

morphology, low-trap density, and high hole extraction capability. As a result, CuSCN-based PSCs treated with diethyl ether showed an increase in PCE from 16.84% to 18.34% while maintaining excellent long-term stability. A combination strategy that uses CuSCN as an HTM and 2D perovskite materials as passivation layers to address the instability of the PSCs that results from the use of spiro-OMeTAD has also been reported. In this re- gard, passivating layers of 2D perovskites such as (phenylethyl) ammonium and [(4-fluorophenyl)ethyl]ammonium cations were found beneficial [135]. The Cs-containing triple cation 3D perovskite layer was covered with these 2D-perovskites layers. The devices delivered efficiencies of up to 19.3% with spiro-OMeTAD and 18% with CuSCN when using passivated 2D-perovskite layers. Moreover, devices with CuSCN and passivated perovskite layers demonstrated improved stability.

The CuSCN was also employed as HTM in the inverted planar PSCs in place of the widely used PEDOT:PSS. The energy loss at the interface between PEDOT:PSS and perovskite may result in a drop in V_{oc} because it is partially governed by the interfaces between perovskites and used charge-transporting interlayers. Compared to PEDOT:PSS, the CuSCN has more effectively tailored energy levels for the perovskites. Moreover, the wide bandgap (Eg 3.6 eV) offers improved transparency across the UVevisenear-infrared spectra, enabling light harvesting materials to capture more light and produce a larger photocurrent in inverted structures. The CuSCN was employed as HTM by Subbiah et al. using the electro- deposition method in the inverted planar PSC, demonstrating a PCE of 3.8% [136]. The CuSCN-based PSCs had poor PV performance since the undesirable thickness of the HTM resulted in a high series resistance and a low shunt resistance. Zhao et al. [137] prepared CuSCN layer through spin-coating before drying out the solvent at a low-temperature of 60 °*C*, as the CuSCN-HTM produced by electrodeposition needed to meet strict standards. When compared to PEDOT:PSS, the CuSCN displayed a VB of 5.3 eV, which more closely matched the VB of perovskite. Compared to the PEDOT:PSS- based counterpart, the CuSCN-based device showed a higher efficiency of 10.8%. The perovskite layer was deposited by Ye et al. using a one-step fast deposition-crystallization method [138]. Compared to the conventional two-step sequential deposition, this deposition process allowed for a reduction in surface roughness and interfacial contact resistance between the perovskite film and selected contacts. Consequently, CuSCN-based device showed a PCE of 16.6% [138]. The CuSCN demonstrated nearly minimal absorption in the UVevisenear infrared spectrum by a simplified deposition process, according to Jung et al. [139], but PEDOT:PSS absorbed light from 350 to 1100 nm. This demonstrated that CuSCN has important potential for usage as HTMs in inverted planar PSCs.

In addition to CuSCN, which has been the subject of the most research, there have only been a few studies on copper seleno- cyanate (CuSeCN) as an effective HTM. The most stable phase of CuSeCN, the 3D phase, was the focus of Wijeyasinghe et al. work [34]. By adding potassium selenocyanate (KSeCN) to a solution of copper ions, they obtained the chemical. They next prepared a solution of CuSeCN in DES. A thin layer (12e16 nm) obtained from

the spin-coated CuSeCN/DES solution showed high transparency after being annealed at 140 °C in a nitrogen environment. The CuSeCN layers were inserted into organic bulk heterojunction solar cells as the HTM. Despite the fact that devices based on PEDOT:PSS showed a slightly higher PCE of 3.6% in comparison to cells con- taining CuSeCN HTMs (3.3%), an increase in the V_{oc} from 0.55 V to 0.57 V was observed, which was primarily attributed to the deeper VB of CuSeCN (—5.1 eV) relative to the work function of PEDOT:PSS(5.0 eV). The mixture solvent of H_2O, ethanolamine (ETA), ethyl- enediamine (EDA), and diethanolamine reported in Zhao et al. [140] work was less volatile and significantly less expensive than the commonly used thioether-based solvents for the solution pro- cessing of CuSCN, which is crucial for practical applications of PSCs. On the thin-film created by spin-coating CuSeCN solution in the mixed solvent of H_2O/ETA/EDA/diethanolamine , a high-quality perovskite film can be generated. With minimal hysteresis and excellent stability, the CuSeCN-based PSC produced PCE of 15.61% at forward scan and 15.97% at reverse scan (Fig. 14).

4.2. *Metal phthalocyanines*

With most of the metals in the periodic table, particularly cop- per and nickel, phthalocyanine produces dye complexes. For instance, the blue dye copper phthalocyanine (CuPc) is used in a variety of industrial coatings, fine art pigments, textile and paper production, and photovoltaics. It has outstanding photoelectric performance and is a typical p-type semiconductor. By using CuPc as HTMs in PSCs, the hole-mobility of CuPc is appropriate for effi- cient hole extraction (10^{-3} to 10^{-2} $cm^2/V/s$, compared to 4 × 10^{-5} $cm^2/V/s$ for spiro-OMeTAD), showing a considerable promise. The CuPc as well as its variants have been employed in regular PSCs that have shown promising PCEs and high stability. For example, when spin-coated on perovskite, copper (II) phthalocyanine with tetra-propyl-substituted function groups (CuPrPc) demonstrated face-on molecular orientation, resulting in enhanced hole mobility and a hydrophobic surface. The CuPrPc was used as the HTM in regular planar PSCs, which showed a maximum PCE of 17.8% [141]. Compared to the spiro- OMeTAD-based devices, the hydrophobic properties of CuPrPc additionally contributed to the devices sta- bility and retained over 94% of their initial PCEs even after 800 h of storage in a humidity of about 75%. Since CuPc is known to have high thermal stability and interfacial bonding capabilities, ther- mally stable PSCs with CuPc can also be fabricated [142]. During more than 1000 h of thermal annealing at 85 °C, the CuPc-based PSCs demonstrated a PCE of 18% and preserved 97% of their initial efficiency. Additionally, the device held up well during 50 cycles of thermal cycling testing (45 to 85 °C). Reports on the use of CuPc in –

inverted PSCs showed satisfactory PCE values (more than 10%) are scarce. Han et al. first used CuPc in inverted planar PSCs by thermal evaporating dopant-free CuPc films onto ITO at ambient tempera- ture [143]. They were able to get PSCs with good reproducibility and homogeneity using this technique, demonstrated highest PCEs of 15.4%. The same group has enhanced the PCE of CuPc-based PSCs to 16.72% in a device using the triple cation perovskite [144]. The improved performance was explained by the fact that C_{60} has better

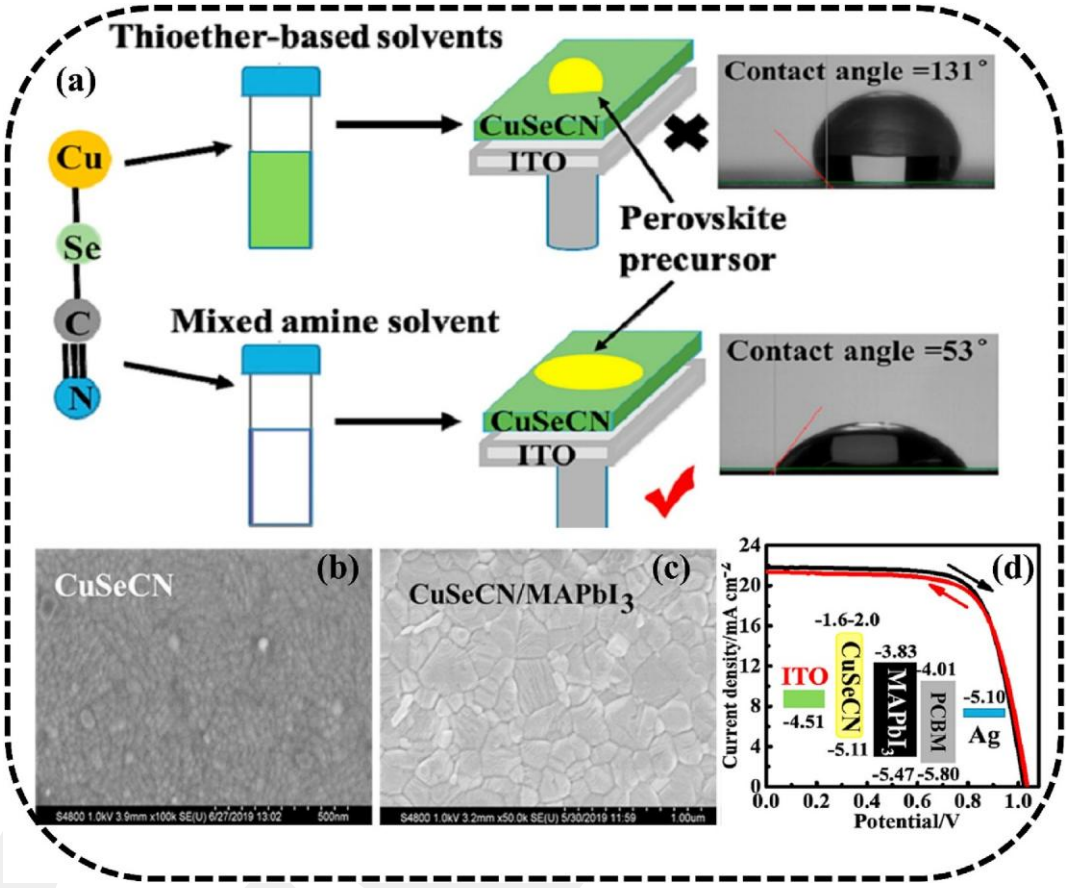

Fig. 14. (a) Schematic illustration and contact angle of the perovskite coated on CuSeCN-HTM; (b, c) SEM images of the CuSeCN thin-film and perovskite coated on CuSeCN thin- film; (d) J-V characteristic curves of the CuSeCN-based PSC accompanied by energy levels diagram of the corresponding materials. Reproduced with permission from the study by Zhao et al. [140]. Copyright 2020, Elsevier B.V. HTM, hole transport material; PSC, perovskite solar cell.

conductivity and electron mobility than phenyl-C61-butyric acid methyl ester (PCBM), which has sped up electron transport and reduced recombination loss. The CuPc derivative Cu- phthalocyanine-tetrasulfonated acid tetra sodium salt (TS-CuPc) exhibits high solubility in polar solvents. In this context, Wang et al. [145] have fabricated composite films of TS-CuPc doped with tet- rafluoro tetracyanoquinodimethane (F4-TCNQ) with increased film conductivity and hole mobility utilizing an aqueous solution method. Inverted planar PSCs made with these films produced ef- ficiencies of 16.14% while simultaneously increasing J_{sc} and

V_{oc} in comparison to the reference PEDOT:PSS device. It is important to note that the undoped TS-CuPc underperformed, generated PCEs lower than 8%, which is a disadvantage given the high cost of the related PSCs.

Nickel phthalocyanine (NiPc) was investigated by Haider et al. [35] as a stable and affordable HTM to take the place of more widely used CuPc and spiro-OMeTAD. The NiPc-based devices out- performed planar devices based on CuPc, delivered a PCE of 12.1% thanks to their high charge-carrier mobility and appropriate energy level alignments. Additionally, the device with NiPc demonstrated significantly greater stability than the one with the standard spiro-OMeTAD. In order to create two non-peripherally octa-alkyl- substituted NiPcs, namely $NiEt_2Pc$ and $NiPr_2Pc$, for usage as dopant-free HTMs in PSCs, structural alteration of NiPc was also presented by Qi et al. [146]. The energy levels of NiPc were dramatically modified by the lengthening of the alkyl chains from ethyl to pro- pyl. This decreased charge-carrier recombination at the perovskite/HTM interface and resulted in the high V_{oc}, J_{sc}, and FF found for the $NiPr_2Pc$-based PSC. Moreover, higher J_{sc} and FF were found for the $NiPr_2Pc$-based device due to higher thin film crystallinity, higher charge-carrier mobility, and lower surface roughness of the $NiPr_2Pc$ HTM in comparison to the $NiEt_2Pc$ one. As a result, the $NiPr_2Pc$- based PSC produced a PCE of 14.07% as compared to 8.63% for the $NiEt_2Pc$-based device. In order to improve the conductivity and hole-mobility in the pristine metal phthalocyanines, Yu et al. [147] produced a NiPc decorated by four methoxyethoxy units as HTMs. In NiPc, the two oxygen atoms in the peripheral substituent have a modified influence on the dipole orientation; however, the central Ni-atom effectively boosted the intramolecular dipole by adding additional electrons to the phthalocyanine ring. According to cal- culations, NiPc's extracted holes were primarily concentrated on the phthalocyanine core where they were caused by the intra-molecular electric field. They were also found to be transmitted by a space channel known as the “stacking space channel” between NiPc molecules. Last but not least, the highest efficiency of PSCs with NiPc as dopant-free HTMs reached a record value of 21.23% (certi- fied 21.03%) [147]. The PSCs also show excellent stability to heat, moisture, and light (Fig. 15).

Furthermore, several other transition metal phthalocyanice-based compounds have been developed as dopant-free HTMs for PSCs, such as tetra-methoxyltriphenylamine substituted zinc phthalocyanine (OTPA-ZnPc). When dimethoxytriphenylamine side chains were added to ZnPc, it had an excellent ability to dissolve in a variety of non-polar solvents, including dichloro- methane, chlorobenzene, and N,N-dimethylformamide [148]. The PSC with OTPA-ZnPc delivered a PCE of 16.23%. In addition, the

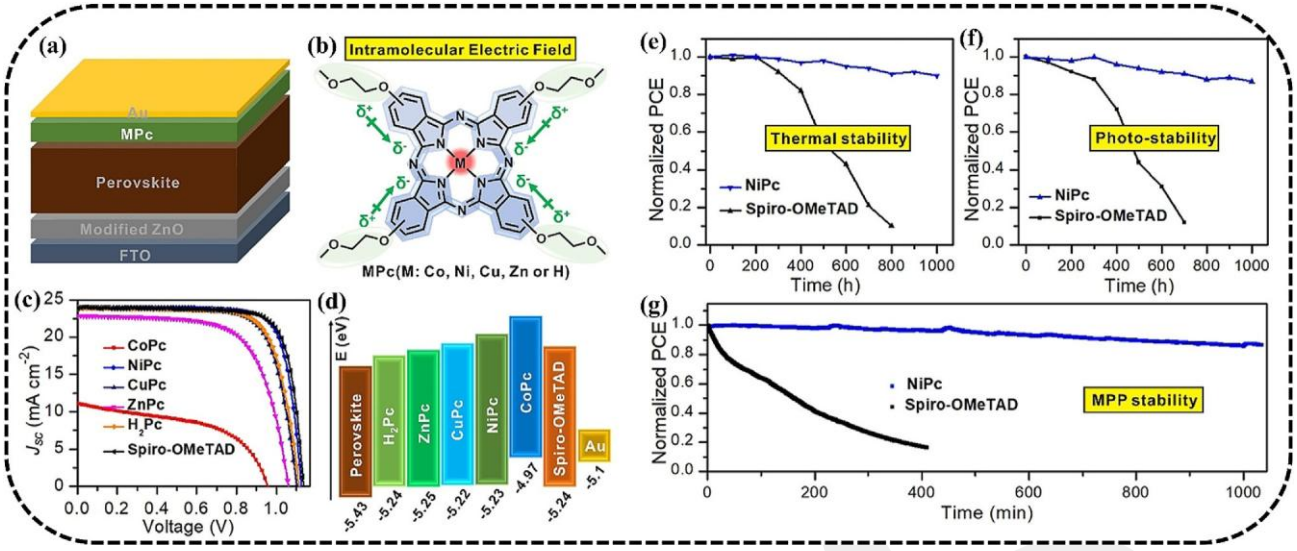

Fig. 15. (a) Scheme illustration of PSCs with metal phthalocyanines (MPcs) as HTMs; (b) MPcs molecular structure and the orientation of the intramolecular electric field; (c) J-V characteristic curves; (d) energy levels of used materials; (eeg) stability analyses of the PSCs using NiPc or spiro-OMeTAD as HTMs. Reproduced with permission from the study by Yu et al. [147]. Copyright 2021, Wiley-VCH GmbH. HTM, hole transport material; PSC, perovskite solar cell.

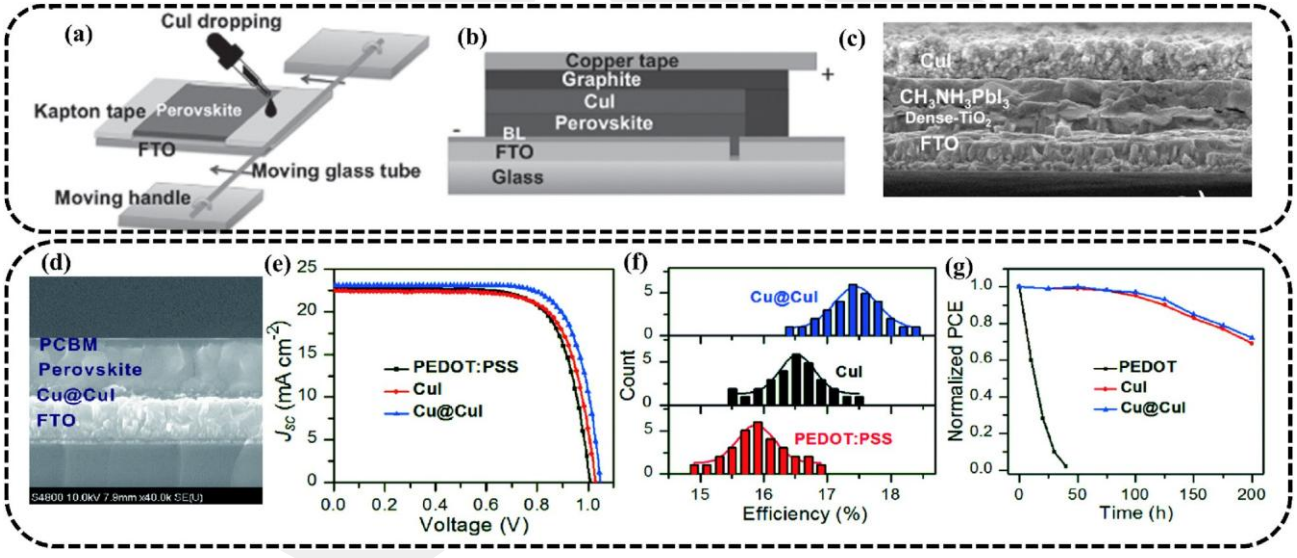

Fig. 16. (a, b) Schematics of the device fabrication and device layout; (c) cross-sectional SEM image of the corresponding device. Reproduced with permission from the study by Sepalage et al. [151]. Copyright 2015, WILEY-VCH Verlag GmbH & Co. KGaA, Weinheim. (d) Cross-sectional SEM image of the Cu@CuI-based PSC; (eeg) J-V characteristic curves, statistical data, and stability of the PSCs using PEDOT:PSS, CuI, and Cu@CuI as HTMs. Reproduced with permission from the study by Cao et

al. [153]. Copyright 2019, Science China Press and Springer-Verlag GmbH Germany. PSC, perovskite solar cell; SEM, scanning electron microscopy.

OTPA-hydrophobic properties of ZnPc allowed the solar cells to maintain around 80% of their initial efficiency even after being exposed to ambient air for 720 h at a humidity level of about 45% without being sealed. Similarly, two tetrapropyl-substituted metal phthalocyanines (PdPrPc and ZnPrPc) were employed as dopant- free HTMs for PSCs. The lowest unoccupied molecular orbital level of the material increased as a result of the substitution of the Pd-atom, but mobility was not considerably reduced. The PdPrPc was predicted to have a longer carrier diffusion length than the ZnPrPc due to spin-orbit interaction. The PCE of the PdPrPc-based device was greater (18.09%) than that of the ZnPrPc-based device due to the higher lowest unoccupied molecular orbital level, longer carrier diffusion length, and lower charge-carrier recombination [149]. Despite the fact that these findings indicate a reasonable improvement in the performance of the PSCs, the presence of

cyanates or phthalocyanines is a serious concern because they have the potential to be poisonous and carcinogenic, which may result in health issues. Moreover, the utilization of unmodified transition metal cyanates and phthalocyanines in solution-processable PSCs is constrained by their poor solubility in the most preferred organic solvents.

4.3. *Metal halide*

In this section, we will only focus on the applications of copper iodide (CuI)-based HTMs due to its broad bandgap (3.1 eV), energy level alignment with perovskite, low extinction coefficient, better hole mobility (40 $cm^2/V/s$), and solution processability. A PCE of 6% was reported in a regular mp-PSC for the first time that used CuI as HTM [150]. A 1.5 m m thick layer of CuI was formed by spin-coating

on top of the perovskite layer. The CuI-based device delivered a lower V_{oc} compared to spiro-OMeTAD. To control CuI layer's thickness and modulate its morphology, Sepalage et al. introduced a rapid doctor-blading method for the deposition of CuI layer on the surface of perovskite layer [151] (Figs. 16aec). Regular planar PSC with CuI-HTM demonstrated a V_{oc} of 0.78 V, a J_{sc} of 16.7 mA/cm^2, and a FF of 55%, led to a PCE of 7.5% [151]. Here, a fast doctor-blading was used to coat the CuI layer in order to prevent the perovskite film from dissolving because the CuI precursor solution contains di- *n*-propylsulfide, which can degrade the perovskite layer. Despite the addition of the graphite layer, the rough surface of the CuI may come into direct contact with the Au electrode and result in a short circuit. The CuI is often utilized in place of PEDOT:PSS in inverted planar PSCs because PEDOT:PSS damages the perovskite layer and lowers the device stability due to its acidic and hygroscopic char- acteristics. In PSCs with inverted design, Chen et al. showed how solution-processed CuI films can be used as HTM and replace the commonly used PEDOT:PSS [152]. An inverted planar PSC displayed a V_{oc} of 1.04 V, a J_{sc} of 21.06 mA/cm^2, a FF of 62%, and a PCE of 13.58%. The CuI-based PSC showed 0.1 eV greater V_{oc} than their PEDOT:PSS counterpart, which was ascribed to well-matched work-function (WF) with perovskite. Over 14 days in an ambient condition, the PSC with CuI-

HTM maintained 90% of its initial PCE while the PEDOT:PSS-based PSCs only retained 27%. The low FF of the CuI-based device, however, was related to their high surface roughness, which was generated on by their large grain size. Furthermore, Saranin et al. [36] used a solution-processed CuI to create a hybrid NiO/CuI HTM in an effort to lower the level of sur- face recombination, improve charge extraction capabilities, and slow down degradation processes. Furthermore, charge transfer was not impeded by the valence band level alignment at perovskite-CuI-NiO junction. The V_{oc} of NiO/CuI HTM increased from 1.02 V to 1.07 V thanks to CuI passivation, which also decreased the series resistance. Ultimately, a best PCE of 15.26% was demonstrated for the NiO/CuI HTM, which represented an improvement of more than 10% over PSCs with NiO HTM and better shelf life as well as light soaking stability. Copper may readily oxidize to CuI when iodide is present. A hybrid nanostructure of CuI coated on Cu can be used to increase the conductivity of the HTM. In this context, Cao et al. [153] pre-deposited a CuI layer on FTO- substrate before depositing copper nanowires on it. Iodide was then used to quickly treat the substrate, producing a Cu@CuI hybrid nanostructure as the HTM for the creation of inverted planar PSCs. The best efficiency of related PSCs attained 18.4% (Figs. 16deg), which was attributed to the efficient charge extraction by the sur- face CuI and the quick transport of the extracted charges to the electrode by the inner Cu [153]. The performance of PSCs using metal cyanates, phthalocyanines, and halide as HTMs is summa- rized in Table 3.

5. Metal chalcogenides

5.1. *Metal sulfides*

Copper sulfide is an inexpensive metal chalcogenide that is often found in the forms of covellite (CuS) and chalcocite (Cu_2S). The CuS in specific exhibits a p-type, metallic-like property due to the highest density of delocalized holes in its VB. The CuS possesses excellent transparency, high hole-mobility, and chemical stability, which gained a lot of attention and has been utilized to replace the commonly used spiro-OMeTAD as HTMs in PSCs. For example, in the inverted planar PSCs, Rao et al. [154] fabricated CuS-HTMs by spin-coating. The substrate's energy level was changed from —4.9 to 5.1 eV to best match with the VB of $MAPbI_3$ (5.4 eV). With various surface coverage brought on by different spin-coating time, the impact of CuS alteration was examined. When the CuS nano- particles were deposited twice with adjusted spin-coating, the PCE reached 16.2%, including a V_{oc} of 1.02 V, a J_{sc} of 22.3 mA/cm^2, and an FF of 71%. Lei et al. have put forth an intriguing method that in- volves the deposition of Cu_xS polycrystalline thin-film on the sur- face of spiro-OMeTAD [155]. Due to the high hole-mobility of the Cu_xS and lower extraction barrier at the spiro-OMeTAD/electrode contact, the as-prepared PSC had a high PCE of 18.58% with improved durability, kept 90% of the initial PCE value after 1000 h. This was possible because the hydrophobic properties of Cu_xS shielded the perovskite layer, extended the device's lifespan. Similar to this, Han et al. demonstrated a PCE of 17.10% and high environmental stability

with the initial efficiency declined only by 4% over 1200 h using a solution-processed HTM made of spiro-OMeTAD and Cu_9S_5 in PSC [156].

Kim et al. constructed a homogeneous and uniform thin-film of tungsten sulfide (WS_2) as HTM in PSC using the chemical vapor deposition [38]. Due to the low V_{oc}, the relevant device showed a PCE of 8.02%, which was lower than that with the PEDOT:PSS. There

Table 3Summary of published data on the performance of PSCs using metal cyanates, phthalocyanines, and halide as HTMs.

HTM	Photoactive layer	Device layout	V_{oc} (V)	J_{sc} (mA cm^{-2})	FF (%)	PCE (%)	Ref.
CuSCN	$MAPbI_3$	n-i-p (meso)	1.02	19.7	62.0	12.4	[129]
CuSCN	$MAPbI_3$	n-i-p (meso)	0.98	21.07	64.0	13.3	[130]
CuSCN	$MAPbI_3$	n-i-p (meso)	1.04	23.1	75.3	18.0	[131]
CuSCN	$MAPbI_3$	n-i-p (planar)	0.981	23.77	72.43	17.0	[133]
CuSCN	$MAPbI_3$	n-i-p (planar)	1.036	24.16	73.2	18.34	[134]
CuSCN	$MAPbI_3$	p-i-n (planar)	1.00	21.9	75.8	16.6	[138]
CuSCN	$MAPbI_3$	p-i-n (planar)	1.07	15.76	63.2	10.8	[137]
CuSCN/rGO	$CsFAMAPbI_2Br$	n-i-p (meso)	1.112	23.24	78.2	20.4	[132]
CuSeCN	$MAPbI_3$	p-i-n (planar)	1.036	21.93	70.29	15.97	[140]
CuPc	$(FAPbI_3)_{0.85}(MAPbBr_3)_{0.15}$	n-i-p (planar)	1.07	22.6	77.5	18.8	[142]
CuPrPc	$MAPbI_3$	n-i-p (planar)	1.01	23.2	76.0	17.8	[141]
CuPc	$MAPbI_3$	p-i-n (planar)	1.03	19.4	77.0	15.4	[143]
CuPc	$Cs_{0.05}(MA_{0.17}FA_{0.83})_{0.95}Pb(I_{0.83}Br_{0.17})_3$	p-i-n (planar)	1.075	20.63	75.4	16.72	[144]

TS-CuPc	$MAPbI_{3-x}Cl_x$	p-i-n (planar)	0.96	21.71	77.0	16.14	[145]
NiPc	$MAPbI_3$	n-i-p (planar)	0.94	17.64	73.0	12.1	[35]
NiPc	$Cs_{0.05}(MA_{0.17}FA_{0.83})_{0.95}Pb(I_{0.83}Br_{0.17})_3$	n-i-p (planar)	1.13	23.92	78.66	21.23	[147]
$NiPr_2Pc$	$MAPbI_3$	n-i-p (planar)	1.04	22.83	59.40	14.07	[146]
ZnPc:OTPA	$(FAPbI_3)_{0.85}(MAPbBr_3)_{0.15}$	n-i-p (planar)	1.02	22.36	71.43	16.23	[148]
CuI	$MAPbI_3$	p-i-n (planar)	1.04	21.06	62.0	13.58	[152]
CuI	$MAPbI_3$	p-i-n (planar)	1.07	20.60	69.0	15.26	[36]
CuI	$(CsFAMA)Pb(BrI)_3$	p-i-n (planar)	1.06	23.31	76.11	18.80	[153]

have also been reports of desirable electronic couplings between WS_2 and perovskite. For instance, altering the electronic structure of WS_2, which was deposited on top of a perovskite layer, improved interface electronic interaction and demonstrated potential for PSCs with high efficiency and stability [157]. Additionally, it was shown that an ultra-thin WS_2 layer can efficiently direct desirable perovskite formation, producing thin films with improved crystal- linity and grain size. Defect formation in perovskite was restricted by WS_2 contact with the perovskite by raising defect formation energy and shallowing deep defect levels, which helped efficient charge extraction and reduced interfacial recombination [158]. Benefiting from these features, inverted planar PSC with WS_2 layer produced a PCE of 20.92% with improved V_{oc} and FF along with 90% shelf-stability under 30% relative humidity for more than 20 days (Figs. 17a and b).

Molybdenum sulfide (MoS_2) has also been used as an effective and stable HTM in PSC because of the facilitated charge transport resulting from suitable interfacial energy level alignment and outstanding homogeneity of the perovskite layer fabricated on it. For example, inverted planar PSCs based on MoS_2 delivered PCEs of 20.43% [159]. The device with MoS_2 flakes demonstrated a PCE of 13.3% with substantial durability improvement preserving the 93% of the initial efficiency after 550 h, while the device without the MoS_2 degraded considerably more quickly with the initial PCE value declining 34% during that same duration [160]. Similarly, Kakavelakis et al. introduced MoS_2 nano-flakes between the PTAA and the perovskite layer to evaluate the stability of inverted planar PSCs in ambient air [161]. The MoS_2 served as a shield for the perovskite layer and inhibited the penetration of water molecules and indium ions that would otherwise migrate from the ITO sub- strate to the perovskite film, degrading the light harvesting layer and shortening the longevity of the cell. Hence,

after 568 h of continuous illumination, MoS_2-based PSCs showed great stability, maintaining 80% of the initial PCE. Furthermore, the MoS_2-based PSCs demonstrated high efficiency due to the better hole transport capabilities originated from the desirable alignment of energy levels. The interface charge transfer processes in a heterojunction made up of MoS_2 and perovskite layers have been studied [162]. It

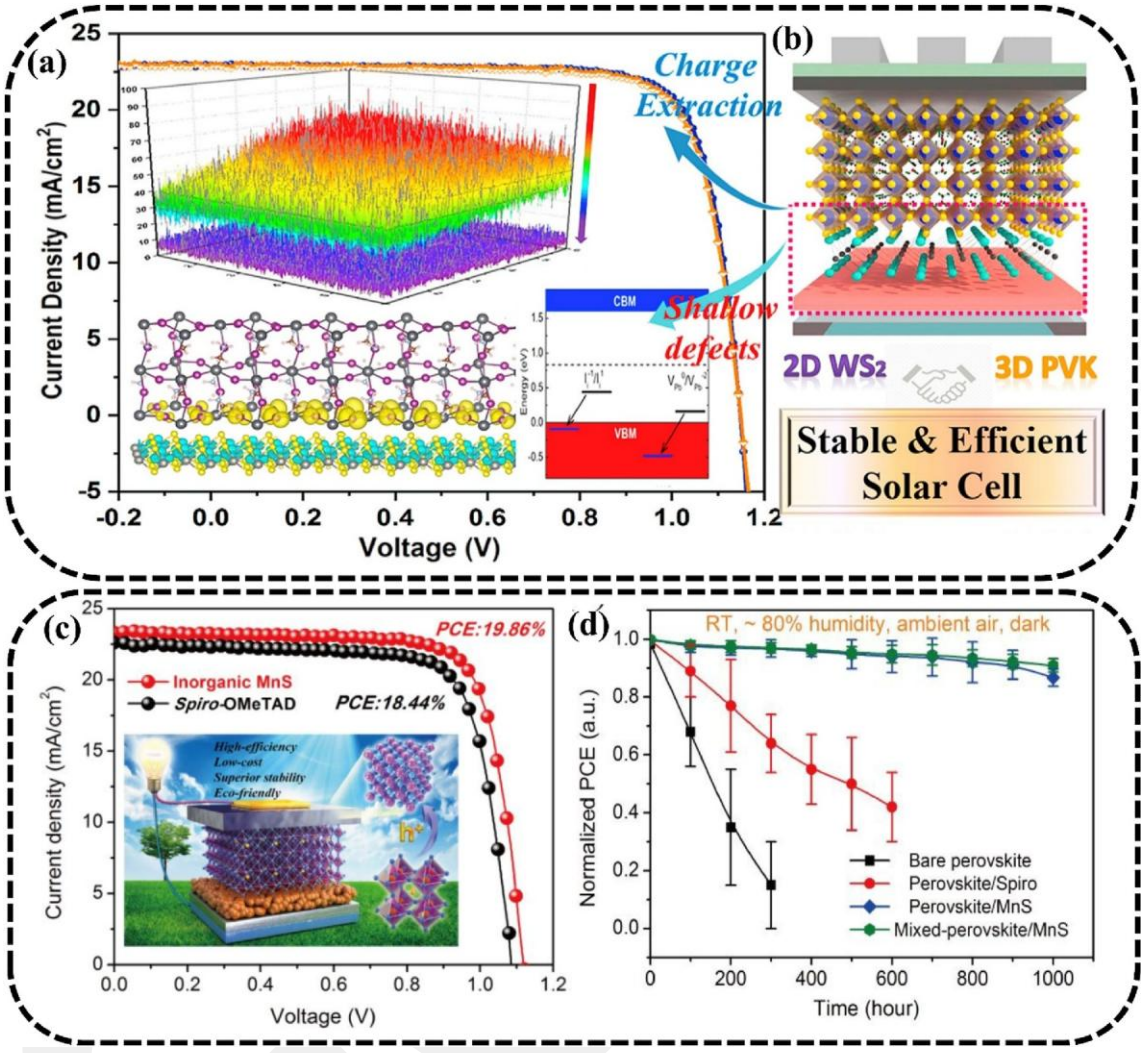

Fig. 17. (a) J-V characteristic curves 2D-WS_2-based PSC (insets are the 3D PL-mapping with 6 m m size in x-y axes, the wavefunctions of VB maxima (yellow) and entirely empty bands (green) of perovskite@WS_2, and after the addition of the WS_2 layer, the schematic diagram in the perovskite's band structure showing the ionization energies of two defects are dropped (from black lines to blue lines); (b) schematics of the based PSC design with 2D-WS_2-HTM. Reproduced with permission from the study by Liu et al. [158]. Copyright 2020, Elsevier Ltd. (c) J-V characteristic curves of the PSCs using MnS or spiro-OMeTAD as HTMs (inset is the schematics of the device design); (d) stability analyses of the corresponding devices. Reproduced with permission from the study by Li et al. [164]. Copyright 2019, Royal Society of Chemistry. HTM, hole transport material; PSC, perovskite solar cell.

was observed that a modest plasma treatment could be utilized to create sulfur vacancies in MoS_2, overcoming the intrinsic band offset at the perovskite/MoS_2 interface that may impede photoin- duced hole transport. As

further evidenced by modeling [163], these vacancies stabilized iodine vacancies at the interface and created an interface dipole that led to low VB maxima mismatch, permitted efficient hole transport. With the right thickness of MoS_2, perovskite, the electron transport layer, and the choice of aluminum or silver back-contacts, the simulation results showed PCE higher than 20% in MoS_2-based device [159], further demonstrating that metal sulfides have great potentials for use as remarkable HTMs in PSCs.

Other metal sulfides such as TiS_2, SnS, PbS, NbS_2, FeS_2, and MnS have been employed as HTMs in PSCs to enhance both efficiency and stability of the resulted devices. In regular planar PSC, for instance, TiS_2 was utilized in place of the frequently used spiro- OMeTAD, which demonstrated PCE of 12.01% [40]. Moreover, Quantum dots (QDs) of tin sulfide (SnS) were used as HTM in regular planar PSC, which yielded PCEs of 12.65% [41]. QDs of lead sulfide (PbS) with hydrophobic nature acted as a barrier for hu- midity in PSCs and led to unprecedented stabilities, maintained 76% of their initial PCEs after 60 days under 70% relative humidity [165]. To minimize charge-carriers recombination and improve charge collection in an inverted planar PSC, Li et al. used a vapor-assisted solution approach to create a high-purity perovskite film and then created a MnS-HTM on top of it [166]. The optimized device produced a PCE of 10.45% and preserved 80% of its initial PCE after

90 days at 80% relative humidity and 85 $^{\circ}C$, demonstrated outstanding long-term stability. Li et al. used vacuum vapor depo- sition to further enhance the efficacy of inexpensive and environ- mentally friendly MnS-HTM [164]. A PCE of 19.86% was attained in MnS-based PSC thanks to favorable band alignment, high hole- mobility, and excellent optical transparency of MnS. Furthermore, the MnS-based devices outperformed their counterparts with organic-HTMs in terms of stability, maintained over 90% of their initial efficiency even after being exposed to 80% relative humidity air for 1000 h without any sealing (Fig. 17c and d). According to these reports, metal sulfide-based HTMs could help PSCs devel- opment by taking the place of frequently employed organic-HTMs, which are difficult to synthesize and are vulnerable to environ- mental disintegration.

5.2. *Metal selenides and tellurides*

The remarkable optoelectronic characteristics of metal selenides and tellurides have attracted a lot of attention. For usage in gas sensors, photovoltaics, and QDs, these materials are particularly desirable. Nevertheless, there are not many studies that have been done on metal selenides and tellurides as HTMs in PSCs. For instance, after annealing at different temperature, $MoSe_2$-HTMs have been used in inverted PSCs. At annealing temperature of 700 $^{\circ}C$, the $MoSe_2$ supported the formation of large grains of the perovskite film. By increasing the contact between the perovskite and $MoSe_2$ layers, fast charge flow and a low series resistance were produced at the junction. The fabricated PSC showed an improved PCE of 8.23% [167].

In order to promote hole transport, decrease trap-states, and impede undesired charge recombination at the perovskite/HTM interface, bismuth telluride (Bi_2Te_3) have previously been employed by Fu et al. as a substitute interlayer to bismuth selenide (Bi_2Se_3) [168]. The improved PCE of 11.96% has been observed in modified PSCs with Bi_2Te_3. Furthermore, Bi_2Te_3 blocked the diffu- sion of silver, iodide ions, and moisture, leading to a significant device stability of over 70% of initial PCE after 50 days without sealing. Computational research has demonstrated that using
Bi_2Se_3 as a shell material for copper nanospheres (NSs) to create a "core/shell" configuration (Cu/Bi_2Se_3) in the absorber layer can boost the light trapping and broad the light absorption of PSC [169]. The optimum values for the Cu-NS radius, Bi_2Se_3 thickness, NSs periodicity, and absorber layer thickness of PSC were 40, 35, 172.5, and 410 nm, respectively. Compared to the bare PSC, which has J_{sc} of 21.8 mA/cm^2, device based on Cu/Bi_2Se_3 core/shell delivered a J_{sc} of 33.01 mA/cm^2 and a maximum normalized absorbed power of 0.89. It was found that the absorption across the entire spectrum can be improved by increasing the Bi_2Se_3 thickness up to 35 nm at a fixed Cu-NS radius of 40 nm. But, at longer wavelengths, this improvement was more pronounced. Compared to the bare Cu-NSs, the extinction cross-section was enhanced by nearly 3.5 times. Comparing the PSC with Cu/Bi_2Se_3 NSs to the controlled PSC, the results revealed a 51.3% increase in absorption. All these primary reports indicate the potential applications of the metal selenides and tellurides for futuristic design engineering and acceptable performance of the PSCs.

5.3. Other metal chalcogenides

Other ternary and quaternary chalcogenides have recently been receiving considerable attention as HTMs in PSCs due to their adequate hole-mobility and adjustable energy levels. For instance, an affordable and stable tetrahedrite ($Cu_{12}Sb_4S_{13}$) ternary HTM allowed an inverted planar PSC to achieve a PCE of 6.5% [170]. The lower V_{oc} of the $Cu_{12}Sb_4S_{13}$-based device compared to its counterpart was attributed to the mismatching between the energy levels of $Cu_{12}Sb_4S_{13}$ and perovskite. The $Cu_{12}Sb_4S_{13}$-based device, on the other hand, demonstrated high stability, maintained 50% of the initial PCE after 15 days, which was attributed to the hydrophobicity of $Cu_{12}Sb_4S_{13}$ nanoparticles. QDs of $Cu_{12}Sb_4S_{13}$ were used as HTM in inverted planar PSCs by Liu et al. to alter energy levels and obtain enhanced hole transport characteristics, which led to a PCE of 14.13% [171]. The initial PCE of the $Cu_{12}Sb_4S_{13}$-based device showed outstanding stability as well, declined by only 9% after 30 days. Similarly, QDs of $CuInSe_2$ were used to prepare HTMs in PSCs. The $CuInSe_2$-based device produced a high PCE of 12.8% and greatly increased long-term stability compared to device using spiro- OMeTAD [172]. Moreover, copper indium sulfide ($CuInS_2$) demon- strated fast hole transport and high PSC's longevity. For instance, Yang et al. [173] developed an inverted planar PSC with $CuInS_2$-HTM, and achieved a PCE of 17.34%. When compared to NiO-based control devices, the $CuInS_2$-based PSCs showed high stability. Liu et al. synthesized $CuInS_2$ QDs via modifying the hot-injection procedure, and used them as an HTM on PSCs [174]. For the optimized PSC using $CuInS_2$ as an HTM, a high PCE of 18.8% was obtained (Fig. 18). Moreover, compared to PSC constructed with spiro-OMeTAD, the stability of $CuInS_2$-based device was significantly increased.

Furthermore, the high chemical stability and suitable hole-mobility in addition to perovskite and Cu_2BaSnS_4 (CBTS) well- aligned energy levels, the CBTS is a viable material for HTM in PSCs. The efficiency was increased by 10% thanks to the usage of quaternary CBTS as the HTM in inverted planar PSC [48]. Another promising HTM is Cu_2ZnSnS_4 (CZTS), which is easy to synthesize, has great chemical stability, and excellent hole-mobility. In this context, Wu et al. successfully used CZTS as HTM, and a high PCE of 12.75% was obtained in regular planar PSC [49]. The high performance of the CZTS-based PSCs was attributed to the enhanced hole transport at the CZTS/perovskite interface and low recombination losses. Additionally, spiro-MeOTAD was replaced with a solution-processed CZTS-HTM in PSC [175]. Together with high stability and minimal hysteresis, the CZTS-based PSC had a matching PCE value of 9.21% to that of spiro-MeOTAD-based device (PCE of 9.88%). Using high purity CZTS nanocrystals made by a hot-injection

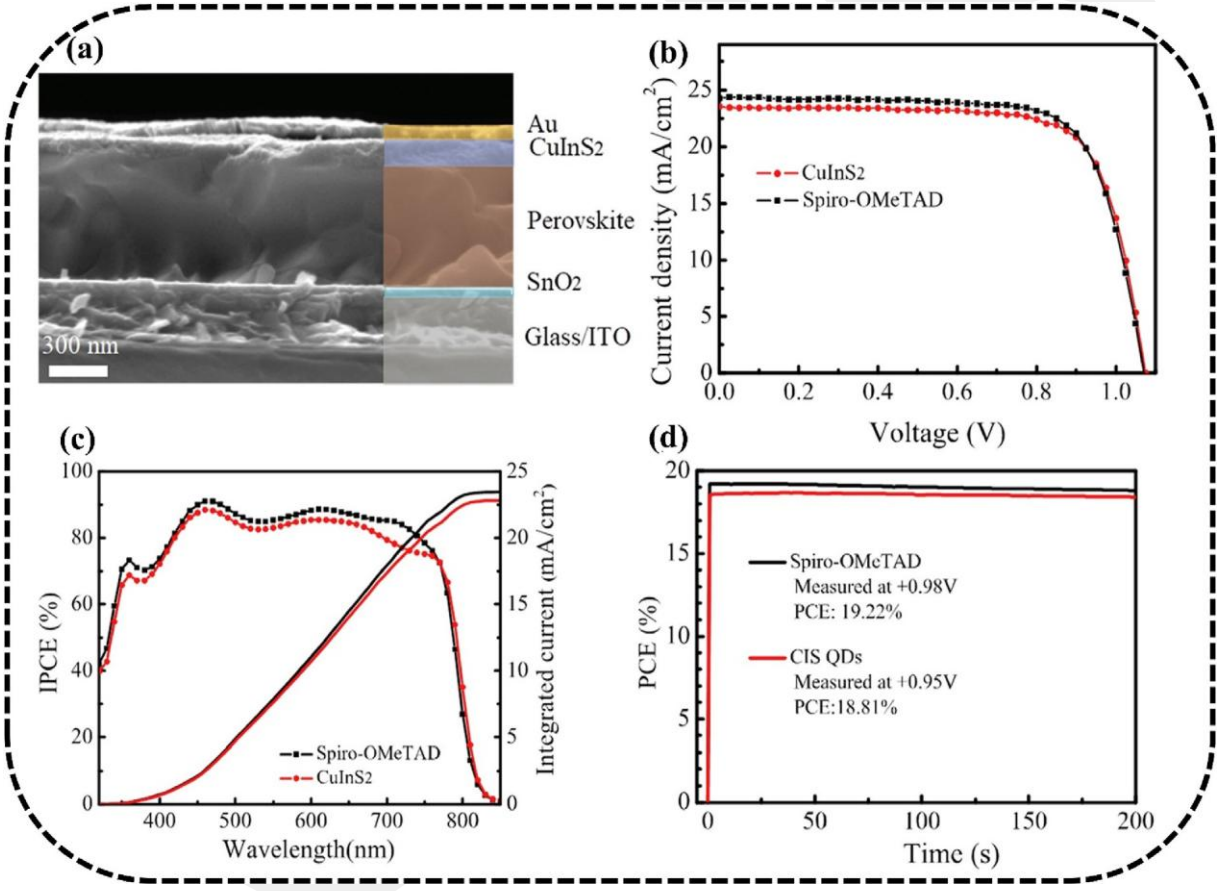

Fig. 18. (a) Cross-sectional SEM image; (b) J-V characteristic curves; (c) quantum efficiencies with integrated Jsc; (d) PCEs at maximum power point tracking of the PSCs using $CuInS_2$ or spiro-OMeTAD as HTMs. Reproduced with permission from the study by Liu et al. [174]. Copyright 2019, Elsevier B.V. HTM, hole transport material; PCE, power conversion efficiency; PSC, perovskite solar cell; SEM, scanning electron microscopy.

Table 4

Published data summarizing the performance of the PSCs using metal chalcogenides.

HTM	Photoactive layer	Device layout	V_{oc} (V)	J_{sc} (mA cm^{-2})	FF (%)	PCE (%)	Ref.
CuS	$MAPbI_3$	p-i-n (planar)	1.02	22.3	71.2	16.2	[154]
Cu_xS	$MAPbI_3$	n-i-p (planar)	1.125	23.10	71.50	18.58	[155]
Cu_9S_5	$MAPbI_3$	n-i-p (planar)	1.05	22.32	73.0	17.10	[156]
WS_2	$MAPbI_3$	p-i-n (planar)	1.14	22.90	79.82	20.92	[158]
TiS_2	$(FAPbI_3)_{0.85}(MAPbBr_3)_{0.15}$	n-i-p (planar)	0.954	21.79	65.0	13.54	[40]
SnS	$MAPbI_3$	n-i-p (planar)	0.944	22.96	63.3	13.72	[41]
MnS	$FA_{0.85}MA_{0.15}Pb(I_{0.85}Br_{0.15})3$	n-i-p (planar)	1.11	23.40	76.48	19.86	[164]
$MoSe_2$	$MAPbI_3$	p-i-n (planar)	1.02	14.45	55.80	8.23	[167]
Bi_2Te_3	$CsPbBrI_2$	n-i-p (planar)	1.14	14.80	71.0	11.96	[168]
Cu12Sb4S13	$MAPbI_3$	p-i-n (planar)	1.05	21.85	61.60	14.13	[171]
$CuInSe_2$	PbI_2/FAI:MABr:MACl	n-i-p (planar)	0.86	22.5	66.0	12.81	[172]
$CuInS_2$	PbI_2/FAI:MABr:MACl	p-i-n (planar)	0.92	23.0	81.95	17.34	[173]
$CuInS_2$	PbI_2/MABr:FAI:MACl	n-i-p (planar)	1.073	23.5	74.5	18.81	[174]
Cu_2ZnSnS_4	$MAPbI_3$	n-i-p (planar)	1.06	20.54	58.7	12.75	[49]
Cu_2ZnSnS_4	$MAPbI_3$	p-i-n (planar)	0.92	20.7	81.0	15.4	[176]
$CuIn_{0.75}Ga_{0.25}S2$	$MAPbBr_3$	n-i-p (planar)	1.08	23.86	62.0	15.93	[177]
$Cu_2ZnSnSe_4$	$MAPbI_3$	p-i-n (planar)	1.10	20.8	76.3	17.4	[178]

procedure with the organic ligand oleylamine, accompanied by the ligand removal before being deposited as HTMs in PSCs, Khanzada et al. was able to achieve one of the highest PCE value of 15.4% in CZTS-based PSCs [176]. The use of $CuIn_{0.75}Ga_{0.25}S_2$ as HTM in a regular PSC resulted in a PCE of 15.9% compared to the device using spiro-OMeTAD (PCE of 16.3%) [177]. In order to function as an HTM in inverted planar PSCs, Tseng et al. developed a new $Cu_2ZnSnSe_4$ chalcogenide [178]. The authors looked at how the processing pa- rameters affected the geometry of the as-prepared $Cu_2ZnSnSe_4$ layers. They were successful in achieving a high PCE of 17.4% in a $Cu_2ZnSnSe_4$-based device through optimization. These results highlighting the crucial role that such materials play in

improving PSCs performance. The performance of the PSCs using metal chal- cogenides as HTMs is summarized in Table 4.

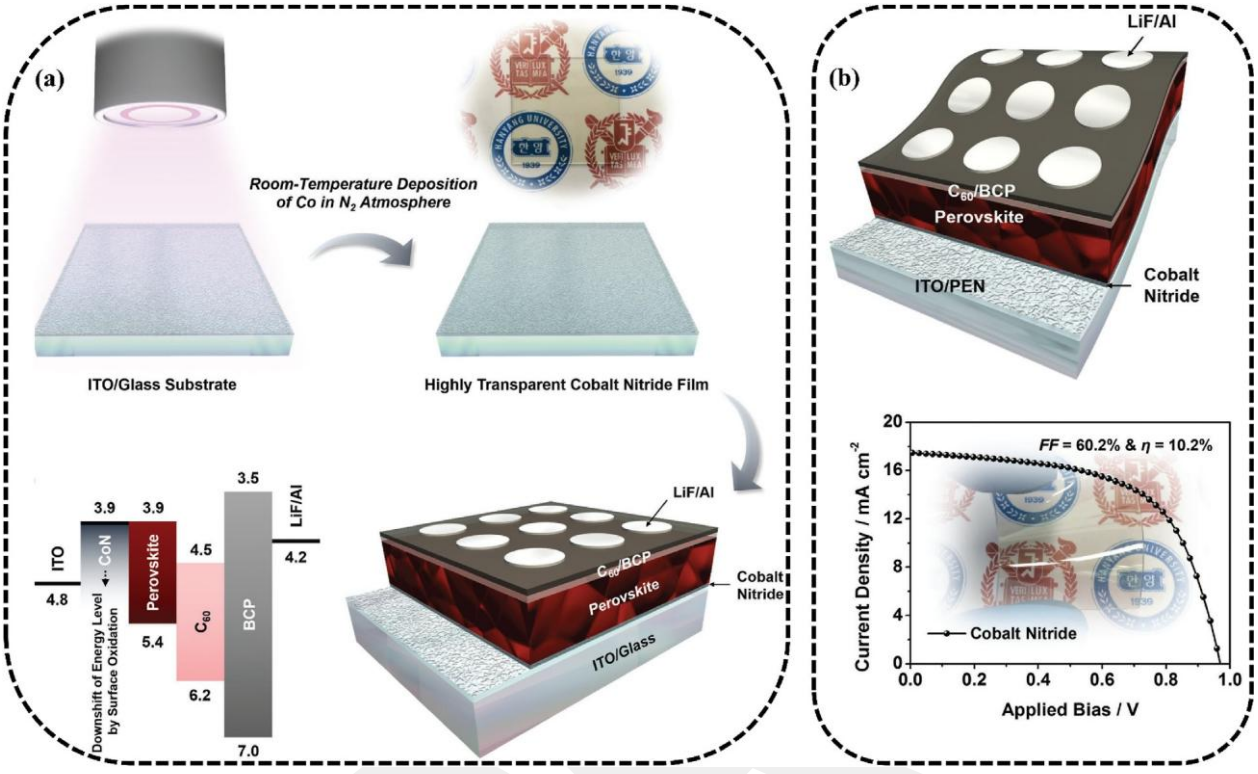

Fig. 19. (a) Schematic illustration of preparing CoN layer on rigid substrate accompanied by energy band diagram and rigid device design; (b) flexible PSC with CoN as HTM accompanied by J-V characteristic curves. Reproduced with permission from the study by Kang et al. [182]. Copyright 2018, WILEY-VCH Verlag GmbH & Co. KGaA, Weinheim. HTM, hole transport material; PSC, perovskite solar cell.

Table 5
Summary of the published data on the performance of PSCs using metal nitrides and carbides as HTMs.

HTM	Photoactive layer	Device layout	V_{oc} (V)	J_{sc} (mA cm^{-2})	FF (%)	PCE (%)	Ref.
Ti_3C_2-MXene	$CsPbBr_3$	n-i-p (planar)	1.444	8.54	73.08	9.01	[180]
$Ti_3C_2T_x$/Glucose	$MAPbI_3$	p-i-n (planar)	1.11	23.58	79.0	20.81	[181]
CoN	$MAPbI_3$	p-i-n (planar)	1.01	21.3	69.7	15.0	[182]

6. Metal carbides and nitrides

Numerous MXene complexes with variable WFs and desirable optoelectronic characteristics have also demonstrated potential use in PSCs. In order to match the WF with perovskite, surface termi- nation functional groups of the MXene can be tuned [179]. By altering the relative concentrations of OH, O, and F terminations, for instance, a strong nonlinear tendency can be generated, indicating that surface functionalization of MXenes provides a path toward improving their characteristics and use in optoelectronic devices. According to Chen et al. [180], the addition of Ti_3C_2-MXene resulted in a more advantageous interfacial energy level matching, which accelerated hole transport and collection, and decreased charge recombination at the perovskite/carbon interface. In perovskite layer, researchers also noticed substantial passivation of deep trap imperfections [180], which was explained by couplings between functional groups on the MXene and the under-coordinated Pb- atoms there. The Ti_3C_2-MXene HTM helped the improved PSCs reach a PCE of 9.01% and outstanding long-term stability, as it kept 80% of its efficiency for more than 1900 h in an environment rich in

humidity as well as more than 600 h under thermal stress at 80 °C

[180]. Zhang et al. [181] has shown that self-assembled gradient $Ti_3C_2T_x$-MXene with PEDOT:PSS can produce high-performance large-area PSCs. The $Ti_3C_2T_x$-MXene nanosheets were spontane- ously dispersed and redistributed at the top area of HTM to

generate the distinctive gradient distribution constituted of MXe- ne:Glucose:PEDOT:PSS by constructing half-caramelization-based glucose-induced MXene redistribution (MG-PEDOT). The MG- PEDOT HTM promoted the film quality of the perovskite layer in addition to providing favorable energy level alignment and effec- tive charge extraction. As a result, when compared to the control device, the PCE of the flexible device based on MG-PEDOT HTM

increased by 36%. When employing MG-PEDOT HTM, the flexible PSC minimodule (15 cm^2 area) attained a PCE of 17.06%. At 85 °*C* in

ambient air (90%), the encapsulated modules display outstanding long-term storage stability.

As hole transport layers in PSCs, transition metal nitrides including cobalt nitride (CoN), gallium nitride (GaN), and titanium nitride (TiN) have recently been presented with outstanding out- comes. PSCs with the combination ITO/CoN/$MAPbI_3$/C_{60}/BCP/LiF/Al (Fig. 19a), for instance, showed a PCE of 15% [182]. The CoN layer was found to facilitate hole extraction and inhibit interfacial recombination. Moreover, CoN applications in flexible planar PSCs were carried out (Fig. 19b), demonstrating the benefits of the room-temperature deposition method and the viability of the CoN nano- films in a variety of applications. These research successes opened the way for the use of carbides and nitrides in PSCs, and further alterations to the composition of carbides and nitrides, such as the addition of suitable dopants, are anticipated to improve the per- formance by enhancing the charge transfer or transport kinetics.

The primary manufacturing procedures provide difficulties for the use of carbides and nitrides in PSCs. For instance, hazardous ammonia is frequently employed as a nitrogen source in chemical synthesis of nitrides,

which often needs high temperature treat- ment. Reactive sputtering, which is carried out at room temperature and uses ecologically friendly N_2 gas as source, can be a good substitute. Hence, research is needed to create new plans and techniques for the commercially viable manufacturing of different nitrides and carbides. Table 5 presents the performance of PSCs using metal nitrides and carbides as HTMs.

7. Conclusion

The compositional engineering of the perovskites and process- ing techniques, as well as the careful selection and engineering of charge transport layers, have contributed to the PCEs of PSCs rapidly improving beyond 26%. Regarding material innovations, there are both organic and inorganic materials that, depending on their optoelectronic properties, show promises as charge transport layers. Numerous different inorganic materials have been used as HTMs in PSCs due to a wide range of favorable features, for example, low cost, appropriate hole-mobility, desired energy levels, and high thermal and chemical stability. In this review, we pro- vided a comprehensive and up-to-date survey of the field of innovative inorganic HTMs, including metal oxides, cyanates, phthalocyanines, halides, chalcogenides, carbides, and nitrides that have been successfully used as HTMs in PSCs. The aforementioned inorganic-HTMs have demonstrated substantial potential in improving device performance while also enhancing overall sta- bility. Current organic-HTMs like spiro-OMeTAD, PEDOT:PSS, and PTAA have now been outperformed by these inorganic-HTMs in terms of performance and low materials' costs, demonstrating their outstanding prospects for improving the efficiencies of PSCs and, probably more significantly, durability. Further developments have been made and more are anticipated as demonstrated by the number of recent studies in this field after mixing these materials with other inorganic/organic materials to form unique hybrid composite materials.

Inorganic-HTMs are particularly appealing options for low-cost devices that are suitable for potential commercialization because of being able to be easily synthesized with a variety of abundant and cost-effective materials. More significantly, the solution process- ability makes it simple to incorporate dopants into inorganic-HTMs to create compounds with enhanced functions. They can also be simply mixed into organic material solutions to create composites with superior optoelectronic capabilities. To prevent malfunctions related to the deterioration of the perovskite layer or electrodes, right integration into the device architecture is necessary.

Materials engineering can be used to develop new sorts of materials with high hole-mobility, acceptable energy levels, transparency, hydrophobicity, high solubility in suitable solvents, and low cost. Such materials might aid in the fabrication of less complex, more economical device architecture, which is required for ultimate production. This excellent design necessitates close cooperation between chemists, materials scientists, and device physicists, which would allow rapid advancement in the develop- ment of such materials.

References

[1] W. Li, Z. Wang, F. Deschler, S. Gao, R.H. Friend, A.K. Cheetham, Chemically diverse and multifunctional hybrid organiceinorganic perovskites, Nat. Rev. Mater. 2 (2017) 16099, https://doi.org/10.1038/natrevmats.2016.99.

[2] S. Sajid, A.M. Elseman, H. Huang, J. Ji, S. Dou, H. Jiang, X. Liu, D. Wei, P. Cui, M. Li, Breakthroughs in NiOx-HTMs towards stable, low-cost and efficient perovskite solar cells, Nano Energy 51 (2018) 408e424, https://doi.org/ 10.1016/j.nanoen.2018.06.082.

[3] J. Sun, J. Lu, B. Li, L. Jiang, A.S.R. Chesman, A.D. Scully, T.R. Gengenbach, Y.-B. Cheng, J.J. Jasieniak, Inverted perovskite solar cells with high fill-factors featuring chemical bath deposited mesoporous NiO hole transporting layers, Nano Energy 49 (2018) 163e171, https://doi.org/10.1016/ j.nanoen.2018.04.026.

[4] M. Cheng, C. Zuo, Y. Wu, Z. Li, B. Xu, Y. Hua, L. Ding, Charge-transport layer engineering in perovskite solar cells, Sci. Bull. 65 (2020) 1237e1241, https:// doi.org/10.1016/j.scib.2020.04.021.

[5] T. Xu, L. Chen, Z. Guo, T. Ma, Strategic improvement of the long-term stability of perovskite materials and perovskite solar cells, Phys. Chem. Chem. Phys. 18 (2016) 27026e27050, https://doi.org/10.1039/C6CP04553G.

[6] M.A. Green, E.D. Dunlop, G. Siefer, M. Yoshita, N. Kopidakis, K. Bothe, X. Hao, Solar cell efficiency tables (Version 61), Prog. Photovoltaics Res. Appl. 31 (2023) 3e16, https://doi.org/10.1002/pip.3646.

[7] X. Zhou, X. Luan, L. Zhang, H. Hu, Z. Jiang, Y. Li, J. Wu, Y. Liu, J. Chen, D. Wang, C. Liu, S. Chen, Y. Zhang, M. Zhang, Y. Peng, P.A. Troshin, X. Wang, Y. Mai, B. Xu, Dual optimization of bulk and interface via the synergistic effect of ligand anchoring and hole transport dopant enables 23.28% efficiency inverted perovskite solar cells, ACS Nano 17 (2023) 3776e3785, https:// doi.org/10.1021/acsnano.2c11615.

[8] L. Nakka, Y. Cheng, A.G. Aberle, F. Lin, Analytical review of spiro-OMeTAD hole transport materials: paths toward stable and efficient perovskite solar cells, Adv. Energy Sustain. Res. 3 (2022) 2200045, https://doi.org/10.1002/ aesr.202200045.

[9] M. Shahbazi, H. Wang, Progress in research on the stability of organometal perovskite solar cells, Sol. Energy 123 (2016) 74e87, https://doi.org/10.1016/ j.solener.2015.11.008.

[10] J. Carrillo, A. Guerrero, S. Rahimnejad, O. Almora, I. Zarazua, E. Mas-Marza, J. Bisquert, G. Garcia-Belmonte, Ionic reactivity at contacts and aging of methylammonium lead triiodide perovskite solar cells, Adv. Energy Mater. 6 (2016) 1502246, https://doi.org/10.1002/aenm.201502246.

[11] K. Domanski, J.-P. Correa-Baena, N. Mine, M.K. Nazeeruddin, A. Abate, M. Saliba, W. Tress, A. Hagfeldt, M. Grätzel, Not all that glitters is gold: metal- migration-induced degradation in perovskite solar cells, ACS Nano 10 (2016) 6306e6314.

[12] A.K. Jena, M. Ikegami, T. Miyasaka, Severe morphological deformation of spiro-OMeTAD in (CH3NH3) PbI3 solar cells at high temperature, ACS Energy Lett. 2 (2017) 1760e1761.

[13] G. Zhu, L. Yang, C. Zhang, G. Du, N. Fan, Z. Luo, X. Zhang, J. Zhang, Unveiling the critical role of oxidants and additives in doped spiro-OMeTAD toward stable and efficient perovskite solar cells, ACS Appl. Energy Mater. 5 (2022) 3595e3604.

[14] J.C. Yu, J.A. Hong, E.D. Jung, D. Bin Kim, S.-M. Baek, S. Lee, S. Cho, S.S. Park, K.J. Choi, M.H. Song, Highly efficient and stable inverted perovskite solar cell employing PEDOT:GO composite layer as a hole transport layer, Sci. Rep. 8 (2018) 1070, https://doi.org/10.1038/s41598-018-19612-7.

[15] P. Guo, J. Dong, C. Xu, Y. Yao, J. You, H. Bian, W. Zeng, G. Zhou, X. He, M. Wang, X. Zhou, M. Wang, Q. Song, Fabrication of an ultrathin PEG- modified PEDOT:PSS HTL for high-efficiency SnePb perovskite solar cells by an eco-friendly solvent etching technique, J. Mater. Chem. A. 11 (2023) 7246e7255, https://doi.org/10.1039/D3TA00455D.

[16] J. Jeng, K. Chen, T. Chiang, P. Lin, T. Tsai, Y. Chang, T. Guo, P. Chen, T. Wen, Y. Hsu, Nickel oxide electrode interlayer in CH3NH3PbI3 perovskite/PCBM planar-heterojunction hybrid solar cells, Adv. Mater. 26 (2014) 4107e4113.

[17] A.M. Elseman, S. Sajid, A.E. Shalan, S.A. Mohamed, M.M. Rashad, Recent progress concerning inorganic holetransport layers for efficient perovskite solar cells, Appl. Phys. A 125 (2019) 476, https://doi.org/10.1007/s00339-019-2766-7.

[18] D. Huang, H. Xiang, R. Ran, W. Wang, W. Zhou, Z. Shao, Recent advances in nanostructured inorganic hole-transporting materials for perovskite solar cells, Nanomaterials 12 (2022), https://doi.org/10.3390/nano12152592.

[19] A. Wang, Z. Cao, J. Wang, S. Wang, C. Li, N. Li, L. Xie, Y. Xiang, T. Li, X. Niu, L. Ding, F. Hao, Vacancy defect modulation in hot-casted NiOx film for effi- cient inverted planar perovskite solar cells, J. Energy Chem. 48 (2020) 426e434, https://doi.org/10.1016/j.jechem.2020.02.034.

[20] Y. Wang, L. Duan, M. Zhang, Z. Hameiri, X. Liu, Y. Bai, X. Hao, PTAA as efficient hole transport materials in perovskite solar cells: a review, Sol. RRL. 6 (2022) 2200234.

[21] S.A. Rutledge, A.S. Helmy, Carrier mobility enhancement in poly (3, 4-ethylenedioxythiophene)-poly (styrenesulfonate) having undergone rapid thermal annealing, J. Appl. Phys. 114 (2013) 133708.

[22] S. Wang, B. Zhang, D. Feng, Z. Lin, J. Zhang, Y. Hao, X. Fan, J. Chang, Achieving high performance and stable inverted planar perovskite solar cells using lithium and cobalt co-doped nickel oxide as hole transport layers, J. Mater. Chem. C 7 (2019) 9270e9277.

[23] X. Gao, Y. Du, X. Meng, Cupric oxide film with a record hole mobility of 48.44 cm2/Vs via directecurrent reactive magnetron sputtering for perovskite solar cell application, Sol. Energy 191 (2019) 205e209.

[24] A. Sekkat, V.H. Nguyen, C.A.M. de La Huerta, L. Rapenne, D. Bellet,

A. Kaminski-Cachopo, G. Chichignoud, D. Munoz-Rojas, Open air printing of Cu2O thin films with high hole mobility for semi-transparent solar har- vesters, Commun. Mater. 2 (2021) 1e10 (n.d.).

[25] C.-H. Chiang, C.-C. Chen, M.K. Nazeeruddin, C.-G. Wu, A newly developed lithium cobalt oxide super hydrophilic film for large area, thermally stable and highly efficient inverted perovskite solar cells, J. Mater. Chem. A. 6 (2018) 13751e13760.

[26] P. Ma, J. Xu, C. Wang, C. Wang, F. Meng, Y. Xie, S. Wen, Enhanced open-circuit voltages and efficiencies: the role of oxidation state of molybdenum oxide buffer layer in polymer solar cells, RSC Adv. 11 (2021) 35141e35146, https:// doi.org/10.1039/D1RA06929B.

[27] M. Cheng, Y. Li, M. Safdari, C. Chen, P. Liu, L. Kloo, L. Sun, Efficient perovskite solar cells based on a solution processable nickel (II) phthalocyanine and vanadium oxide integrated hole transport layer, Adv. Energy Mater. 7 (2017) 1602556.

[28] S. Jiang, S. Xiong, W. Dong, D. Li, Y. Yan, M. Jia, Y. Dai, Q. Zhao, K. Jiang, X. Liu, Constructing chromium multioxide hole-selective heterojunction for high- performance perovskite solar cells, Adv. Sci. 9 (2022) 2203681.

[29] B. Gil, J. Kim, A.J. Yun, K. Park, J. Cho, M. Park, B. Park, CuCrO2 nanoparticles incorporated into PTAA as a hole transport layer for 85° C and light stabilities in perovskite solar cells, Nanomaterials 10 (2020) 1669.

[30] H. Zhang, H. Wang, W. Chen, A.K. Jen, CuGaO2: a promising inorganic hole- transporting material for highly efficient and stable perovskite solar cells, Adv. Mater. 29 (2017) 1604984.

[31] S. Akin, F. Sadegh, S. Turan, S. Sonmezoglu, Inorganic CuFeO2 delafossite nanoparticles as effective hole transport materials for highly efficient and long-term stable perovskite solar cells, ACS Appl. Mater. Interfaces 11 (2019) 45142e45149.

[32] L. Mohan, S.R. Ratnasingham, J. Panidi, M. Daboczi, J.-S. Kim, T.D. Anthopoulos, J. Briscoe, M.A. McLachlan, T. Kreouzis, Determining out- of-plane hole mobility in CuSCN via the time-of-flight technique to eluci- date its function in perovskite solar cells, ACS Appl. Mater. Interfaces 13 (2021) 38499e38507.

[33] N. Wijeyasinghe, L. Tsetseris, A. Regoutz, W. Sit, Z. Fei, T. Du, X. Wang, M.A. McLachlan, G. Vourlias, P.A. Patsalas, Copper (I) selenocyanate (CuSeCN) as a novel hole-transport layer for transistors, organic solar cells, and light- emitting diodes, Adv. Funct. Mater. 28 (2018) 1707319.

[34] M. Bidikoudi, E. Kymakis, Novel approaches and scalability prospects of copper based hole transporting materials for planar perovskite solar cells, J. Mater. Chem. C 7 (2019) 13680e13708.

[35] M. Haider, C. Zhen, T. Wu, G. Liu, H.-M. Cheng, Boosting efficiency and sta- bility of perovskite solar cells with nickel phthalocyanine as a low-cost hole transporting layer material, J. Mater. Sci. Technol. 34 (2018) 1474e1480.

[36] D. Saranin, P. Gostischev, D. Tatarinov, I. Ermanova, V. Mazov, D. Muratov,

A. Tameev, D. Kuznetsov, S. Didenko, A. Di Carlo, Copper iodide interlayer for improved charge extraction and stability of inverted perovskite solar cells, Materials 12 (2019), https://doi.org/10.3390/ma12091406.

[37] H. Lei, G. Fang, F. Cheng, W. Ke, P. Qin, Z. Song, Q. Zheng, X. Fan, H. Huang, X. Zhao, Enhanced efficiency in organic solar cells via in situ fabricated p-type copper sulfide as the hole transporting layer, Sol. Energy Mater. Sol. Cells 128 (2014) 77e84.

[38] Y.G. Kim, K.C. Kwon, Q. Van Le, K. Hong, H.W. Jang, S.Y. Kim, Atomically thin two-dimensional materials as hole extraction layers in organolead halide perovskite photovoltaic cells, J. Power Sources 319 (2016) 1e8.

[39] A.D. Al-Ghiffari, N.A. Ludin, M.L. Davies, R.M. Yunus, M.S. Suait, Systematic review of molybdenum disulfide for solar cell applications: properties, mechanism and application, Mater. Today Commun. (2022) 104078.

[40] A.J. Huckaba, S. Gharibzadeh, M. Ralaiarisoa, C. Roldán-Carmona, N. Mohammadian, G. Grancini, Y. Lee, P. Amsalem, E.J. Plichta, N. Koch, Low-cost TiS2 as hole-transport material for perovskite solar cells, Small Methods 1 (2017) 1700250.

[41] M. Grätzel, P. Wang, SnS quantum dots as hole transporter of perovskite solar cells, ACS Appl. Energy Mater. 2 (2019) 3822e3829.

[42] U. Chalapathi, S.-H. Park, W.J. Choi, Two-step chemical bath deposition enhanced mobility of PbS thin films, Mater. Sci. Semicond. Process. 136 (2021) 106147.

[43] I.G. Orletsky, M.I. Ilashchuk, E. V Maistruk, H.P. Parkhomenko, P.D. Marianchuk, I.P. Koziarskyi, D.P. Koziarskyi, Electrical properties of heterostructures MnS/n-CdZnTe obtained by spray pyrolysis, Mater. Res. Express 8 (2021) 15905.

[44] D. Vikraman, H. Liu, S. Hussain, S.H.A. Jaffery, K. Karuppasamy, E. Jo, Z. Abbas, J. Jung, J. Kang, H. Kim, Impact of molybdenum dichalcogenides on the active and hole-transport layers for perovskite solar cells, X-ray detectors, and photodetectors, Small 18 (2022) 2104216.

[45] C.H. Champness, A.L. Kipling, The Hall and Seebeck effects in non-stoichiometric bismuth telluride, Can. J. Phys. 44 (1966) 769e788.

[46] V. Vinayakumar, S. Shaji, D. Avellaneda, J.A. Aguilar-Martínez, B. Krishnan, Copper antimony sulfide thin films for visible to near infrared photodetector applications, RSC Adv. 8 (2018) 31055e31065.

[47] M. Ye, R. Tang, S. Ma, Q. Tao, X. Wang, Y. Li, P. Zhu, Electrical transport properties and band structure of CuInSe2 under high pressure, J. Phys. Chem. C 123 (2019) 20757e20763.

[48] J. Ge, C.R. Grice, Y. Yan, Cu-based quaternary chalcogenide Cu 2 BaSnS 4 thin films acting as hole transport layers in inverted perovskite CH 3 NH 3 PbI 3 solar cells, J. Mater. Chem. A. 5 (2017) 2920e2928.

[49] Q. Wu, C. Xue, Y. Li, P. Zhou, W. Liu, J. Zhu, S. Dai, C. Zhu, S. Yang, Kesterite Cu2ZnSnS4 as a low-cost inorganic hole-transporting material for high- efficiency perovskite solar cells, ACS Appl. Mater. Interfaces 7 (2015) 28466e28473.

[50] A. Miranda, J. Halim, M.W. Barsoum, A. Lorke, Electronic properties of free- standing Ti3C2Tx MXene monolayers, Appl. Phys. Lett. 108 (2016) 33102, https://doi.org/10.1063/1.4939971.

[51] X. Zheng, Z. Song, Z. Chen, S.S. Bista, P. Gui, N. Shrestha, C. Chen, C. Li, X. Yin, R.A. Awni, H. Lei, C. Tao, R.J. Ellingson, Y. Yan, G. Fang, Interface modification of sputtered NiOx as the hole-transporting layer for efficient inverted planar perovskite solar cells, J. Mater. Chem. C 8 (2020) 1972e1980, https://doi.org/ 10.1039/C9TC05759E.

[52] Y. Nishihara, M. Chikamatsu, S. Kazaoui, T. Miyadera, Y. Yoshida, Influence of O2 plasma treatment on NiOx layer in perovskite solar cells, Jpn. J. Appl. Phys. 57 (2018) 04FS07.

[53] P. Docampo, J.M. Ball, M. Darwich, G.E. Eperon, H.J. Snaith, Efficient orga- nometal trihalide perovskite planar-heterojunction solar cells on flexible polymer substrates, Nat. Commun. 4 (2013) 2761, https://doi.org/10.1038/ ncomms3761.

[54] K.-C. Wang, J.-Y. Jeng, P.-S. Shen, Y.-C. Chang, E.W.-G. Diau, C.-H. Tsai, T.-Y. Chao, H.-C. Hsu, P.-Y. Lin, P. Chen, P-type mesoscopic nickel oxide/ organometallic perovskite heterojunction solar cells, Sci. Rep. 4 (2014) 4756.

[55] W. Chen, Y. Wu, J. Liu, C. Qin, X. Yang, A. Islam, Y.-B. Cheng, L. Han, Hybrid interfacial layer leads to solid performance improvement of inverted perovskite solar cells, Energy Environ. Sci. 8 (2015) 629e640, https://doi.org/ 10.1039/C4EE02833C.

[56] Z. Liu, J. Chang, Z. Lin, L. Zhou, Z. Yang, D. Chen, C. Zhang, S. Liu, Y. Hao, High-performance planar perovskite solar cells using low temperature, sol- utionecombustion-based nickel oxide hole transporting layer with efficiency exceeding 20, Adv. Energy Mater. 8 (2018) 1703432.

[57] L. Zhou, Z. Lin, Z. Ning, T. Li, X. Guo, J. Ma, J. Su, C. Zhang, J. Zhang, S. Liu, Highly efficient and stable planar perovskite solar cells with modulated diffusion passivation toward high power conversion efficiency and ultrahigh fill factor, Sol. RRL. 3 (2019) 1900293.

[58] D.S. Mann, S.-N. Kwon, P. Patil, S.-I. Na, Revivification of nickel oxide- perovskite interfaces via nickel nitrate to boost performance in perovskite solar cells, Nano Energy 106 (2023) 108062, https://doi.org/10.1016/ j.nanoen.2022.108062.

[59] J. You, L. Meng, T.-B. Song, T.-F. Guo, Y. (Michael) Yang, W.-H. Chang, Z. Hong, H. Chen, H. Zhou, Q. Chen, Y. Liu, N. De Marco, Y. Yang, Improved air stability of perovskite solar cells via solution-processed metal oxide transport layers, Nat. Nanotechnol. 11 (2016) 75e81, https://doi.org/10.1038/nnano. 2015.230.

[60] Z. Liu, A. Zhu, F. Cai, L. Tao, Y. Zhou, Z. Zhao, Q. Chen, Y.-B. Cheng, H. Zhou, Nickel oxide nanoparticles for efficient hole transport in p-i-n and n-i-p perovskite solar cells, J. Mater. Chem. A. 5 (2017) 6597e6605, https:// doi.org/10.1039/C7TA01593C.

[61] J. Tirado, M. Vásquez-Montoya, C. Roldán-Carmona, M. Ralaiarisoa, N. Koch,

M.K. Nazeeruddin, F. Jaramillo, Air-stable neiep planar perovskite solar cells using nickel oxide nanocrystals as sole hole-transporting material, ACS Appl. Energy Mater. 2 (2019) 4890e4899, https://doi.org/10.1021/acsaem. 9b00603.

[62] R. Li, P. Wang, B. Chen, X. Cui, Y. Ding, Y. Li, D. Zhang, Y. Zhao, X. Zhang, NiOx/ spiro hole transport bilayers for stable perovskite solar cells with efficiency exceeding 21, ACS Energy Lett. 5 (2020) 79e86, https://doi.org/10.1021/ acsenergylett.9b02112.

[63] K.-C. Wang, P.-S. Shen, M.-H. Li, S. Chen, M.-W. Lin, P. Chen, T.-F. Guo, Low- temperature sputtered nickel oxide compact thin film as effective electron blocking layer for mesoscopic NiO/CH3NH3PbI3 perovskite heterojunction solar cells, ACS Appl. Mater. Interfaces 6 (2014) 11851e11858, https:// doi.org/10.1021/am503610u.

[64] J. Cui, F. Meng, H. Zhang, K. Cao, H. Yuan, Y. Cheng, F. Huang, M. Wang, CH3NH3PbI3-Based planar solar cells with magnetron-sputtered nickel ox- ide, ACS Appl. Mater. Interfaces 6 (2014) 22862e22870, https://doi.org/ 10.1021/am507108u.

[65] E. Aydin, J. Troughton, M. De Bastiani, E. Ugur, M. Sajjad, A. Alzahrani, M. Neophytou, U. Schwingenschlögl, F. Laquai, D. Baran, S. De Wolf, Room- temperature-sputtered nanocrystalline nickel oxide as hole transport layer for peien perovskite solar cells, ACS Appl. Energy Mater. 1 (2018) 6227e6233, https://doi.org/10.1021/acsaem.8b01263.

[66] J.H. Park, J. Seo, S. Park, S.S. Shin, Y.C. Kim, N.J. Jeon, H.-W. Shin, T.K. Ahn, J.H. Noh, S.C. Yoon, C.S. Hwang, S. Il Seok, Efficient CH3NH3PbI3 perovskite solar cells employing nanostructured p-type NiO electrode formed by a pulsed laser deposition, Adv. Mater. 27 (2015) 4013e4019, https://doi.org/ 10.1002/adma.201500523.

[67] A.E. Shalan, T. Oshikiri, H. Sawayanagi, K. Nakamura, K. Ueno, Q. Sun, H.-P. Wu, E.W.-G. Diau, H. Misawa, Versatile plasmonic-effects at the interface of inverted perovskite solar cells, Nanoscale 9 (2017) 1229e1236, https:// doi.org/10.1039/C6NR06741G.

[68] J.H. Kim, P.-W. Liang, S.T. Williams, N. Cho, C.-C. Chueh, M.S. Glaz, D.S. Ginger, A.K.-Y. Jen, High-performance and environmentally stable planar hetero- junction perovskite solar cells based on a solution-processed copper-doped nickel oxide hole-transporting layer, Adv. Mater. 27 (2015) 695e701, https:// doi.org/10.1002/adma.201404189.

[69] S. Yue, K. Liu, R. Xu, M. Li, M. Azam, K. Ren, J. Liu, Y. Sun, Z. Wang, D. Cao, Efficacious engineering on charge extraction for realizing highly efficient perovskite solar cells, Energy Environ. Sci. 10 (2017) 2570e2578.

[70] J.W. Jung, C.-C. Chueh, A.K.-Y. Jen, A low-temperature, solution-processable, Cu-doped nickel oxide hole-transporting layer via the combustion method for high-performance thin-film perovskite solar cells, Adv. Mater. 27 (2015) 7874e7880, https://doi.org/10.1002/adma.201503298.

[71] K. Yao, F. Li, Q. He, X. Wang, Y. Jiang, H. Huang, A.K.-Y. Jen, A copper-doped nickel oxide bilayer for enhancing efficiency and stability of hysteresis-free inverted mesoporous perovskite solar cells, Nano Energy 40 (2017) 155e162, https://doi.org/10.1016/j.nanoen.2017.08.014.

[72] Q. He, K. Yao, X. Wang, X. Xia, S. Leng, F. Li, Room-temperature and solution- processable Cu-doped nickel oxide nanoparticles for efficient hole-transport layers of flexible large-area perovskite solar cells, ACS Appl. Mater. Interfaces 9 (2017) 41887e41897, https://doi.org/10.1021/acsami.7b13621.

[73] W. Chen, Y. Wu, J. Fan, A.B. Djurišić, F. Liu, H.W. Tam, A. Ng, C. Surya, W.K. Chan, D. Wang, Z.-B. He, Understanding the doping effect on NiO: to- ward high-performance inverted perovskite solar cells, Adv. Energy Mater. 8 (2018) 1703519, https://doi.org/10.1002/aenm.201703519.

[74] W. Chen, F.-Z. Liu, X.-Y. Feng, A.B. Djurišić, W.K. Chan, Z.-B. He, Cesium doped NiOx as an efficient hole extraction layer for inverted planar perovskite solar cells, Adv. Energy Mater. 7 (2017) 1700722, https://doi.org/10.1002/ aenm.201700722.

[75] X. Yin, J. Han, Y. Zhou, Y. Gu, M. Tai, H. Nan, Y. Zhou, J. Li, H. Lin, Critical roles of potassium in charge-carrier balance and diffusion induced defect passiv- ation for efficient inverted perovskite solar cells, J. Mater. Chem. A. 7 (2019) 5666e5676, https://doi.org/10.1039/C8TA11782A.

[76] B. Ge, H.W. Qiao, Z.Q. Lin, Z.R. Zhou, A.P. Chen, S. Yang, Y. Hou, H.G. Yang, Deepening the valance band edges of NiOx contacts by alkaline earth metal doping for efficient perovskite photovoltaics with high open-circuit voltage, Sol. RRL. 3 (2019) 1900192, https://doi.org/10.1002/solr.201900192.

[77] W. Chen, Y. Wu, Y. Yue, J. Liu, W. Zhang, X. Yang, H. Chen, E. Bi, I. Ashraful, M. Grätzel, Efficient and stable large-area perovskite solar cells with inor- ganic charge extraction layers, Science 350 (80) (2015) 944e948.

[78] B. Ge, Z.Q. Lin, Z.R. Zhou, H.W. Qiao, A.P. Chen, Y. Hou, S. Yang, H.G. Yang, Boric acid mediated formation and doping of NiOx layers for perovskite solar cells with efficiency over 21, Sol. RRL 5 (2021) 2000810, https://doi.org/ 10.1002/solr.202000810.

[79] P. Zhou, B. Li, Z. Fang, W. Zhou, M. Zhang, W. Hu, T. Chen, Z. Xiao, S. Yang, Nitrogen-doped nickel oxide as hole transport layer for high-efficiency inverted planar perovskite solar cells, Sol. RRL. 3 (2019) 1900164, https:// doi.org/10.1002/solr.201900164.

[80] S. Wang, Y. Li, J. Yang, T. Wang, B. Yang, Q. Cao, X. Pu, L. Etgar, J. Han, J. Zhao, X. Li, A. Hagfeldt, Critical role of removing impurities in nickel oxide on high- efficiency and long-term stability of inverted perovskite solar cells, Angew. Chem. Int. Ed. 61 (2022) e202116534, https://doi.org/10.1002/ anie.202116534.

[81] C. Li, Y. Zhang, X. Zhang, P. Zhang, X. Yang, H. Chen, Efficient inverted perovskite solar cells with a fill factor over 86% via surface modification of the nickel oxide hole contact, Adv. Funct. Mater. 33 (2023) 2214774, https:// doi.org/10.1002/adfm.202214774.

[82] S. Sajid, S. Alzahmi, I.B. Salem, I.M. Obaidat, Guidelines for fabricating highly efficient perovskite solar cells with Cu2O as the hole transport material, Nanomaterials 12 (2022), https://doi.org/10.3390/nano12193315.

[83] M.I. Hossain, F.H. Alharbi, N. Tabet, Copper oxide as inorganic hole transport material for lead halide perovskite based solar cells, Sol. Energy (2015), https://doi.org/10.1016/j.solener.2015.07.040.

[84] B.A. Nejand, V. Ahmadi, S. Gharibzadeh, H.R. Shahverdi, Cuprous oxide as a potential low-cost hole-transport material for stable perovskite solar cells, ChemSusChem 9 (2016) 302e313, https://doi.org/10.1002/cssc.201501273.

[85] Y. Guo, H. Lei, L. Xiong, B. Li, G. Fang, An integrated organiceinorganic hole transport layer for efficient and stable perovskite solar cells, J. Mater. Chem. A. 6 (2018) 2157e2165, https://doi.org/10.1039/C7TA09946K.

[86] C. Zuo, L. Ding, Solution-processed Cu2O and CuO as hole transport materials for efficient perovskite solar cells, Small 11 (2015) 5528e5532, https:// doi.org/10.1002/smll.201501330.

[87] S. Chatterjee, A.J. Pal, Introducing Cu2O thin films as a hole-transport layer in efficient planar perovskite solar cell structures, J. Phys. Chem. C 120 (2016) 1428e1437, https://doi.org/10.1021/acs.jpcc.5b11540.

[88] W. Yu, F. Li, H. Wang, E. Alarousu, Y. Chen, B. Lin, L. Wang, M.N. Hedhili, Y. Li, K. Wu, X. Wang, O.F. Mohammed, T. Wu, Ultrathin Cu2O as an efficient inorganic hole transporting material for perovskite solar cells, Nanoscale 8 (2016) 6173e6179, https://doi.org/10.1039/C5NR07758C.

[89] W. Sun, Y. Li, S. Ye, H. Rao, W. Yan, H. Peng, Y. Li, Z. Liu, S. Wang, Z. Chen, L. Xiao, Z. Bian, C. Huang, High-performance inverted planar heterojunction perovskite solar cells based on a solution-processed CuOx hole transport layer, Nanoscale 8 (2016) 10806e10813, https://doi.org/10.1039/ C6NR01927G.

[90] Z.-K. Yu, W.-F. Fu, W.-Q. Liu, Z.-Q. Zhang, Y.-J. Liu, J.-L. Yan, T. Ye, W.-T. Yang, H.-Y. Li, H.-Z. Chen, Solution-processed CuOx as an efficient hole-extraction layer for inverted planar heterojunction perovskite solar cells, Chin. Chem. Lett. 28 (2017) 13e18, https://doi.org/10.1016/j.cclet.2016.06.021.

[91] F. Galatopoulos, A. Savva, I.T. Papadas, S.A. Choulis, The effect of hole transporting layer in charge accumulation properties of p-i-n perovskite solar cells, Apl. Mater. 5 (2017) 76102, https://doi.org/10.1063/1.4991030.

[92] H. Rao, S. Ye, W. Sun, W. Yan, Y. Li, H. Peng, Z. Liu, Z. Bian, Y. Li, C. Huang, A 19.0% efficiency achieved in CuOx-based inverted CH3NH3PbI3 xClx solar cells by an effective Cl doping method, Nano Energy 27 (2016) 51e57, https://doi.org/10.1016/j.nanoen.2016.06.044.

[93] I.Y.Y. Bu, Y.-S. Fu, J.-F. Li, T.-F. Guo, Large-area electrospray-deposited nanocrystalline CuXO hole transport layer for perovskite solar cells, RSC Adv. 7 (2017) 46651e46656, https://doi.org/10.1039/C7RA07725D.

[94] L. Liu, Q. Xi, G. Gao, W. Yang, H. Zhou, Y. Zhao, C. Wu, L. Wang, J. Xu, Cu2O particles mediated growth of perovskite for high efficient hole-transporting- layer free solar cells in ambient

conditions, Sol. Energy Mater. Sol. Cells 157 (2016) 937e942, https://doi.org/10.1016/j.solmat.2016.08.013.

[95] Z. Shi, D. Zhou, X. Zhuang, S. Liu, R. Sun, W. Xu, L. Liu, H. Song, Light man- agement through organic bulk heterojunction and carrier interfacial engi- neering for perovskite solar cells with 23.5% efficiency, Adv. Funct. Mater. 32 (2022) 2203873, https://doi.org/10.1002/adfm.202203873.

[96] A.E. Shalan, T. Oshikiri, S. Narra, M.M. Elshanawany, K. Ueno, H.-P. Wu, K. Nakamura, X. Shi, E.W.-G. Diau, H. Misawa, Cobalt oxide (CoOx) as an efficient hole-extracting layer for high-performance inverted planar perov- skite solar cells, ACS Appl. Mater. Interfaces 8 (2016) 33592e33600, https:// doi.org/10.1021/acsami.6b10803.

[97] A. Huang, L. Lei, J. Zhu, Y. Yu, Y. Liu, S. Yang, S. Bao, X. Cao, P. Jin, Fast fabrication of a stable perovskite solar cell with an ultrathin effective novel inorganic hole transport layer, Langmuir 33 (2017) 3624e3634, https:// doi.org/10.1021/acs.langmuir.7b00127.

[98] A. Bashir, S. Shukla, J.H. Lew, S. Shukla, A. Bruno, D. Gupta, T. Baikie, R. Patidar, Z. Akhter, A. Priyadarshi, N. Mathews, S.G. Mhaisalkar, Spinel Co3O4 nanomaterials for efficient and stable large area carbon-based printed perovskite solar cells, Nanoscale 10 (2018) 2341e2350, https://doi.org/ 10.1039/C7NR08289D.

[99] J.H. Lee, Y.W. Noh, I.S. Jin, S.H. Park, J.W. Jung, Efficient perovskite solar cells with negligible hysteresis achieved by solegel-driven spinel nickel cobalt oxide thin films as the hole transport layer, J. Mater. Chem. C 7 (2019) 7288e7298, https://doi.org/10.1039/C9TC00902G.

[100] B.-S. Kim, T.-M. Kim, M.-S. Choi, H.-S. Shim, J.-J. Kim, Fully vacuumeprocessed perovskite solar cells with high open circuit voltage using MoO3/NPB as hole extraction layers, Org. Electron. 17 (2015) 102e106.

[101] Y. Jiang, C. Li, H. Liu, R. Qin, H. Ma, Poly(3,4-ethylenedioxythiophene):pol- y(styrenesulfonate)(PEDOT:PSS)emolybdenum oxide composite films as hole conductors for efficient planar perovskite solar cells, J. Mater. Chem. A. 4 (2016) 9958e9966, https://doi.org/10.1039/C6TA03658A.

[102] W. Zhang, Y. Ding, Y. Jiang, M. Zheng, S. Wu, X. Lu, M. Zeng, X. Gao, Q. Wang, G. Zhou, J. Liu, K. Kempa, J. Gao, Simultaneously enhanced Jsc and FF by employing two solution-processed interfacial layers for inverted planar perovskite solar cells, RSC Adv. 7 (2017) 39523e39529, https://doi.org/ 10.1039/C7RA07475A.

[103] Y. Zhao, A.M. Nardes, K. Zhu, Effective hole extraction using MoOx-Al contact in perovskite CH3NH3PbI3 solar cells, Appl. Phys. Lett. 104 (2014) 213906, https://doi.org/10.1063/1.4880899.

[104] S. Sun, M. Xu, Y. Zhang, R. Liu, X. Wang, L. Zhang, Y. Fang, P. Wang, Study of molybdenum oxide optimized hole carrier transport in perovskite solar cells, Org. Electron. 113 (2023) 106697, https://doi.org/10.1016/ j.orgel.2022.106697.

[105] H. Sun, X. Hou, Q. Wei, H. Liu, K. Yang, W. Wang, Q. An, Y. Rong, Low-tem- perature solution-processed p-type vanadium oxide for perovskite solar cells, Chem. Commun. 52 (2016) 8099e8102, https://doi.org/10.1039/ C6CC03740B.

[106] X. Yao, W. Xu, X. Huang, J. Qi, Q. Yin, X. Jiang, F. Huang, X. Gong, Y. Cao, Solution-processed vanadium oxide thin film as the hole extraction layer for efficient hysteresis-free perovskite hybrid solar cells, Org. Electron. 47 (2017) 85e93, https://doi.org/10.1016/j.orgel.2017.05.006.

[107] D. Li, C. Tong, W. Ji, Z. Fu, Z. Wan, Q. Huang, Y. Ming, A. Mei, Y. Hu, Y. Rong, H. Han, Vanadium oxide post-treatment for enhanced photovoltage of printable perovskite solar cells, ACS Sustain. Chem. Eng. 7 (2019) 2619e2625, https://doi.org/10.1021/acssuschemeng.8b05653.

[108] H. Peng, W. Sun, Y. Li, S. Ye, H. Rao, W. Yan, H. Zhou, Z. Bian, C. Huang, So- lution processed inorganic V2Oxas interfacial function materials for inverted planar-heterojunction perovskite solar cells with enhanced efficiency, Nano Res. 9 (2016) 2960e2971, https://doi.org/10.1007/s12274-016-1181-z.

[109] T.H. Schloemer, J.A. Raiford, T.S. Gehan, T. Moot, S. Nanayakkara, S.P. Harvey, R.C. Bramante, S. Dunfield, A.E. Louks, A.E. Maughan, L. Bliss, M.D. McGehee, M.F.A.M. van Hest, M.O. Reese, S.F. Bent, J.J. Berry, J.M. Luther, A. Sellinger, The molybdenum oxide interface limits the high-temperature operational stability of unencapsulated perovskite solar cells, ACS Energy Lett. 5 (2020) 2349e2360, https://doi.org/10.1021/acsenergylett.0c01023.

[110] M. Kaltenbrunner, G. Adam, E.D. Głowacki, M. Drack, R. Schwödiauer, L. Leonat, D.H. Apaydin, H. Groiss, M.C. Scharber, M.S. White, Flexible high power-per-weight perovskite solar cells with chromium oxideemetal con- tacts for improved stability in air, Nat. Mater. 14 (2015) 1032e1039.

[111] P.-L. Qin, H.-W. Lei, X.-L. Zheng, Q. Liu, H. Tao, G. Yang, W.-J. Ke, L.-B. Xiong, M.-C. Qin, X.-Z. Zhao, G.-J. Fang, Copper-doped chromium oxide hole- transporting layer for perovskite solar cells: interface engineering and per- formance improvement, Adv. Mater. Interfac. 3 (2016) 1500799, https:// doi.org/10.1002/admi.201500799.

[112] Y. Zheng, B. Ge, L.R. Zheng, Y. Hou, S. Yang, H.G. Yang, Solution-processable nickelechromium ternary oxide as an efficient hole transport layer for inverted planar perovskite solar cells, J. Mater. Chem. A. 9 (2021) 21792e21798, https://doi.org/10.1039/D1TA06565C.

[113] P. Salehi-Abar, H. Ashassi-Sorkhabi, MWCNT/Cr2O3 nanocomposite as a solution-processed hole transport layer for cost-effective perovskite solar cells with long-term stability, Sol. Energy 251 (2023) 382e391, https:// doi.org/10.1016/j.solener.2023.01.024.

[114] N.N. Som, V. Sharma, V. Mankad, M.L.C. Attygalle, P.K. Jha, Role of CuAlO2 as an absorber layer for solar energy converter, Sol. Energy 193 (2019) 799e805, https://doi.org/10.1016/j.solener.2019.09.098.

[115] F. Igbari, M. Li, Y. Hu, Z.-K. Wang, L.-S. Liao, A room-temperature CuAlO2 hole interfacial layer for efficient and stable planar perovskite solar cells, J. Mater. Chem. A. 4 (2016) 1326e1335, https://doi.org/10.1039/C5TA07957H.

[116] S. Akin, Y. Liu, M.I. Dar, S.M. Zakeeruddin, M. Grätzel, S. Turan, S. Sonmezoglu, Hydrothermally processed CuCrO2 nanoparticles as an inorganic hole transporting material for low-cost perovskite solar cells with superior stability, J. Mater. Chem. A. 6 (2018) 20327e20337, https://doi.org/ 10.1039/C8TA07368F.

[117] H. Zhang, H. Wang, H. Zhu, C.-C. Chueh, W. Chen, S. Yang, A.K.-Y. Jen, Low- temperature solution-processed CuCrO2 hole-transporting layer for efficient and photostable perovskite solar cells, Adv. Energy Mater. 8 (2018) 1702762, https://doi.org/10.1002/aenm.201702762.

[118] P.-L. Qin, Q. He, C. Chen, X.-L. Zheng, G. Yang, H. Tao, L.-B. Xiong, L. Xiong, G. Li, G.-J. Fang, High-performance rigid and flexible perovskite solar cells with low-temperature solution-processable binary metal oxide hole- transporting materials, Sol. RRL. 1 (2017) 1700058, https://doi.org/10.1002/ solr.201700058.

[119] S. Wang, L. Wang, C. Liu, Y. Shan, F. Li, L. Sun, Spray pyrolysis deposition of CuCrO2 films as promising inorganic hole transport layers for highly efficient perovskite solar cells, Energy Technol. 10 (2022) 2200518, https://doi.org/ 10.1002/ente.202200518.

[120] Y. Chen, Z. Yang, S. Wang, X. Zheng, Y. Wu, N. Yuan, W.-H. Zhang, S. (Frank) Liu, Design of an inorganic mesoporous hole-transporting layer for highly efficient and stable inverted perovskite solar cells, Adv. Mater. 30 (2018) 1805660, https://doi.org/10.1002/adma.201805660.

[121] H. Zhang, J. Cheng, F. Lin, H. He, J. Mao, K.S. Wong, A.K.-Y. Jen, W.C.H. Choy, Pinhole-free and surface-nanostructured NiO x film by room-temperature solution process for high-performance flexible perovskite solar cells with good stability and reproducibility, ACS Nano 10 (2016) 1503e1511.

[122] C. Zhang, X. Shen, M. Chen, Y. Zhao, X. Lin, Z. Qin, Y. Wang, L. Han, Con- structing a stable and efficient buried heterojunction via halogen bonding for inverted perovskite solar cells, Adv. Energy Mater. 13 (2023) 2203250, https://doi.org/10.1002/aenm.202203250.

[123] M. Yang, X. Zhu, K. Mo, S. Li, S. Cheng, Y. Liu, N. Yan, Z. Wang, Tuning surface oxidation states of nickel oxide for efficient inverted perovskite solar cells, ACS Appl. Energy Mater. 6 (2023) 1332e1339, https://doi.org/10.1021/ acsaem.2c03072.

[124] S. Ito, S. Tanaka, H. Nishino, Lead-halide perovskite solar cells by CH3NH3I dripping on PbI2eCH3NH3IeDMSO precursor layer for planar and porous structures using CuSCN hole-transporting material, J. Phys. Chem. Lett. 6 (2015) 881e886.

[125] S. Ito, S. Tanaka, H. Vahlman, H. Nishino, K. Manabe, P. Lund, Carbon-double- bond-free printed solar cells from TiO2/CH3NH3PbI3/CuSCN/Au: structural control and photoaging effects, ChemPhysChem 15 (2014) 1194e1200, https://doi.org/10.1002/cphc.201301047.

[126] J. Burschka, N. Pellet, S.J. Moon, R. Humphry-Baker, P. Gao, M.K. Nazeeruddin,

M. Grätzel, Sequential deposition as a route to high-performance perovskite- sensitized solar cells, Nature 499 (2013) 316e319, https://doi.org/10.1038/ nature12340.

[127] S. Chavhan, O. Miguel, H.-J. Grande, V. Gonzalez-Pedro, R.S. Sánchez, E.M. Barea, I. Mora-Seró, R. Tena-Zaera, Organo-metal halide perovskite-based solar cells with CuSCN as the inorganic hole selective contact, J. Mater. Chem. A. 2 (2014) 12754e12760.

[128] G.A. Sepalage, S. Meyer, A.R. Pascoe, A.D. Scully, U. Bach, Y.-B. Cheng, L. Spiccia, A facile deposition method for CuSCN: exploring the influence of CuSCN on JV hysteresis in planar perovskite solar cells, Nano Energy 32 (2017) 310e319.

[129] P. Qin, S. Tanaka, S. Ito, N. Tetreault, K. Manabe, H. Nishino, M.K. Nazeeruddin, M. Grätzel, Inorganic hole conductor-based lead halide perovskite solar cells with 12.4% conversion efficiency, Nat. Commun. 5 (2014) 1e6.

[130] J. Liu, S.K. Pathak, N. Sakai, R. Sheng, S. Bai, Z. Wang, H.J. Snaith, Identification and mitigation of a critical interfacial instability in perovskite solar cells employing copper thiocyanate hole-transporter, Adv. Mater. Interfac. 3 (2016) 1600571.

[131] M. Jung, Y.C. Kim, N.J. Jeon, W.S. Yang, J. Seo, J.H. Noh, S. Il Seok, Thermal stability of CuSCN hole conductor-based perovskite solar cells, Chem- SusChem 9 (2016) 2592e2596.

[132] N. Arora, M.I. Dar, A. Hinderhofer, N. Pellet, F. Schreiber, S.M. Zakeeruddin, M. Grätzel, Perovskite solar cells with CuSCN hole extraction layers yield stabilized efficiencies greater than 20, Science 358 (80) (2017) 768e771.

[133] G. Kim, N. Kwon, D. Lee, M. Kim, M. Kim, Y. Lee, W. Kim, D. Hyeon, B. Kim, M.S. Jeong, Methylammonium compensation effects in MAPbI3 perovskite solar cells for high-quality inorganic CuSCN hole transport layers, ACS Appl. Mater. Interfaces 14 (2022) 5203e5210.

[134] N. Perumbalathodi, T.-S. Su, T.-C. Wei, Antisolvent treatment on wet solution-processed CuSCN hole transport layer enables efficient and stable perovskite solar cells, Adv. Mater. Interfac. 9 (2022) 2201191, https://doi.org/ 10.1002/admi.202201191.

[135] V.E. Madhavan, I. Zimmermann, A.A.B. Baloch, A. Manekkathodi, A. Belaidi, N. Tabet, M.K. Nazeeruddin, CuSCN as hole transport material with 3D/2D perovskite solar cells, ACS Appl. Energy Mater. 3 (2019) 114e121.

[136] A.S. Subbiah, A. Halder, S. Ghosh, N. Mahuli, G. Hodes, S.K. Sarkar, Inorganic hole conducting layers for perovskite-based solar cells, J. Phys. Chem. Lett. 5 (2014) 1748e1753.

[137] K. Zhao, R. Munir, B. Yan, Y. Yang, T. Kim, A. Amassian, Solution-processed inorganic copper (I) thiocyanate (CuSCN) hole transporting layers for effi- cient peien perovskite solar cells, J. Mater. Chem. A. 3 (2015) 20554e20559.

[138] S. Ye, W. Sun, Y. Li, W. Yan, H. Peng, Z. Bian, Z. Liu, C. Huang, CuSCN-based inverted planar perovskite solar cell with an average PCE of 15.6, Nano Lett. 15 (2015) 3723e3728.

[139] J.W. Jung, C. Chueh, A.K. Jen, High-performance semitransparent perovskite solar cells with 10% power conversion efficiency and 25% average visible transmittance based on transparent CuSCN as the hole-transporting mate- rial, Adv. Energy Mater. 5 (2015) 1500486.

[140] K. Zhao, Y. Li, H. Cheng, K. Hu, Z.-S. Wang, Efficient inverted perovskite solar cells with CuSeCN as the hole transport material, J. Power Sources 472 (2020) 228505.

[141] X. Liu, Y. Wang, E. Rezaee, Q. Chen, Y. Feng, X. Sun, L. Dong, Q. Hu, C. Li, Z. Xu, Tetra-propyl-substituted copper (II) phthalocyanine as dopant-free hole transporting material for planar perovskite solar cells, Sol. RRL. 2 (2018) 1800050.

[142] Y.C. Kim, T.-Y. Yang, N.J. Jeon, J. Im, S. Jang, T.J. Shin, H.-W. Shin, S. Kim, E. Lee, J.H. Noh, Engineering interface structures between lead halide perovskite and copper phthalocyanine for efficient and stable perovskite solar cells, Energy Environ. Sci. 10 (2017) 2109e2116.

[143] J. Han, Y. Tu, Z. Liu, X. Liu, H. Ye, Z. Tang, T. Shi, G. Liao, Efficient and stable inverted planar perovskite solar cells using dopant-free CuPc as hole transport layer, Electrochim. Acta 273 (2018) 273e281, https://doi.org/ 10.1016/j.electacta.2018.04.055.

[144] X. Liu, Z. Liu, H. Ye, Y. Tu, B. Sun, X. Tan, T. Shi, Z. Tang, G. Liao, Novel efficient C60-based inverted perovskite solar cells with negligible hysteresis, Elec- trochim. Acta 288 (2018) 115e125.

[145] J. Wang, Z. Wang, M. Li, C. Zhang, L. Jiang, K. Hu, Q. Ye, L. Liao, Doped copper phthalocyanine via an aqueous solution process for normal and inverted perovskite solar cells, Adv. Energy Mater. 8 (2018) 1701688.

[146] F. Qi, B. Wu, J. Xu, Q. Chen, H. Shan, J. Xu, Z.-X. Xu, Non-peripherally octaalkyl-substituted nickel phthalocyanines used as non-dopant hole transport materials in perovskite solar cells, Chin. Phys. B 30 (2021) 108801.

[147] Z. Yu, L. Wang, X. Mu, C. Chen, Y. Wu, J. Cao, Y. Tang, Intramolecular electric field construction in metal phthalocyanine as dopant-free hole transporting material for stable perovskite solar cells with> 21% efficiency, Angew. Chem. Int. Ed. 60 (2021) 6294e6299.

[148] Z. Cui, Y. Wang, Y. Chen, X. Chen, X. Deng, W. Chen, C. Shi, Soluble tetra-methoxyltriphenylamine substituted zinc phthalocyanine as dopant-free hole transporting materials for perovskite solar cells, Org. Electron. 69 (2019) 248e254, https://doi.org/10.1016/j.orgel.2019.03.035.

[149] C. Li, Q. Hu, Q. Chen, W. Yu, J. Xu, Z.-X. Xu, Tetrapropyl-substituted palladium phthalocyanine used as an efficient hole transport material in perovskite solar cells, Org. Electron. 88 (2021) 106018.

[150] J.A. Christians, R.C.M. Fung, P. V Kamat, An inorganic hole conductor for organo-lead halide perovskite solar cells. Improved hole conductivity with copper iodide, J. Am. Chem. Soc. 136 (2014) 758e764.

[151] G.A. Sepalage, S. Meyer, A. Pascoe, A.D. Scully, F. Huang, U. Bach, Y. Cheng, L. Spiccia, Copper (I) iodide as hole-conductor in planar perovskite solar

cells: probing the origin of JeV hysteresis, Adv. Funct. Mater. 25 (2015) 5650e5661.

[152] W.-Y. Chen, L.-L. Deng, S.-M. Dai, X. Wang, C.-B. Tian, X.-X. Zhan, S.-Y. Xie, R.-B. Huang, L.-S. Zheng, Low-cost solution-processed copper iodide as an alternative to PEDOT: PSS hole transport layer for efficient and stable inverted planar heterojunction perovskite solar cells, J. Mater. Chem. A. 3 (2015) 19353e19359.

[153] J. Cao, B. Wu, J. Peng, X. Feng, C. Li, Y. Tang, Copper-copper iodide hybrid nanostructure as hole transport material for efficient and stable inverted perovskite solar cells, Sci. China Chem. 62 (2019) 363e369.

[154] H. Rao, W. Sun, S. Ye, W. Yan, Y. Li, H. Peng, Z. Liu, Z. Bian, C. Huang, Solution-processed CuS NPs as an inorganic hole-selective contact material for inverted planar perovskite solar cells, ACS Appl. Mater. Interfaces 8 (2016) 7800e7805.

[155] H. Lei, G. Yang, X. Zheng, Z. Zhang, C. Chen, J. Ma, Y. Guo, Z. Chen, P. Qin, Y. Li, Incorporation of high-mobility and room-temperature-deposited CuxS as a hole transport layer for efficient and stable organo-lead halide perovskite solar cells, Sol. RRL. 1 (2017) 1700038.

[156] D. Han, C. Wu, Q. Zhang, S. Wei, X. Qi, Y. Zhao, Y. Chen, Y. Chen, L. Xiao, Z. Zhao, Solution-processed Cu9S5 as a hole transport layer for efficient and stable perovskite solar cells, ACS Appl. Mater. Interfaces 10 (2018) 31535e31540.

[157] A. Yang, J.-C. Blancon, W. Jiang, H. Zhang, J. Wong, E. Yan, Y.-R. Lin, J. Crochet, M.G. Kanatzidis, D. Jariwala, Giant enhancement of photoluminescence emission in WS2-two-dimensional perovskite heterostructures, Nano Lett. 19 (2019) 4852e4860.

[158] X. Liu, Y. Cheng, B. Tang, Z.G. Yu, M. Li, F. Lin, S. Zhang, Y.-W. Zhang, J. Ouyang, H. Gong, Shallow defects levels and extract detrapped charges to stabilize highly efficient and hysteresis-free perovskite photovoltaic devices, Nano Energy 71 (2020) 104556.

[159] S. Kohnehpoushi, P. Nazari, B.A. Nejand, M. Eskandari, MoS2: a two- dimensional hole-transporting material for high-efficiency, low-cost perov- skite solar cells, Nanotechnology 29 (2018) 205201.

[160] A. Capasso, F. Matteocci, L. Najafi, M. Prato, J. Buha, L. Cinà, V. Pellegrini, A. Di Carlo, F. Bonaccorso, Few-layer MoS2 flakes as active buffer layer for stable perovskite solar cells, Adv. Energy Mater. 6 (2016) 1600920.

[161] G. Kakavelakis, I. Paradisanos, B. Paci, A. Generosi, M. Papachatzakis, T. Maksudov, L. Najafi, A.E. Del Rio Castillo, G. Kioseoglou, E. Stratakis, Extending the continuous operating lifetime of perovskite solar cells with a molybdenum disulfide hole extraction interlayer, Adv. Energy Mater. 8 (2018) 1702287.

[162] B. Peng, G. Yu, Y. Zhao, Q. Xu, G. Xing, X. Liu, D. Fu, B. Liu, J.R.S. Tan, W. Tang, Achieving ultrafast hole transfer at the monolayer MoS2 and CH3NH3PbI3 perovskite interface by defect engineering, ACS Nano 10 (2016) 6383e6391.

[163] Y. Shi, O. V Prezhdo, J. Zhao, W.A. Saidi, Iodine and sulfur vacancy cooper- ation promotes ultrafast charge extraction at MAPbI3/MoS2 interface, ACS Energy Lett. 5 (2020) 1346e1354.

[164] X. Li, J. Yang, Q. Jiang, H. Lai, S. Li, Y. Tan, Y. Chen, S. Li, Perovskite solar cells employing an eco-friendly and low-cost inorganic hole transport layer for enhanced photovoltaic performance and operational stability, J. Mater. Chem. A. 7 (2019) 7065e7073.

[165] S. Sidhik, C.R. Pérez, M.A.S. Estrada, T. López-Luke, A. Torres, E. De la Rosa, Improving the stability of perovskite solar cells under harsh environmental conditions, Sol. Energy 202 (2020) 438e445.

[166] X. Li, Y. Tan, H. Lai, S. Li, Y. Chen, S. Li, P. Xu, J. Yang, All-inorganic CsPbBr3 perovskite solar cells with 10.45% efficiency by evaporation-assisted

deposition and setting intermediate energy levels, ACS Appl. Mater. In- terfaces 11 (2019) 29746e29752.

[167] L.-C. Chen, Z.-L. Tseng, C.-C. Chen, S.H. Chang, C.-H. Ho, Fabrication and characteristics of CH3NH3PbI3 perovskite solar cells with molybdenum- selenide hole-transport layer, APEX 9 (2016) 122301.

[168] L. Fu, Y. Nie, B. Li, N. Li, B. Cao, L. Yin, Bismuth telluride interlayer for all- inorganic perovskite solar cells with enhanced efficiency and stability, Sol. Rrl. 3 (2019) 1900233.

[169] A. Abdolhay, A. Kashaninia, M. Banihashemi, Effect of a metal-semiconductor hetero nanostructure of Cu/Bi2Se3 on optical properties of perovskite solar cells, Phys. Status Solidi (n.d.). 260 (2023) 2200482.

[170] M. Tamilselvan, A.J. Bhattacharyya, Tetrahedrite (Cu12Sb4S13) ternary inorganic hole conductor for ambient processed stable perovskite solar cells, ACS Appl. Energy Mater. 1 (2018) 4227e4234.

[171] Y. Liu, Q. Chen, A. Mei, B. Hu, Z. Yang, W. Chen, Bandgap aligned Cu 12 Sb 4 S 13 quantum dots as efficient inorganic hole transport materials in planar perovskite solar cells with enhanced stability, Sustain. Energy Fuels 3 (2019) 831e840.

[172] Y. Zhang, Z. Zhang, Y. Liu, Y. Liu, H. Gao, Y. Mao, An inorganic hole-transport material of CuInSe2 for stable and efficient perovskite solar cells, Org. Electron. 67 (2019) 168e174.

[173] S. Yang, W. Ma, Z. Zhang, J. Zhu, Y. Liu, H. Zhang, Y. Mao, Inverted perovskite solar cells based on inorganic hole transport material of CuInS2 with high efficiency and stability, Sol. Energy 230 (2021) 485e491.

[174] Y. Liu, Z. Zhang, H. Gao, H. Zhang, Y. Mao, A novel inorganic hole- transporting material of CuInS2 for perovskite solar cells with high effi- ciency and improved stability, Org. Electron. 75 (2019) 105430.

[175] S.B. Patel, A.H. Patel, J. V Gohel, A novel and cost effective CZTS hole transport material applied in perovskite solar cells, CrystEngComm 20 (2018) 7677e7687.

[176] L.S. Khanzada, I. Levchuk, Y. Hou, H. Azimi, A. Osvet, R. Ahmad, M. Brandl, P. Herre, M. Distaso, R. Hock, Effective ligand engineering of the Cu2ZnSnS4 nanocrystal surface for increasing hole transport efficiency in perovskite solar cells, Adv. Funct. Mater. 26 (2016) 8300e8306.

[177] F. Behrouznejad, M. Forouzandeh, R. Khosroshahi, K. Meraji, M.N. Badrabadi, M. Dehghani, X. Li, Y. Zhan, Y. Liao, Z. Ning, Effective carbon composite electrode for low-cost perovskite solar cell with inorganic CuIn0. 75Ga0. 25S2 hole transport material, Sol. Rrl. 4 (2020) 1900564.

[178] C.-C. Tseng, G. Wu, L.-B. Chang, M.-J. Jeng, W.-S. Feng, D.W. Chen, L.-C. Chen, K.-L. Lee, Effects of annealing on characteristics of Cu2ZnSnSe4/ CH3NH3PbI3/ZnS/IZO nanostructures for enhanced photovoltaic solar cells, Nanomaterials 10 (2020) 521.

[179] A. Di Vito, A. Pecchia, M. Auf der Maur, A. Di Carlo, Nonlinear work function tuning of lead-halide perovskites by MXenes with mixed terminations, Adv. Funct. Mater. 30 (2020) 1909028, https://doi.org/10.1002/adfm.201909028.

[180] T. Chen, G. Tong, E. Xu, H. Li, P. Li, Z. Zhu, J. Tang, Y. Qi, Y. Jiang, Accelerating hole extraction by inserting 2D Ti 3 C 2-MXene interlayer to all inorganic perovskite solar cells with long-term stability, J. Mater. Chem. A. 7 (2019) 20597e20603.

[181] R. Zhang, Z. Huang, W. Chen, B. Lyu, H. Zhang, X. He, X. Hu, Y. Song, W.C.H. Choy, A self-assembled vertical-gradient and well-dispersed MXene structure for flexible large-area perovskite modules, Adv. Funct. Mater. 33 (2023) 2210063.

[182] J.S. Kang, J. Kim, J. Yoon, J. Kim, J. Yang, D.Y. Chung, M. Kim, H. Jeong, Y.J. Son, B.G. Kim, Room-temperature vapor deposition of cobalt nitride nanofilms for mesoscopic and perovskite solar cells, Adv. Energy Mater. 8 (2018) 1703114.